# Connectivity, Plasticity, and Function of Neuronal Circuits in the Zebrafish Olfactory Forebrain

## Inaugural Dissertation

**zur Erlangung der Doktorwürde**

**vorgelegt der**

**Philosophisch-Naturwissenschaftlichen Fakultät**

**der Universität Basel**

**von**


## Ming Zou

**aus Guangdong, P. R. China**


**Basel, 2014**

Genehmigt von der Philosophisch-Naturwissenschaftlichen Fakultät auf Antrag von:

**Prof. Dr. Rainer W. Friedrich**

(Dissertationsleiter und Fakultätsverantwortliche)

**Dr. Georg Keller**

(Korreferent)

Basel, 24 June 2014

**Prof. Dr. Jörg Schibler**

(Dekan)

The work presented in this thesis was carried out at the Friedrich Miescher Institute for Biomedical Research, Basel, Switzerland, under the supervision of Prof. Dr. Rainer W. Friedrich. All experiments and data analysis of this work were performed by Ming Zou.

About one third of the results presented here have been published recently in:

Zou M, De Koninck P, Neve RL and Friedrich RW (2014)

**Fast gene transfer into the adult zebrafish brain by herpes simplex virus 1 (HSV-1) and electroporation: methods and optogenetic applications.**

*Front. Neural Circuits* **8**:41. doi: 10.3389/fncir.2014.00041

# Acknowledgements:

First of all, I would like to thank all members in the Friedrich Group for generous help and nice atmosphere. Especially, those who contributed to this study:

Martin Naegeli for maintaining the zebrafish facility;

Estelle Arn for help with molecular cloning;

Gilad Jacobson for valuable instructions and advice on data analysis;

Adrian Wanner and Iori Namekawa for advice on data analysis and helpful discussions;

Thomas Frank and Anastasios Moressis for helpful discussions;

Yan-Ping Zhang Schaerer for help with electrophysiology experiments.

Special thanks to Prof. Dr. Rainer W. Friedrich for giving me the opportunity to study neural circuits and computations in his laboratory where I have gained a lot of advanced knowledge and interesting ideas through interactions with colleagues of diverse backgrounds.

Special thanks to Prof. Dr. Carl Petersen, Prof. Dr. Thomas Oertner, Prof. Dr. Paul De Koninck and Dr. Georg Keller for taking part in my thesis committee and for valuable instructions.

Sincere thanks to Dr. Sheng-Jia Zhang, who told me about FMI and gave strong support to my application of FMI, and who continues to provide valuable guidance.

Many thanks to all the colleagues at FMI and particularly those in the neurobiology groups. Without you, I would not be able to enjoy so much the stimulating environment, excellent research, and fantastic scientific discussions.

Many thanks to the FMI football team and ACSSB basketball team for a lot of fun during my PhD study in Basel.

Last but not least, thanks to Liying Wang. You know how important you are to me.

***Standing on the shoulders of giants…***

*— To pioneers of olfactory research*

# *Contents*

## *Abbreviations*

AUC: Area under curve

CCh: cholinergic agonist carbachol

ChR2: Channelrhodopsin-2

Dp: Posterior zone of dorsal telencephalon

chrDp: Blue light stimulation of Dp ChR2 positive neurons

EEP: External-electrode-electroporation

EPSC: Excitatory post-synaptic current

GECI: Genetically encoded calcium indicator

HSV-1: Herpes simplex virus type I

IEP: Internal-electrode-electroporation

IPSC: Inhibitory post-synaptic current

LTD: long-term depression

LTP: long-term potentiation

OB: Olfactory bulb

eleOB: Electrical stimulation of OB output fibers

MC: Mitral cell

SD: Standard deviation

SE: Standard error

STDP: Spike-timing-dependent plasticity

# *Preface*

For most living animals such as worms, insects, fishes, rodents and humans, chemical cues from the environment (odorants) play critical roles in guiding behaviors important for survival, including preying, mating, breeding, and escaping. How those odorants are detected, identified, learned, remembered, and used by the nervous system is a longstanding interest for neuroscientists. An animal that is well-suited to study the processing of odor information at the level of neuronal circuits is the zebrafish (*Danio rerio*) because its small brain size allows for exhaustive quantitative measurements of neuronal activity patterns.

In vertebrates, odorants are detected by olfactory sensory neurons in the nose and transmitted to the first olfactory processing center in the brain, the olfactory bulb (OB), as patterns of neuronal activities. In the OB, neuronal activity patterns from the nose are transformed into odor-specific spatiotemporal activity patterns across second order neurons, the mitral cells. These discrete neuronal activity patterns are broadcast to various target areas. The largest of these higher brain areas is piriform cortex or its teleost homolog, the posterior zone of dorsal telencephalon (Dp). In this higher brain region, an odor-encoding neuronal activity pattern from the OB is thought to be encoded as a “gestalt”, or “odor object”, and possibly stored in memory by specific modifications of functional connections between distributed neuronal ensembles. Such neuronal ensembles are also thought to be connected with other brain regions that involved in the control of different behaviors. Therefore, by inducing a specific activity pattern in the OB, which then retrieves related neuronal ensemble activities in a higher brain region, an odor cue (or even partial cue) recalls an odor object memory that may further trigger a specific set of behavioral responses in the animal.

The mechanisms by which odor object memory is synthesized, stored, and recalled is of major interest in neuroscience because it may provide fundamental insights into associative memory functions. However, dissecting higher brain functions such as associative memory will first require basic understanding of connectivity, plasticity, and related modulating factors for the underlying neuronal circuits. In this inaugural dissertation, I present an approach to study the connectivity, plasticity, and cholinergic modulation of the neural circuits in Dp and present new insights into the synaptic organizations of this neuronal network.

In results part one, I show that transgenes can be introduced directly into the adult zebrafish brain by herpes simplex type I viruses (HSV-1) or electroporation. I developed a new procedure to target electroporation to defined brain areas, e.g. Dp, and identified promoters that produced strong long-term expression. These new methods fill an important gap in the spectrum of molecular tools for zebrafish and are likely to have a wide range of applications. In results part two, I used a combination of electroporation, optogenetics, electrophysiology, and pharmacology to study the intrinsic connectivity and plasticity in neural circuits of Dp. I found that connectivity between any pair of excitatory neurons in Dp is extremely sparse (connection probability < 1.5 %). The connection probability of inhibitory synapses is also sparse but slightly higher (< 2.5 %). Furthermore, I found that connectivity can be functionally modified by activity-dependent synaptic plasticity including spike timing-dependent long-term potentiation. Moreover, I show that cholinergic agonists differentially modulate excitatory and inhibitory synaptic transmissions in Dp, consistent with the notion that cholinergic neuromodulation controls experience-dependent changes in functional connectivity. These findings show that the synaptic organization of Dp is similar to mammalian piriform cortex and provide quantitative insights into the functional organization of a brain area that is likely to be involved in associative memory.

# *Chapter 1: Introduction*

Chemical cues in our environment plays a critical role in the daily life of essentially all animals. For example, odor cues are important for mate choice and recognition (Brennan and Keverne, 1997), mother-infant interactions (Kendrick et al., 1992), food localization and preferences (Mennella and Beauchamp, 2002), predator avoidance (Apfelbach et al., 2005), as well as emotional state (Otto et al., 2000). Memory of odor information allows animals to react to chemosensory stimuli with different behaviors to maximize their survival. These phenomena raise fundamental questions about how odors are detected, learned, memorized, and retrieved by the animal's nervous system. Such questions have captured long-lasting scientific interests, last but not least because they concern fundamental questions in neuroscience. Addressing these questions requires multi-disciplinary approaches and has recently been facilitated by rapid technical developments in different fields including genetics, physiology, pharmacology, behavior, and computation. Small model organisms such as the zebrafish (*Danio rerio*), which are rare among vertebrates, provide important advantages to combine the different technologies.

## 1.1 Advantages of zebrafish for circuit neuroscience

Zebrafish is a small freshwater teleost species that comes from still or slow waters with a lot of green plants (e.g. rice fields) in India and Bangladesh (Engeszer et al., 2007; Spence et al., 2008). It has various advantages that make it a unique model organism for circuit neuroscience. First, many brain regions of the zebrafish have gross structures that similar to that of other vertebrates, for instance, the retina, OB,

cerebellum and spinal cord (Friedrich et al., 2010; Wullimann and Mueller, 2004). This enables knowledge transfer and comparison among species.

Secondly, an important advantage, maybe the most important advantage, for exhaustive quantitative measurements of neuronal activity patterns is its small brain size **(Figure 1A, B)**. As a consequence, neuronal activity in brain areas such as Dp can be measured from relatively large fractions of all neurons, which would not be possible in homologous brain areas of mammals such as piriform cortex. In the future, the small brain size may also allow for large-scale reconstructions of wiring diagrams by electron microscopy (Friedrich et al., 2013a). Exhaustive measurements of neuronal activity and wiring diagrams are important because crucial processing functions could be carried out by only small subset of neurons that can hardly be detected through sparse sampling (Briggman et al., 2011; Niessing and Friedrich, 2010). Without exhaustive sampling of the neuronal activities or connections in a feasibly sized brain, such important features of neuronal circuits may not be discovered.

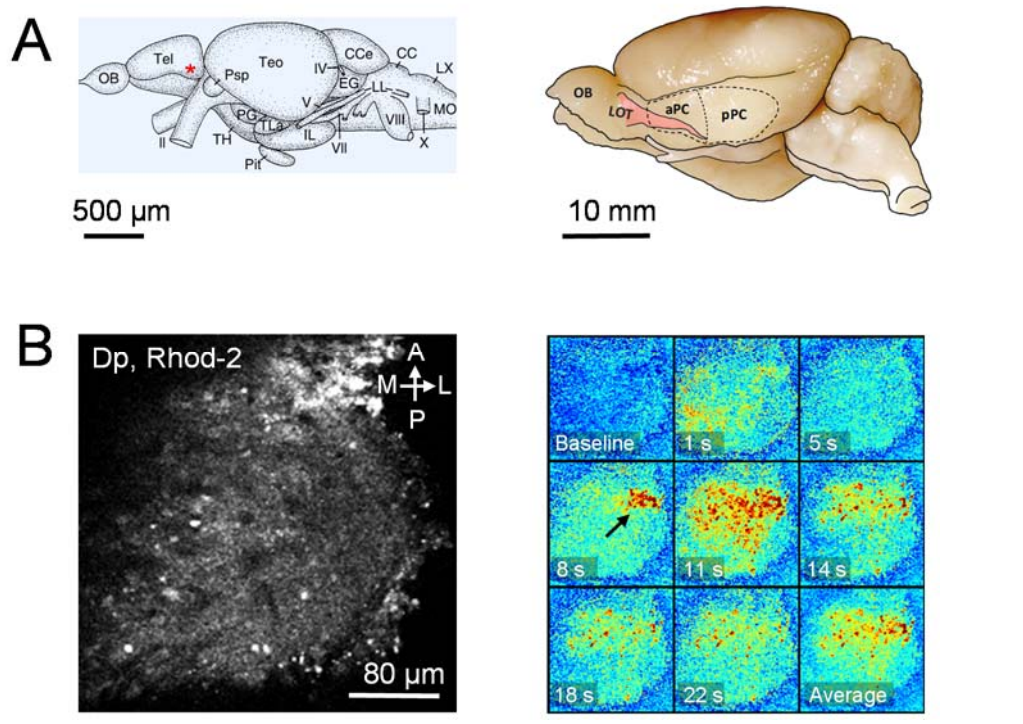


**FIGURE 1 | Small brain size is an important advantage of zebrafish for circuit neuroscience. (A)** Comparison of the zebrafish brain (left, adapted from Wullimann and Mueller 2004) and the rat brain (right, adapted from Bekkers and Suzuki 2013). **(B)** Dp of adult zebrafish (red asterisk in A) was loaded with calcium sensitive dye Rhod-2 and stimulated with food odor extract during two-photon imaging. Left, raw fluorescence of an optical section through Dp viewed under the two-photon microscope; right, fluorescence signal change (dF/F) at different time points of the optical section at the left (odor is applied at 1s). Arrow points to a subset of early responding neurons. (Ming Zou, unpublished data)

In addition, zebrafish are cheap, easy to breed, and transparent during early development, which enables deep tissue live imaging. Zebrafish are also accessible to many sophisticated genetic manipulations that are important for dissecting the structures and functions of neural circuits (see below). Therefore, taken together, zebrafish provide unique advantages among vertebrates to study olfactory information processing.

## 1.2 Genetic approaches for dissecting neural circuits

Understanding the principles of odor information processing in neural circuits requires systematic characterization of the participating cell types and their connections. Furthermore, it requires the ability to measure and intervene with the activity of these neurons. To achieve cell-type-specific marking, measurements, and manipulations, genetic approaches are particularly powerful (Friedrich et al., 2010, 2013a; Luo et al., 2008; Weber and Köster, 2013).

In recent years, various genetically encoded protein markers, sensors, and transducers have been synthesized and optimized for the application in neuroscience or other fields. These tools include the optogenetic actuators channelrhodopsin-2 (ChR2) and halorhodopsin (Yizhar et al., 2011), genetically encoded calcium indicators (GECIs) with different colors (Pérez Koldenkova and Nagai, 2013), and other light-responsive synthetic proteins (Chudakov et al., 2010; Knöpfel et al., 2010; Müller and Weber, 2013). The applications of these new tools have produced significant insights into mechanisms underlying circuit functions or behavior (Blumhagen et al., 2011; Chen et al., 2013; Liu et al., 2012) and will most likely continue to be extremely important in neuroscience.

Using such tools requires genetic approaches to express transgenes in neurons, ideally with a high degree of control over the expression patterns. Among vertebrates, mouse and zebrafish are the most advanced genetic model organisms. Available methods to achieve cell-type-specific protein expression in these model organisms include (1) direct endogenous *cis*-regulatory elements (enhancers and promoters), (2) bacterial artificial chromosomes (BACs), and (3) enhancer or repressor trap approaches. Amplification of gene expression and easy exchange of transgenes can be achieved using two-component expression systems such as the binary Gal4/UAS and tTA/TetO systems, and the intersectional Flp/FRT and Cre/loxP systems (**Figure 2**). Further, temporal control of expression can be achieved by inducible systems that depend on small molecules such as Doxycycline (rtTA/TetO system, **Figure 2G'**) or tamoxifen (CreER system) or heat-shock-based system such as heat-shock/MAZe system (Collins et al., 2010). Particularly powerful tools for the expression of transgenes are viral vectors, which have been engineered extensively for applications in rodents (Luo et al., 2008). However, very few viral vectors for gene transfer have been identified that work efficiently in zebrafish.

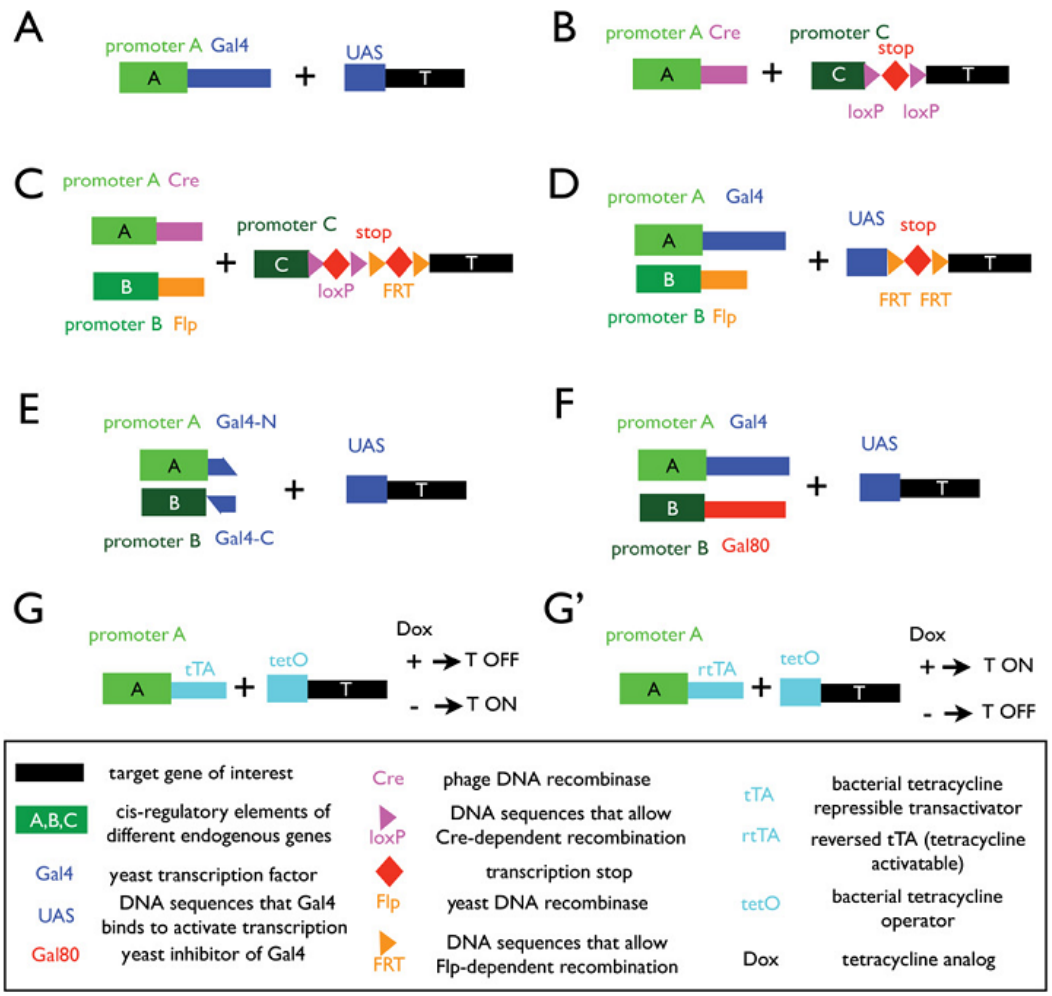


**FIGURE 2 | Binary and Intersectional Methods of Gene Expression. (A)** Yeast transcription factor Gal4 binds to UAS and activates expression of target gene T in cells where promoter A is active. The same scheme applies to other transcription factor/binding site-based binary expression systems. **(B)** Cre/loxP-mediated recombination removes the transcription stop, allowing target gene T to be expressed in cells where both promoters A and C are active. Promoter C is often constitutive for general application. If promoter C is also specific, it can provide intersectional restrictions with promoter A. Cre can be replaced with a tamoxifen-inducible CreER to allow control of timing and amount of recombination. The same scheme also applies to other site-directed recombination systems, such as Flp/FRT. **(C)** Combination of Cre/loxP and Flp/FRT recombination systems allow target genes of interest to be expressed in cells that are active for both promoters A and B (and C). **(D)** The combination of Gal4/UAS and Flp/FRT allows the target gene of interest to be expressed in cells that are active for both promoters A and B. Gal4/UAS can be replaced with other binary expression systems; Flp/FRT can be replaced by other recombination systems. **(E)** Intersectional method that utilizes the reconstitution of N- and C-terminal parts of Gal4. **(F)** Target gene is expressed in cells that are active for promoter A but not promoter B, as Gal80 inhibits Gal4 activity. **(G and G')** Tetracycline-inducible transcription of target gene T. Dox, doxycycline, a tetracycline analog. (Adapted from Luo et al. 2008).

Moreover, multiple genetic tools can be combined with each other to allow sophisticated genetic approaches to dissect neuronal circuit function (**Figure 2**). In zebrafish older than a few days, however, most genetic approaches rely on the generation of stable transgenic lines. As a consequence, genetic approaches for zebrafish are usually time-consuming, particularly when multiple genetic manipulations are to be combined. In rodents, this problem can often be circumvented by direct gene transfer into the developing or adult brain using viral vectors. It is therefore of major interest to develop viral vectors or other methods to achieve fast and efficient gene transfer into neurons of adult zebrafish. Although quite some efforts have been made to employ baculoviruses (Wagle and Jesuthasan, 2003), pseudotyped lentiviruses and murine leukemia viruses (Rothenaigner et al., 2011), Rabies virus and Sindbis virus (Zhu et al., 2009), and electroporation (Barnabé-Heider et al., 2008; Nishi et al., 1996; Rambabu et al., 2005), so far these methods are still not satisfying. Other viral vectors, e.g. herpes simplex virus type I (HSV-1), have not been tested for transgene expression in zebrafish neurons and the electroporation has not been optimized for their applications in the adult zebrafish brain.

## 1.3 Zebrafish olfactory system and odor information processing

Odorants are detected by zebrafish in an aqueous environment. Unlike rodents, zebrafish do not sniff but may actively control odor delivery into their nose by swimming through the environment. However, in general, odor processing in the zebrafish olfactory nervous system is similar to that of other vertebrates (Friedrich, 2013b). Briefly, odorants are first detected by periphery epithelium olfactory sensory neurons (OSNs) in the nose and encoded as neuronal activities. These activity patterns are then processed by the OB and the higher olfactory forebrain including Dp (**Figure 3A**).

### Olfactory bulb basic anatomy and function

In the first processing center OB, OSNs terminate in an array of glomeruli, each of which receives convergent input from OSNs expressing the same odorant receptor (Axel, 1995; Buck, 2000; Shi and Zhang, 2009). There are up to 300 odorant receptor genes in the zebrafish genome (Shi and Zhang, 2009) and at least 140 stereotyped glomeruli, as well as a large number of loosely defined, small axonal termination fields in the zebrafish OB (Baier and Korsching, 1994; Braubach et al.). Neuronal circuits in the OB consist of principal neurons, the mitral cells (MCs), and a large number of interneurons that perform feedforward and feedback inhibition (**Figure 3A**). It is estimated that in total the adult OB contains ~25,000 – 30,000 neurons, including ~1,500 MCs (Wiechert et al., 2010). MC axons are the principle outputs of OB and they project in parallel to multiple pallial and subpallial target regions in the

telencephalon, including higher olfactory forebrain Vv and Dp (Miyasaka et al., 2009; Yaksi et al., 2009; Kermen et al., 2013; Miyasaka et al., 2014) (**Figure 3B**).

It has been shown that in OB, the neuronal activities containing odor information of the environment from OSNs are decorrelated and transformed into discrete MC spatiotemporal activity patterns (Friedrich and Laurent, 2001; Niessing and Friedrich, 2010; Yaksi et al., 2007) that are further presented to higher brain areas Vv and Dp (Blumhagen et al., 2011; Yaksi et al., 2009).

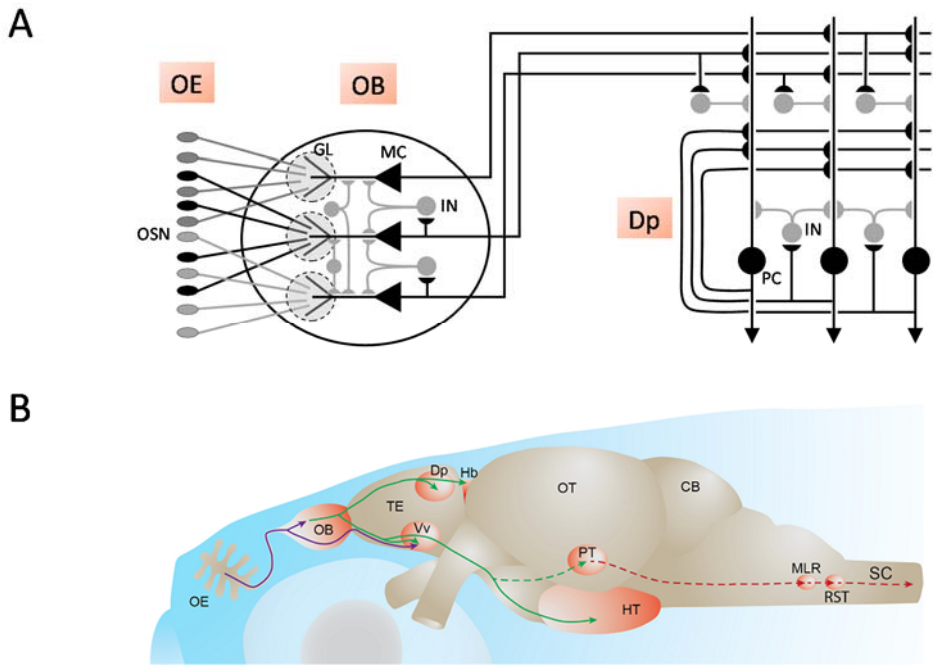


**FIGURE 3 | Zebrafish olfactory system. (A)** Circuit scheme for zebrafish olfactory system. In general, major circuits in the zebrafish olfactory system are similar to those in the mammalian olfactory system. OE: olfactory epithelium, OB: olfactory bulb, Dp: posterior zone of dorsal telencephalon, OSN: olfactory sensory neurons, GL: glomerulus, MC: mitral cell, IN: interneuron, PC: principal cell. **(B)** Primary projections from the olfactory sensory neurons to the olfactory bulb or telencephalon are depicted in purple. Secondary olfactory projections from the olfactory bulb to the telencephalon and diencephalon are depicted in green. A putative olfacto-motor pathway connecting the posterior tubercle to executive motor centers in the mesencephalon, described in lampreys, is depicted in red. Solid lines represent connections described in zebrafish. Dotted lines represent connections described in other fish species. TE: telencephalon, Hb: habenula, Vv: ventral nucleus of the ventral telencephalon, OT: optic tectum, PT: posterior tubercle, HT: hypothalamus, CB: cerebellum, MLR: mesencephalic locomotor region; RST: reticulo-spinal tract, SC: spinal cord. (Adapted from Kermen et al. 2013)

### Basic anatomy and function of Dp

The second processing center Dp, is the main target of OB and directly homologous to the mammalian piriform cortex (Mueller et al., 2011; Wullimann and Mueller, 2004). The structures and functions of Dp have, however, not been thoroughly

studied. The mammalian piriform cortex is a paleocortical area that receives divergent, nontopographic input from the OB and has widespread intracortical associative connections among pyramidal neurons (Davison and Ehlers, 2011; Franks et al., 2011; Johnson et al., 2000; Miyamichi et al., 2011). Teleost Dp is relocated by morphogenetic movements during ontogeny and does not possess the same gross histological structure as mammals (Mueller et al., 2011; Wullimann and Mueller, 2004). Nevertheless, immunohistological, electrophysiological, and live imaging experiments suggest that Dp shares functional similarities with the piriform cortex (Friedrich, 2013; Wilson and Sullivan, 2011; Bekkers and Suzuki) (**Figure 3A**). For example, Dp receives mono- and polysynaptic convergence of diverse channels from the OB (Yaksi et al., 2009); there are divergent projections from the OB to Dp without pronounced topography (Miyasaka et al., 2009); Dp receives a lot cholinergic fibers from higher brain region (Clemente et al., 2004); and there are scattered but not extremely sparse activity patterns and pronounced mixture suppression in Dp (Blumhagen et al., 2011; Schärer et al., 2012; Yaksi et al., 2009). However, the precise synaptic architecture of Dp has not been analyzed. In particular, it remains unclear whether connectivity among Dp neurons is very sparse, as found in piriform cortex. Moreover, the overall connection probability of inhibitory neurons has not been quantified, both in Dp and in piriform cortex. Measurements of these connection probabilities are of key importance to analyze the potential associative role of Dp neuronal circuits.

**Autoassociative network hypothesis**

Based on the structural and functional properties of piriform cortex it has been hypothesized that this brain area functions as an autoassociative network for synthetic representations of odor objects (Haberly, 2001; Wilson and Sullivan, 2011). The autoassociative network hypothesis is arising from a serial of theoretical and modeling studies (Marr, 1971; Kohonen, 1989; Kanerva, 1988; Hasselmo et al., 1990), as well as experimental findings (Barnes et al., 2008; Chapuis and Wilson, 2011; Choi et al., 2011; Wilson, 2003). It is a far-reaching notion for studying archicortical function. By homology, it is assumed that Dp subserves similar functions, which allows some features of this hypothesis to be addressed experimentally: (a) odorant-induced spatiotemporal activity patterns of MCs representing specific environmental information, are delineated in Dp as an “object” without topographic patterns; (b) the odor object is learned and stored in neuronal ensembles connected together but distributed across the whole Dp; (c) the connectivity across the whole network may be sparse; (d) recurrent synaptic connections in this network should be able to undergo Hebbian synaptic plasticity; (e) after storage, the circuit should perform separation and completion of learned patterns; (f) the circuit functions are regulated by cholinergic modulation; (g) principle neurons of this network also connect to and receive connections from other higher brain regions (Haberly, 2001).

One of the most challenging steps to address these issues is to obtain detailed information on structural and functional properties of neuronal connections in Dp. In particular, the probability and potential plasticity of neuronal connections, as well as the possible role of cholinergic modulation in Dp are still unkown.

## 1.4 Specific aims of this thesis project

In this thesis project, I sought to address the following questions with experiments: (1) the possible application of HSV-1 viral vectors for fast gene expression in zebrafish neurons; (2) optimization of an in vivo electroporation protocol for adult zebrafish brain fast gene expression; (3) quantitative measurements of excitatory and inhibitory neuronal connection probabilities in Dp; (4) the potential plasticity of synaptic connections in Dp; and (5) the possible cholinergic modulation of functional connections in Dp.

In results part one (*Chapter 2*), I show that both HSV-1 vectors and electroporation can be efficiently used for fast gene expression in the zebrafish brain and these new methods largely increase the flexibility for applying many advanced genetic tools in zebrafish. In results part two (*Chapter 3*), I used a combination of electroporation, optogenetics, electrophysiology, and pharmacology to probe the connectivity and plasticity of neuronal connections in Dp. I found that both intrinsic excitatory and inhibitory connectivity in Dp are sparse and there is activity-dependent synaptic plasticity including spike timing-dependent long-term potentiation in functional synapses of Dp. Moreover, I found that cholinergic innvervation could reduce inhibitory synaptic transmission in Dp. My results characterized key features of neuronal circuits in Dp and provide quantitative insights into the synaptic organization of a brain area in zebrafish that is likely to have associative memory. These findings will guide future experiments to examine the circuit mechanisms underlying associative learning.

## 1.5 References

Apfelbach, R., Blanchard, C.D., Blanchard, R.J., Hayes, R.A., and McGregor, I.S. (2005). The effects of predator odors in mammalian prey species: A review of field and laboratory studies. Neurosci. Biobehav. Rev. *29*, 1123–1144.

Axel, R. (1995). The molecular logic of smell. Sci. Am. *273*, 154–159.

Baier, H., and Korsching, S. (1994). Olfactory glomeruli in the zebrafish form an invariant pattern and are identifiable across animals. J. Neurosci. Off. J. Soc. Neurosci. *14*, 219–230.

Barnabé-Heider, F., Meletis, K., Eriksson, M., Bergmann, O., Sabelström, H., Harvey, M.A., Mikkers, H., and Frisén, J. (2008). Genetic manipulation of adult mouse neurogenic niches by in vivo electroporation. Nat. Methods *5*, 189–196.

Barnes, D.C., Hofacer, R.D., Zaman, A.R., Rennaker, R.L., and Wilson, D.A. (2008). Olfactory perceptual stability and discrimination. Nat. Neurosci. *11*, 1378–1380.

Bekkers, J.M., and Suzuki, N. Neurons and circuits for odor processing in the piriform cortex. Trends Neurosci.

Blumhagen, F., Zhu, P., Shum, J., Schärer, Y.-P.Z., Yaksi, E., Deisseroth, K., and Friedrich, R.W. (2011). Neuronal filtering of multiplexed odour representations. Nature *479*, 493–498.

Braubach, O.R., Fine, A., and Croll, R.P. Distribution and functional organization of glomeruli in the olfactory bulbs of zebrafish (Danio rerio). J. Comp. Neurol.

Brennan, P.A., and Keverne, E.B. (1997). Neural mechanisms of mammalian olfactory learning. Prog. Neurobiol. *51*, 457–481.

Briggman, K.L., Helmstaedter, M., and Denk, W. (2011). Wiring specificity in the direction-selectivity circuit of the retina. Nature *471*, 183–188.

Buck, L.B. (2000). The molecular architecture of odor and pheromone sensing in mammals. Cell *100*, 611–618.

Chapuis, J., and Wilson, D.A. (2011). Bidirectional plasticity of cortical pattern recognition and behavioral sensory acuity. Nat. Neurosci. *15*, 155–161.

Chen, T.-W., Wardill, T.J., Sun, Y., Pulver, S.R., Renninger, S.L., Baohan, A., Schreiter, E.R., Kerr, R.A., Orger, M.B., Jayaraman, V., et al. (2013). Ultrasensitive fluorescent proteins for imaging neuronal activity. Nature *499*, 295–300.

Choi, G.B., Stettler, D.D., Kallman, B.R., Bhaskar, S.T., Fleischmann, A., and Axel, R. (2011). Driving Opposing Behaviors with Ensembles of Piriform Neurons. Cell *146*, 1004–1015.

Chudakov, D.M., Matz, M.V., Lukyanov, S., and Lukyanov, K.A. (2010). Fluorescent Proteins and Their Applications in Imaging Living Cells and Tissues. Physiol. Rev. *90*, 1103–1163.

Clemente, D., Porteros, Á., Weruaga, E., Alonso, J.R., Arenzana, F.J., Aijón, J., and Arévalo, R. (2004). Cholinergic elements in the zebrafish central nervous system: Histochemical and immunohistochemical analysis. J. Comp. Neurol. *474*, 75–107.

Collins, R.T., Linker, C., and Lewis, J. (2010). MAZe: a tool for mosaic analysis of gene function in zebrafish. Nat. Methods *7*, 219–223.

Davison, I.G., and Ehlers, M.D. (2011). Neural Circuit Mechanisms for Pattern Detection and Feature Combination in Olfactory Cortex. Neuron *70*, 82–94.

Engeszer, R.E., Patterson, L.B., Rao, A.A., and Parichy, D.M. (2007). Zebrafish in The Wild: A Review of Natural History And New Notes from The Field. Zebrafish *4*, 21–40.

Franks, K.M., Russo, M.J., Sosulski, D.L., Mulligan, A.A., Siegelbaum, S.A., and Axel, R. (2011). Recurrent Circuitry Dynamically Shapes the Activation of Piriform Cortex. Neuron *72*, 49–56.

Friedrich, R.W. (2013). Neuronal Computations in the Olfactory System of Zebrafish. Annu. Rev. Neurosci. *36*, 383–402.

Friedrich, R.W., and Laurent, G. (2001). Dynamic optimization of odor representations by slow temporal patterning of mitral cell activity. Science *291*, 889–894.

Friedrich, R.W., Jacobson, G.A., and Zhu, P. (2010). Circuit neuroscience in zebrafish. Curr. Biol. CB *20*, R371–381.

Friedrich, R.W., Genoud, C., and Wanner, A.A. (2013). Analyzing the structure and function of neuronal circuits in zebrafish. Front. Neural Circuits *7*, 71.

Haberly, L.B. (2001). Parallel-distributed Processing in Olfactory Cortex: New Insights from Morphological and Physiological Analysis of Neuronal Circuitry. Chem. Senses *26*, 551–576.

Hasselmo, M.E., Wilson, M.A., Anderson, B.P., and Bower, J.M. (1990). Associative memory function in piriform (olfactory) cortex: computational modeling and neuropharmacology. Cold Spring Harb. Symp. Quant. Biol. *55*, 599–610.

Johnson, D.M.G., Illig, K.R., Behan, M., and Haberly, L.B. (2000). New Features of Connectivity in Piriform Cortex Visualized by Intracellular Injection of Pyramidal Cells Suggest that "Primary" Olfactory Cortex Functions Like "Association" Cortex in Other Sensory Systems. J. Neurosci. *20*, 6974–6982.

Kanerva, P. (1988). Sparse Distributed Memory (Cambridge, Mass: The MIT Press).

Kendrick, K.M., Lévy, F., and Keverne, E.B. (1992). Changes in the sensory processing of olfactory signals induced by birth in sheep. Science *256*, 833–836.

Kermen, F., Franco, L.M., Wyatt, C., and Yaksi, E. (2013). Neural circuits mediating olfactory-driven behavior in fish. Front. Neural Circuits *7*, 62.

Knöpfel, T., Lin, M.Z., Levskaya, A., Tian, L., Lin, J.Y., and Boyden, E.S. (2010). Toward the Second Generation of Optogenetic Tools. J. Neurosci. *30*, 14998 –15004.

Kohonen, T. (1989). Self-Organization and Associative Memory (Berlin, Heidelberg: Springer Berlin Heidelberg).

Liu, X., Ramirez, S., Pang, P.T., Puryear, C.B., Govindarajan, A., Deisseroth, K., and Tonegawa, S. (2012). Optogenetic stimulation of a hippocampal engram activates fear memory recall. Nature.

Luo, L., Callaway, E.M., and Svoboda, K. (2008). Genetic dissection of neural circuits. Neuron *57*, 634–660.

Marr, D. (1971). Simple memory: a theory for archicortex. Philos. Trans. R. Soc. Lond. B. Biol. Sci. *262*, 23–81.

Mennella, J.A., and Beauchamp, G.K. (2002). Flavor experiences during formula feeding are related to preferences during childhood. Early Hum. Dev. *68*, 71–82.

Miyamichi, K., Amat, F., Moussavi, F., Wang, C., Wickersham, I., Wall, N.R., Taniguchi, H., Tasic, B., Huang, Z.J., He, Z., et al. (2011). Cortical representations of olfactory input by trans-synaptic tracing. Nature *472*, 191–196.

Miyasaka, N., Morimoto, K., Tsubokawa, T., Higashijima, S., Okamoto, H., and Yoshihara, Y. (2009). From the Olfactory Bulb to Higher Brain Centers: Genetic Visualization of Secondary Olfactory Pathways in Zebrafish. J. Neurosci. *29*, 4756 –4767.

Miyasaka, N., Arganda-Carreras, I., Wakisaka, N., Masuda, M., Sümbül, U., Seung, H.S., and Yoshihara, Y. (2014). Olfactory projectome in the zebrafish forebrain revealed by genetic single-neuron labelling. Nat. Commun. *5*.

Mueller, T., Dong, Z., Berberoglu, M.A., and Guo, S. (2011). The dorsal pallium in zebrafish, Danio rerio (Cyprinidae, Teleostei). Brain Res. *1381*, 95–105.

Müller, K., and Weber, W. (2013). Optogenetic tools for mammalian systems. Mol. Biosyst.

Niessing, J., and Friedrich, R.W. (2010). Olfactory pattern classification by discrete neuronal network states. Nature *465*, 47–52.

Nishi, T., Yoshizato, K., Yamashiro, S., Takeshima, H., Sato, K., Hamada, K., Kitamura, I., Yoshimura, T., Saya, H., Kuratsu, J., et al. (1996). High-Efficiency in Vivo Gene Transfer Using Intraarterial Plasmid DNA Injection following in Vivo Electroporation. Cancer Res. *56*, 1050–1055.

Otto, T., Cousens, G., and Herzog, C. (2000). Behavioral and neuropsychological foundations of olfactory fear conditioning. Behav. Brain Res. *110*, 119–128.

Pérez Koldenkova, V., and Nagai, T. (2013). Genetically encoded Ca2 + indicators: Properties and evaluation. Biochim. Biophys. Acta BBA - Mol. Cell Res. *1833*, 1787–1797.

Rambabu, K.M., Rao, S.H.N., and Rao, N.M. (2005). Efficient expression of transgenes in adult zebrafish by electroporation. BMC Biotechnol. *5*, 29.

Rothenaigner, I., Krecsmarik, M., Hayes, J.A., Bahn, B., Lepier, A., Fortin, G., Götz, M., Jagasia, R., and Bally-Cuif, L. (2011). Clonal analysis by distinct viral vectors identifies bona fide neural stem cells in the adult zebrafish telencephalon and characterizes their division properties and fate. Development *138*, 1459–1469.

Schärer, Y.-P.Z., Shum, J., Moressis, A., and Friedrich, R.W. (2012). Dopaminergic modulation of synaptic transmission and neuronal activity patterns in the zebrafish homolog of olfactory cortex. Front. Neural Circuits *6*, 76.

Shi, P., and Zhang, J. (2009). Extraordinary diversity of chemosensory receptor gene repertoires among vertebrates. Results Probl. Cell Differ. *47*, 1–23.

Spence, R., Gerlach, G., Lawrence, C., and Smith, C. (2008). The behaviour and ecology of the zebrafish, Danio rerio. Biol. Rev. Camb. Philos. Soc. *83*, 13–34.

Wagle, M., and Jesuthasan, S. (2003). Baculovirus-mediated gene expression in zebrafish. Mar. Biotechnol. N. Y. N *5*, 58–63.

Weber, T., and Köster, R. (2013). Genetic tools for multicolor imaging in zebrafish larvae. Methods *62*, 279–291.

Wiechert, M.T., Judkewitz, B., Riecke, H., and Friedrich, R.W. (2010). Mechanisms of pattern decorrelation by recurrent neuronal circuits. Nat. Neurosci. *13*, 1003–1010.

Wilson, D.A. (2003). Rapid, Experience-Induced Enhancement in Odorant Discrimination by Anterior Piriform Cortex Neurons. J. Neurophysiol. *90*, 65–72.

Wilson, D.A., and Sullivan, R.M. (2011). Cortical Processing of Odor Objects. Neuron *72*, 506–519.

Wullimann, M.F., and Mueller, T. (2004). Teleostean and mammalian forebrains contrasted: Evidence from genes to behavior. J. Comp. Neurol. *475*, 143–162.

Yaksi, E., Judkewitz, B., and Friedrich, R.W. (2007). Topological reorganization of odor representations in the olfactory bulb. PLoS Biol. *5*, e178.

Yaksi, E., von Saint Paul, F., Niessing, J., Bundschuh, S.T., and Friedrich, R.W. (2009). Transformation of odor representations in target areas of the olfactory bulb. Nat. Neurosci. *12*, 474–482.

Yizhar, O., Fenno, L.E., Davidson, T.J., Mogri, M., and Deisseroth, K. (2011). Optogenetics in Neural Systems. Neuron *71*, 9–34.

Zhu, P., Narita, Y., Bundschuh, S.T., Fajardo, O., Schärer, Y.-P.Z., Chattopadhyaya, B., Bouldoires, E.A., Stepien, A.E., Deisseroth, K., Arber, S., et al. (2009). Optogenetic dissection of neuronal circuits in zebrafish using viral gene transfer and the Tet system. Front. Neural Circuits *3*, 21.

# *Chapter 2: Results Part I*

## Fast gene transfer into the adult zebrafish brain by herpes simplex virus 1 (HSV-1) and electroporation: methods and optogenetic applications.

Ming Zou*, Paul De Koninck, Rachael L. Neve, Rainer W. Friedrich

*Front. Neural Circuits.* 2014 May 06; 8:41.

*Correspondence

**Contributions:**

MZ performed all experiments and data analysis, PDK and RLN provided reagents and commented on experiments, MZ and RWF conceived the study and wrote the manuscript.

frontiers in
NEURAL CIRCUITS

METHODS ARTICLE
published: 06 May 2014
doi: 10.3389/fncir.2014.00041

# Fast gene transfer into the adult zebrafish brain by herpes simplex virus 1 (HSV-1) and electroporation: methods and optogenetic applications

***Ming Zou*[1,2]*, *Paul De Koninck*[1,3,4], *Rachael L. Neve*[5] and *Rainer W. Friedrich*[1,2]**

[1] *Friedrich Miescher Institute for Biomedical Research, Basel, Switzerland*
[2] *University of Basel, Basel, Switzerland*
[3] *Institut Universitaire en Santé Mentale de Québec, Québec, QC, Canada*
[4] *Département de Biochimie, Microbiologie et Bio-informatique, Université Laval, Québec, QC, Canada*
[5] *McGovern Institute for Brain Research, Massachusetts Institute of Technology, Cambridge, MA, USA*

***Edited by:***
*Florian Engert, Harvard University, USA*

***Reviewed by:***
*Isaac Henry Bianco, Harvard University, USA*
*Yuchin Albert Pan, Georgia Regents University, USA*

****Correspondence:***
*Ming Zou, Friedrich Miescher Institute for Biomedical Research, Maulbeerstrasse 66, CH-4058 Basel, Switzerland*
*e-mail: ming.zou@fmi.ch*

The zebrafish has various advantages as a model organism to analyze the structure and function of neural circuits but efficient viruses or other tools for fast gene transfer are lacking. We show that transgenes can be introduced directly into the adult zebrafish brain by herpes simplex type I viruses (HSV-1) or electroporation. We developed a new procedure to target electroporation to defined brain areas and identified promoters that produced strong long-term expression. The fast workflow of electroporation was exploited to express multiple channelrhodopsin-2 variants and genetically encoded calcium indicators in telencephalic neurons for measurements of neuronal activity and synaptic connectivity. The results demonstrate that HSV-1 and targeted electroporation are efficient tools for gene delivery into the zebrafish brain, similar to adeno-associated viruses and lentiviruses in other species. These methods fill an important gap in the spectrum of molecular tools for zebrafish and are likely to have a wide range of applications.

**Keywords: zebrafish, adult brain, gene transfer, herpes simplex virus type I, electroporation, optogenetics, genetically encoded calcium indicator**

## INTRODUCTION

The zebrafish is an attractive vertebrate model to analyze the structure and function of neural circuits because it is small, transparent at early developmental stages, genetically modifiable, and amenable to electrophysiological and optical measurements of neuronal activity (Friedrich et al., 2010, 2013; Leung et al., 2013). However, zebrafish do not offer efficient methods for fast neuronal gene transfer *in vivo* at post-embryonic stages. In rodents and other vertebrates, gene transfer in the brain is often accomplished by the injection of viral vectors, particularly adeno-associated viruses (AAVs) or lentiviruses (Luo et al., 2008). These vectors allow for the rapid expression of transgenes in spatially defined brain areas and can be targeted to defined subsets of cells by specific promoters and intersectional genetic approaches. As a consequence, viral gene transfer has become an important tool for a wide range of applications including optical measurements and manipulations of neuronal activity using genetically encoded calcium indicators (GECIs) and optogenetic probes, respectively (Knöpfel et al., 2010; Yizhar et al., 2011; Pérez Koldenkova and Nagai, 2013). In zebrafish, however, commonly used AAVs or lentiviruses failed to produce detectable expression of transgenes in the brain (Zhu et al., 2009). Fast, flexible and cost-effective methods are therefore desired to express transgenes in zebrafish without the need for time-consuming production of stable transgenic lines. Here we explored other viral vectors and non-viral methods to achieve fast, robust and long-term expression of transgenes in the zebrafish brain.

Viral gene transfer in zebrafish has been achieved using baculoviruses, Rabies virus, and Sindbis virus (Wagle and Jesuthasan, 2003; Wagle et al., 2004; Zhu et al., 2009). However, these vectors have practical disadvantages including toxicity (Sindbis), complex procedures for virus production and modification (Rabies, baculoviruses), and the difficulty to produce high titers (Rabies). One possibility to circumvent these problems is to use pseudotyped letiviruses or murine leukemia viruses (Rothenaigner et al., 2011). Another class of viral vectors with favorable properties are modified herpes simplex viruses 1 (HSV-1) (Luo et al., 2008). Although HSV-1 can infect zebrafish (Burgos et al., 2008), HSV-1-derived vectors have, to our knowledge, not yet been explored as tools to introduce transgenes into zebrafish neurons.

An alternative approach for fast gene transfer is electroporation, which uses brief electrical pulses to transiently permeabilize the plasma membrane and transfer nucleic acids into cells (De Vry et al., 2010). This method does not require the production of specialized vectors, is cost-effective, and has additional advantages (Barnabé-Heider et al., 2008). Electroporation is a popular method to manipulate neurons during development ("*in utero* electroporation") (Tabata and Nakajima, 2001) and has been used in various species (Barnabé-Heider et al., 2008; De Vry et al., 2010) including zebrafish (Rambabu et al., 2005; Cerda et al., 2006; Hendricks and Jesuthasan, 2007; Bianco et al., 2008). However, despite promising reports (Nishi et al., 1996; Rambabu et al., 2005; Barnabé-Heider et al., 2008), electroporation is not

a common method to introduce transgenes directly into spatially restricted neuronal populations in the adult brain.

We found that HSV-1-derived vectors and electroporation can be used to transfer transgenes into spatially restricted populations of neurons in the adult zebrafish brain with high efficiency. Using these approaches to express different ChR2 variants and GECIs, we explored the potential of optogenetic approaches to analyze functional synaptic connectivity among sparsely connected neurons in the posterior zone of the dorsal telencephalon (Dp), the teleost homolog of olfactory cortex.

## MATERIALS AND METHODS

### ANIMALS AND HANDLING FOR SURGICAL PROCEDURES

Experiments were performed in wild-type zebrafish (Danio rerio) of both sexes that were raised at 25–28°C on a 14/10 h on/off light cycle. Adult fish were > 3 months old. All experimental protocols were approved by the Veterinary Department of the Canton Basel-Stadt (Switzerland).

For surgical procedures, fish were anesthetized with 0.01% tricaine methanesulfonate (MS-222, Sigma-Aldrich). Larvae were embedded in low-melting agarose using standard procedures. Adult fish were held dorsal side up by a fish holder made from wet sponges inside a flexible plastic tube. The body of the fish was held by the sponges while the head was free. The tube was integrated in a custom-made stereotactic chamber with lateral stabilizers that were used when high spatial precision and stability was required. The chamber was placed on a tilted stage under a stereomicroscope (Olympus SZX16 or Wild; **Figure 1A** left). A cannula was inserted into the mouth of the fish to continuously apply fresh fish water with MS-222 to the mouth and gills. The skin was kept wet by regular supply of fish water. After surgery, fish were returned to standard tanks.

In order to monitor expression of fluorescent proteins through the skull, fish were anesthetized with MS-222 and mounted as described above. Fish were then imaged from the dorsal side using an Olympus SZX16 fluorescence stereomicroscope equipped with a color CCD camera (Olympus) and returned to their home tanks afterwards.

### HSV-1 AND DNA CONSTRUCTS

HSV-1vectors were obtained from three different sources: (1) BioVex (USA; kindly provided by Dr. J. Letzkus), (2) SinoGenomax (China), (3) the Massachusetts Institute of Technology (MIT) viral core (USA). Note that sources (1) and (2) have recently discontinued the custom production of HSV-1. All HSV-1 viruses used in this study and their inserts, sources, titers, and production methods (Simonato et al., 1999) are summarized in **Table 1**.

Plasmids used for electroporation are summarized in **Table 2**. Self-made constructs were generated from the components described by standard procedures including PCR, restriction cloning, and the gateway system (Kwan et al., 2007). For *in vivo* electroporation, plasmids were dissolved in calcium-free Ringer's solution (NaCl 119 mM, KCl 2.9 mM, HEPES 5 mM; pH 7.2) or, in a few cases, in 0.9% NaCl. Plasmid concentrations were between 0.2 μg/μl and 4 μg/μl. In most experiments, a concentration of approximately 1 μg/μl was used. Co-electroportation

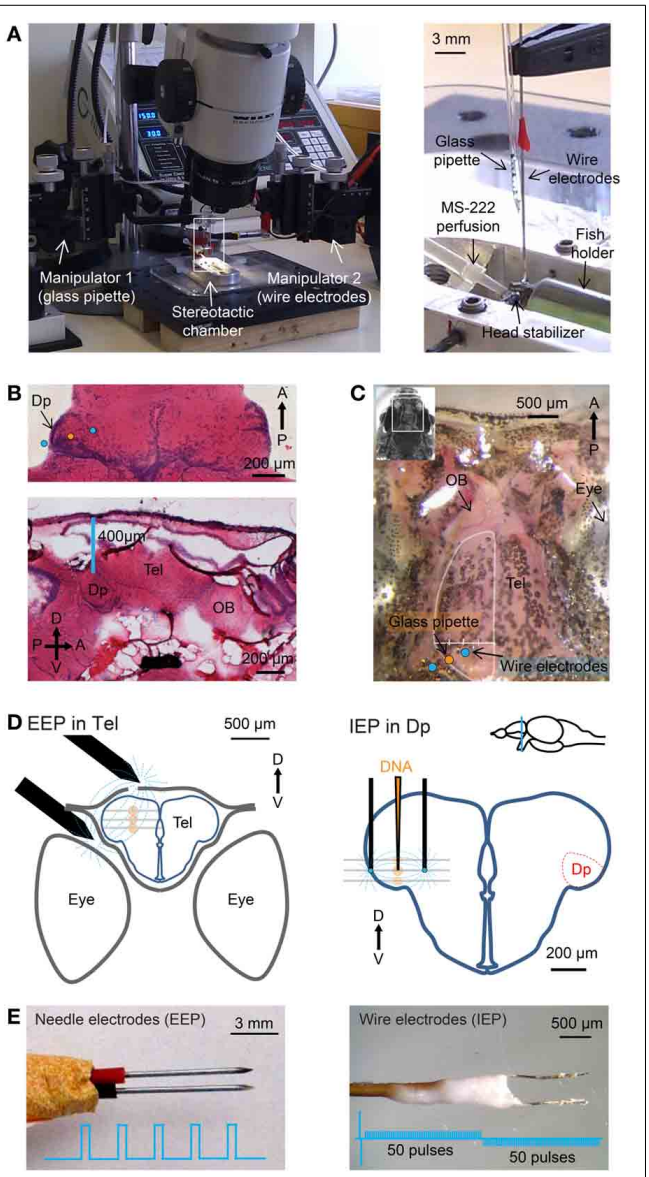


**FIGURE 1 | Stereotactic injection and electroporation. (A)** Left: apparatus for injection and electroporation. Right: Arrangement of wire electrodes and glass micropipette for targeted electroporation with internal electrodes (IEP) in the stereotactic chamber. Positions of electrodes and micropipette relative to Dp are shown schematically in **(D)**. **(B)** Top: hematoxylin and eosin (H&E) staining of a horizontal brain section through Dp. Somata are stained blue. Approximate positions of injection pipette and wire electrodes for targeted IEP in Dp are indicated. Bottom: sagittal section. D, dorsal; V, ventral; A, anterior; P, posterior. **(C)** Dorsal view of the skull over the telencephalon (Tel) and olfactory bulb (OB). The bone over the left olfactory bulb has been removed. Positions of the glass pipette and wire electrodes for targeted IEP in Dp are indicated. A virtual line between the lateral edge of the telencephalon and the midline (white) was used to determine the position of the injection pipette along the medial-lateral axis (Methods). **(D)** Approximate positions of electrodes (black) and injection sites (orange) for EEP in the dorsal telencephalon (left) and targeted IEP in Dp (right). Plasmid was injected and electroporated sequentially at three different depths (gray lines). **(E)** Needle electrodes for "external-electrode-electroporation" (EEP; left) and wire electrodes for "internal-electrode-electroporation" (IEP; right). Insets show electrical pulse protocols.

**Table 1 | HSV-1 viruses and expression in the dorsal telencephalon of adult zebrafish.**

| No. | Virus insert (promoter :: gene) | Virus source | Titer (units/ml) | Production method* | Number of fish | Expression strength |
|---|---|---|---|---|---|---|
| 1 | hEF1α::GFP | BioVex | n.a. | Amplicons | $n = 9$ | +++ |
| 2 | hEF1α::ChR2-2A-NpHR2.0YFP | BioVex | $1.4 \times 10^{10}$ | Amplicons | $n = 3$ | – |
| 3 | CMV::GFP | SinoGenomax | $2 \times 10^{8}$ | Replication-defective vector | $n = 4$ | + |
| 4 | hEF1α::GFP | SinoGenomax | $2 \times 10^{8}$ | Replication-defective vector | $n = 4$ | – |
| 5 | ST-IE4/5::DsRed2 | MIT viral core | $3 \times 10^{8}$ | Amplicons | $n = 8$ | ++ |
| 6 | ST-CMV::GFP | MIT viral core | $3 \times 10^{8}$ | Amplicons | $n = 4$ | + |
| 7 | LT-CMV::DsRed2 | MIT viral core | $3 \times 10^{8}$ | Amplicons | $n = 10$ | +++ |
| 8 | CaMKII::GFP | MIT viral core | $3 \times 10^{8}$ | Amplicons | $n = 4$ | – |
| 9 | rEF1α::GFP | MIT viral core | $3 \times 10^{8}$ | Amplicons | $n = 4$ | – |
| 10 | hEF1α::GFP | MIT viral core | $3 \times 10^{8}$ | Amplicons | $n = 4$ | + |
| 11 | LT-CMV::RG-GFP | MIT viral core | $4.5 \times 10^{8}$ | Amplicons | $n = 4$ | +++ |

*hEF1α, human elongation factor 1 alpha; CMV, cytomegalovirus immediate-early gene; ST- IE4/5, immediate early gene 4/5 promoter with short-term expression; ST-CMV, CMV promoter with short-term expression; LT-CMV, CMV promoter modified for long-term expression; CaMKII, $Ca^{2+}$/calmodulin-dependent protein kinase II; rEF1α, rat elongation factor 1 alpha; 2A, self-processing viral peptide cleavage site for co-expression of multiple polypeptides; RG-GFP, fusion of rabies virus glycoprotein and GFP; n.a., not available. For further information on viruses from MIT Viral Core see http://mcgovern.mit.edu/technology/viral-core-facility. *For further information on production methods see Simonato et al. (1999). Titers of HSV-1 from MIT Viral Core have been estimated based on previous measurements but not measured directly for each batch. Expression strength was scored on a scale ranging from no detectable expression (–) to strong expression (+++).*

of two plasmids was performed using equal concentrations of each plasmid.

### STEREOTACTIC PROCEDURES IN ADULT FISH AND MICROINJECTION OF VIRAL VECTORS

Virus suspensions were injected into the dorsal telencephalon (areas Dm, Dc, and/or Dl), the olfactory bulb, or Dp. All procedures were performed under a stereomicroscope. Experiments in the dorsal telencephalon did not require high spatial precision. In these cases, the fish was held by the sponge holder without lateral stabilizers. A craniotomy was made over the dorsal telencephalon near the midline using a dentist's drill. Micropipettes were inserted vertically through the craniotomy into the dorsal telencephalon using a manual 3-axis manipulator (WPI; **Figure 1A**). Care was taken to avoid major blood vessels. Three injections of 50 to a few 100 nl were made 250, 350, and 450 μm below the level of the bone.

Injections into the olfactory bulb or Dp were performed using the stereotactic chamber and lateral stabilizers. Dp was targeted by a stereotactic procedure that was developed based on the zebrafish brain atlas (Wullimann and Reichert, 1996). Hematoxylin and eosin (H&E) staining of coronal, horizontal and sagittal brain sections through Dp were performed to confirm the cell body distribution within Dp and the position of Dp relative to the skull (**Figure 1B**). A craniotomy was made on the suture between the bones over the telencephalon and tectum. In the lateral-medial direction the craniotomy was located approximately 25% along a virtual line between the lateral edge of the telencephalon and the midline (**Figure 1C**). A micropipette containing virus suspension was inserted through the craniotomy slightly anterior to the suture, avoiding blood vessels (**Figure 1C**, orange dot). Three injections were made approximately 400, 500, and 600 μm below the level of the bone (**Figure 1D**). The precise depths of injection points were adjusted slightly based on the size of each fish. In order to target injections to the olfactory bulb a craniotomy was made at the anterior edge of the telencephalic skull (**Figure 1C**) and virus was injected 200, 300, and 400 μm below the level of the bone.

Virus suspensions were injected using glass micropipettes with a long shaft that were prepared from borosilicate capillaries (1 mm diameter, Hilgenberg) using an electrode puller (P-2000, Sutter). The tip was broken to obtain a diameter of 10–20 μm. At each injection point, the capillary was pressurized using a syringe connected with flexible tubing and the ejected volume was measured by monitoring the movement of the meniscus inside the capillary.

### ELECTROPORATION

Stereotactic procedures for electroporation were equivalent to those used for viral injections. For electroporation in the dorsal telencephalon using external electrodes, 100–300 nl of plasmid suspension was injected at each of three injection points approximately 250, 350, and 450 μm below the level of the bone (**Figure 1D**, left). The glass pipette was then retracted and a pair of parallel sharp steel electrodes (**Figure 1E** left; 0.5 mm diameter), separated by approximately 1 mm, was positioned so that one electrode was placed on the craniotomy and the other was located between the eye and the skull. Electrodes were custom made from steel needles (BTX, USA) and not insulated. Electrical pulses (5 × 25 ms, 70 V, 1 Hz, square; **Table 3** and **Figure 1E**, left) were applied with a NEPA21 electroporator (NEPAGENE, Japan) or a Gene Pulser Xcell electroporator (Bio-Rad, USA). The delay between DNA injection and electrical stimulation was approximately 20 s. This procedure is relatively simple, reliable, and allows for the detection of fluorescent protein expression through the intact skull using a fluorescence stereomicroscope. The procedure was used to analyze the time course of protein expression *in vivo* and to test the efficiency of different promoters.

Targeted electroporation in Dp using internal electrodes was performed using lateral stabilizers in the stereotactic chamber.

**Table 2 | Plasmids used for electroporation.**

| No. | Plasmid (promoter :: gene) | Description/source/references |
|---|---|---|
| 1 | hEF1α::GFP | The plasmid was constructed by combining the human EF1α promoter (Kim et al., 1990) (Gift from C. Xu) with green fluorescent protein (GFP). |
| 2 | hEF1α::ChR2tc-GFP | The plasmid was constructed based on plasmid #1. ChR2tc is a ChR2 mutant with the T159C mutation, which increases the photocurrent (Berndt et al., 2011). ChR2tc cDNA was a gift from T. Oertner and fused to GFP. |
| 3 | hEF1α::ChR2tc-mEos2 | The plasmid was constructed based on plasmid #1 and ChR2tc-mEos2, a gift from T. Oertner. ChR2tc-mEos2 is a fusion of ChR2tc (described above) and the photoconvertible fluorescent protein mEos2 (McKinney et al., 2009), Addgene 20341. |
| 4 | xEF1α::GFP | The plasmid was constructed by combining the Xenopus EF1α promoter (Johnson and Krieg, 1994) (gift of K. Kawakami) with GFP. |
| 5 | zHsp70l::GFP | The plasmid was constructed by combining the zebrafish Hsp70l promoter (Halloran et al., 2000) from the Tol2-kit (Kwan et al., 2007) with GFP. |
| 6 | zHsp70l::GCaMP5 | The plasmid was constructed by combining the zebrafish zHsp70l (Halloran et al., 2000) from the Tol2-kit (Kwan et al., 2007) with GCaMP5, a green fluorescent calcium indicator (Akerboom et al., 2012). GCaMP5 cDNA was a gift from L. Looger and D. Kim. |
| 7 | CAG::Cre-GFP | CAG is a chimeric promoter (Miyazaki et al., 1989), Cre-GFP is a recombinase fused to GFP (Matsuda and Cepko, 2007). |
| 8 | αCaMKII::GFP(1) | Gift from A. Fine (Mayford et al., 1996). The plasmid contains a short version of the αCaMKII promoter (0.4 kb) and GFP. |
| 9 | αCaMKII::GFP(2) | Gift from A. Fine (Mayford et al., 1996). The plasmid contains a longer version of the αCaMKII promoter (1.3 kb) and GFP. |
| 10 | hSyn::ChR2wt-GFP-mbd | Gift from S. Wiegert and T. Oertner; the plasmid contains the human Synapsin-1 promoter (Kügler et al., 2003) and wild type ChR2 fused to GFP and a myosin binding domain (mbd) that can target ChR2 to the somato-dendritic compartments (Lewis et al., 2009). |
| 11 | zElavl3::GCaMP5 | Gift from A. Schier. The plasmid contains the zebrafish Elavl3 (HuC) promoter (Park et al., 2000) and the GECI GCaMP5 (Akerboom et al., 2012). |
| 12 | zElavl3::itTA | The plasmid contains the zElavl3 promoter and the Tet activator (itTA), a transcription activator that binds specifically to tet operator (tetO) (Zhu et al., 2009). |
| 13 | tetO7::ChR2wt-YFP | The plasmid contains seven repeats of the tet operator with a minimum CMV promoter (tetO7) and wild type ChR2 fused to yellow fluorescent protein (YFP) (Zhu et al., 2009). |
| 14 | CMV::mRuby | The plasmid contains the CMV promoter (Thomsen et al., 1984) and mRuby, a monomeric red fluorescent protein (Kredel et al., 2009). |
| 15 | CMV:: mGFP-αCaMKII | The alpha $Ca^{2+}$ /calmodulin-dependent protein kinase II (αCaMKII) gene was fused to monomeric GFP (Hudmon et al., 2005). |
| 16 | CMV::GCaMP6f | Obtained from Addgene 40755 (Chen et al., 2013). GCaMP6f is a green fluorescent calcium indicator with fast kinetics. |
| 17 | CMV::GCaMP6s | Obtained from Addgene 40753 (Chen et al., 2013). GCaMP6s is a green fluorescent calcium indicator with slow kinetics. |
| 18 | CMV::RGECO1.0 | The plasmid contains the CMV promoter and RGECO1.0, a red fluorescent GECI (Zhao et al., 2011). |
| 19 | CMV::RCaMP1.07 | The plasmid contains the CMV promoter and RCaMP1.07, a red-fluorescent GECI (Ohkura et al., 2012). |

*hEF1α, human elongation factor 1 alpha; xEF1α, Xenopus elongation factor 1 alpha; zHsp70l, zebrafish heat-shock protein 70l; CAG, chimeric promoter with sequences from cytomegalovirus immediate-early gene, chicken beta-actin gene, and rabbit beta-globin gene; αCaMKII, $Ca^{2+}$/calmodulin-dependent protein kinase II; hSyn, human synapsin-1 gene; zElavl3, zebrafish Elavl3 (HuC) gene; CMV, cytomegalovirus immediate-early gene; tetO7, minimum CMV promoter with seven repeats of tet operator. Other abbreviations are explained in the right column.*

DNA solution was loaded into a micropipette that was held vertically by a manual 3-axis manipulator as described above (**Figure 1A**). A pair of custom-made parallel thin Pt electrodes (25 μm diameter, approximately 400 μm distance, shank insulated, tip exposed, modified from FHC Inc. CE2C40; **Figure 1E**, right) was mounted on a second 3-axis manual manipulator. Electrodes were almost parallel to the micropipette (**Figure 1A** right) and positioned so that the injection pipette was between the electrodes above the craniotomy. The glass pipette and the pair of electrodes were then inserted together into the tissue. Three injections were made approximately 400, 500, and 600 μm below the level of the bone (**Figure 1D**). At each injection point, approximately 70 nl of DNA solution was ejected and the tissue impedance was measured immediately afterwards. Based on the measured impedance, a set of pre-programmed square electrical pulses was selected (**Table 3**) and applied 1–2 times immediately after DNA injection using the NEPA21 electroporator.

The two electroporators used in this study included a basic instrument (Gene Pulser Xcell, Bio-Rad, USA) and a more advanced instrument (NEPA21, NEPAGENE, Japan). Targeted local electroporation was performed exclusively using the NEPA21 electroporator because this instrument allowed for fine

**Table 3 | Pulse settings for electroporation.**

| No. | Tissue impedance | Poring pulse | | | | | Transferring pulse | | | | |
|---|---|---|---|---|---|---|---|---|---|---|---|
| | | Voltage (V) | Pulse duration (ms) | Interval (ms) | Number of pulse | Polarity switch | Voltage (V) | Pulse duration (ms) | Interval (ms) | Number of pulse | Polarity switch |
| **GENE PULSER XCELL ELECTROPORATOR, FOR EEP** | | | | | | | | | | | |
| 1 | n.a. | n.a. | n.a. | n.a. | n.a. | n.a. | 70 | 25 | 1 s | 5 | No |
| **NEPA21 ELECTROPORATOR, FOR EEP** | | | | | | | | | | | |
| 2 | n.a. | 100 | 0.1 | 999.9 | 2 × 1 | Yes | 20 | 5 | 95 | 2 × 25 | Yes |
| **NEPA21 ELECTROPORATOR, FOR IEP, PORING VOLTAGE CALCULATED FOR MAXIMUM CURRENT OF 6 mA** | | | | | | | | | | | |
| 3 | 6–9 kΩ | 36 | 0.1 | 999.9 | 2 × 1 | Yes | 7.2 | 1 | 99 | 2 × 50 | Yes |
| 4 | 9–12 kΩ | 54 | 0.1 | 999.9 | 2 × 1 | Yes | 10.8 | 1 | 99 | 2 × 50 | Yes |
| 5 | 12–16 kΩ | 72 | 0.1 | 999.9 | 2 × 1 | Yes | 14.4 | 1 | 99 | 2 × 50 | Yes |
| 6 | 16–20 kΩ | 96 | 0.1 | 999.9 | 2 × 1 | Yes | 19.2 | 1 | 99 | 2 × 50 | Yes |
| 7 | 20–25 kΩ | 120 | 0.1 | 999.9 | 2 × 1 | Yes | 24 | 1 | 99 | 2 × 50 | Yes |
| 8 | 25–30 kΩ | 150 | 0.1 | 999.9 | 2 × 1 | Yes | 30 | 1 | 99 | 2 × 50 | Yes |
| 9 | 30–36 kΩ | 180 | 0.1 | 999.9 | 2 × 1 | Yes | 36 | 1 | 99 | 2 × 50 | Yes |
| 10 | 36–42 kΩ | 216 | 0.1 | 999.9 | 2 × 1 | Yes | 43.2 | 1 | 99 | 2 × 50 | Yes |
| 11 | 42–50 kΩ | 252 | 0.1 | 999.9 | 2 × 1 | Yes | 50.4 | 1 | 99 | 2 × 50 | Yes |
| 12 | >50 kΩ | 300 | 0.1 | 999.9 | 2 × 1 | Yes | 60 | 1 | 99 | 2 × 50 | Yes |

*n.a., not applicable. Settings #6 and #7 were used most frequently for IEP.*

tuning of the pulse protocol based on tissue impedance. Pulse trains consisted of a pair of high-amplitude poring pulses with opposite polarity followed by a train of lower-amplitude transfer pulses. The polarity of the transfer pulses was reversed after 50% of pulses were applied (**Figure 1E**, right). The amplitude of the pulses was adjusted based on tissue impedance, which was measured using the NEPA21 electroporator. Highest cell survival and expression levels were obtained when the voltage of the poring pulse was set to yield currents of 4–6 mA and the voltage of the transfer pulses was 20% of that of the poring pulse. The pulse duration was kept short (0.1–1 ms) in order to avoid accumulation of heat. For tissue with an impedance of 16–20 kΩ, for example, the pulse train consisted of a pair of square pulses of 0.1 ms and ±96 V for membrane poring followed by 50 square pulses of 1 ms, 19.2 V and 10 Hz for DNA transfer and another 50 square pulses with the same parameters but opposite polarity (**Table 3**). In order to minimize the time delay between impedance measurements and pulse application, predefined pulse trains were stored in the memory of the electroporator (**Table 3**).

### *EX-VIVO* PREPARATION, MULTIPHOTON IMAGING, ELECTROPHYSIOLOGY, ODOR APPLICATION, AND OPTICAL STIMULATION

Multiphoton imaging and electrophysiological experiments were performed in an *ex-vivo* preparation of the adult zebrafish brain as described (Zhu et al., 2012). Briefly, fish were cold-anesthetized, decapitated, and the dorsal or ventral forebrain was exposed. The preparation was then transferred to a custom-made imaging chamber, continuously perfused with teleost artificial cerebrospinal fluid (ACSF) (Mathieson and Maler, 1988), and warmed up to room temperature.

High-resolution imaging of fluorescent protein expression and calcium signals were performed using a custom-made multiphoton microscope that was constructed around the body of an Olympus BX-51 microscope. The microscope was equipped with a 20× water immersion objective (NA 0.95, Olympus), a Ti:Sapphire laser (Spectra Physics, USA), a custom-built unit containing galvanometric scanners (6215H, Cambridge Technology, USA) and custom-built external detection optics with photomultipliers (H7422P-40MOD, Hamamatsu). GFP/YFP were excited at 860 or 980 nm; red-fluorescent proteins were excited at 980 nm. Fluorescence emission was detected in two channels using green (535/50 nm) and red (640/75 nm) emission filters. A third channel was used to acquire the signal of a position-sensitive detector for transmitted infrared light. This channel produced a contrast-enhanced transmitted light image that was used to direct the recording pipette for patch clamp recordings. The microscope and related equipment were controlled by ScanImage and Ephus software (Pologruto et al., 2003; Suter et al., 2010). For calcium imaging, series of fluorescence images were collected at 128 ms/frame, in some cases 512 ms/frame or 64 ms/frame, for approximately 20 s. Laser intensity was adjusted to minimize photobleaching.

Whole-cell patch clamp recordings were performed using borosilicate pipettes (8–12 MΩ), a Multiclamp 700 B amplifier (Molecular Devices) and Ephus software (Suter et al., 2010). Neurons were targeted by a combination of multiphoton fluorescence and contrast-enhanced transmitted-light optics (transmitted light channel). Pipettes were filled with an intracellular solution containing 130 mM potassium gluconate, 10 mM sodium gluconate, 10 mM sodium phosphocreatine, 4 mM sodium chloride, 4 mM magnesium-ATP, 0.3 mM sodium-GTP, 10 mM HEPES (pH 7.2, 300 mOsm) and 10 μM Alexa Fluor 594 (Invitrogen). Signals were digitized at 10 kHz.

Electrical stimulation in the olfactory bulb was performed by placing a glass pipette (tip diameter, 30–50 μm) filled with

1 M NaCl at the posterior end of the olfactory bulb. A train of 10 pulses (0.5 ms pulse width, −35 V, 20 Hz) was delivered 10 times at an inter-trial interval of 12 s. In order to induce slow, epileptiform population activity, the $GABA_A$ receptor antagonist Gabazine (1 μM) was added to the ACSF.

Optical stimulation of ChR2 with blue light was performed with a strong LED (460 nm; Luxeon, USA) that was mounted in the epifluorescence lamphouse attached to the Olympus BX-51 microscope body. Optical stimuli consisted of trains of light pulses (10 ms duration; 10 pulses at 5 or 10 Hz; light power under objective approximately 250–300 $\mu W/mm^2$). At least 15 trials were acquired for each cell. In some electrophysiological recordings, optical stimulation caused a small stimulus artifact that was removed from the recorded traces by replacing voltage values with a constant value.

Odors were delivered through a constant stream of carrier medium directed at the ipsilateral naris using a computer controlled HPLC injection valve (Rheodyne, USA) as described (Tabor et al., 2004). Odor stimulation was repeated at least three times with an inter-trial interval of at least 2 min to avoid adaptation. Food extract was prepared from standard dry fish food (SDS, UK) as described (Tabor et al., 2004) and diluted 1:1000 before the experiment.

### DATA ANALYSIS

Electrophysiology or calcium imaging data were analyzed using custom routines written in Matlab or IGOR Pro. Synaptic currents evoked by optical stimulation were measured by whole-cell voltage clamp recordings and averaged over 150 pulses (15 trials with 10 pulses each). The synaptic latency was estimated as the time between the offset of the 10 ms light pulse and the first inflection of the current trace. The inflection point was usually sharply defined within a time window of < 2 ms and determined manually by inspection of each trace. The amplitudes of averaged EPSCs and IPSCs were measured as the peak currents within a 20 ms time window after the offset of the light pulse relative to pre-stimulus baseline.

Calcium signals (ΔF/F) were calculated as changes in fluorescence intensity (ΔF) relative to a baseline period of 2–4 s before response or stimulus onset (F). To quantify calcium signals of individual neurons, regions of interest were outlined manually on time-averaged ΔF/F maps. In order to quantify fluorescence changes of GECIs during epileptiform activity, 9 neurons from 3 fish were analyzed for each GECI. In each neuron, ΔF/F of calcium transients were measured at the soma and at a dendritic location that showed large ΔF/F values in time-averaged maps. Amplitudes of multiple large calcium transients were then averaged for each neuron, and mean calcium transients were then averaged over neurons for each GECI.

In order to assess the fluorescence intensity in the dorsal telencephalon through the intact skull, individual fish were anesthetized and viewed through a fluorescence stereomicroscope. Fluorescence intensity was scored manually relative to the mean fluorescence intensity observed 10 days after electroporation of plasmid #10. This plasmid contained the hSyn promoter and was chosen as a reference because it produced an intermediate fluorescence intensity.

## RESULTS

### *IN VIVO* GENE TRANSFER USING HSV-1

Replication-incompetent HSV-1 viruses have been used successfully as vectors to express transgenes in the brain of rodents and other vertebrates (Palella et al., 1989; Luo et al., 2008; Yonehara et al., 2011). Because many HSV-1 viruses infect neurons retrogradely via their axon terminals they can be used to target projection neurons by injections into their terminal areas (Ugolini et al., 1987; Yonehara et al., 2011). We tested the ability of 11 replication-incompetent HSV-1 viruses (**Table 1**) to express transgenes in neurons of the adult zebrafish brain. Using stereotactic procedures, HSV-1 viruses were injected through small craniotomies into the dorsal telencephalon, into Dp, or into the olfactory bulb (Methods). Each HSV-1 virus was injected into 3–10 fish. Expression was scored *in vivo* by imaging fluorescence through the intact skull at different time points after injection. In addition, high resolution images of neurons expressing fluorescent markers were obtained by multiphoton microscopy in an *ex-vivo* preparation of the brain (Zhu et al., 2012).

A subset of HSV-1 viruses (e.g., #1, #7, and #11; **Table 1**; **Figures 2A–C**) produced dense and robust expression of fluorescent marker proteins while injection of other HSV-1 viruses produced weak or no detectable fluorescence (e.g., #2, #4, #8, and #9; **Table 1**). These differences were consistently observed in multiple experiments, indicating that they were not caused by stochastic factors such as variable success of injections. Moreover, independent batches of one of the HSV-1 viruses (#7) produced consistent results, suggesting that variation in the efficiency of virus production is unlikely to account for the observed differences. Generally, HSV-1 viruses produced by replication-defective vectors resulted in less fluorescence than HSV-1 viruses produced by amplicons, suggesting that viral infection, transgene expression or cell survival depend on the method of virus production (Simonato et al., 1999). In addition, expression may depend on promoters, transgenes, titers, and other factors.

Most HSV-1 viruses produced fluorescence that could be observed through the intact skull. Fluorescence was first observed 2 days post-injection (dpi), reached a maximum around 9 dpi and declined slowly thereafter (**Figure 2A**), often lasting more than 4 weeks. Expression driven by a CMV promoter for short-term expression (#6) decayed rapidly after approximately 7 dpi while expression driven by a CMV promoter designed for long-term expression (#7) remained high even 28 dpi (not shown). High resolution imaging of infected neurons revealed fluorescence in many somata and neuronal processes (**Figures 2B,C**). No fragmented cells, fluorescent aggregates or other obvious signs of cell death were observed, and no obvious tissue damage was apparent. Injection of 100–200 nl of virus #1 caused transgene expression in approximately 150 ± 50 cells ($n = 4$ fish, mean ± SD) within a volume of approximately $200 \times 200 \times 100\,\mu m^3$ around the injection site.

Injections of HSV-1 virus into Dp labeled neurons in the outer layer of the olfactory bulb where mitral cells projecting to Dp are located (**Figure 2D**, $n = 3$ fish). Few labeled neurons were found in telencephalic areas between the olfactory bulb and Dp and no labeled neurons were found in deep layers of the olfactory bulb (**Figure 2D**), which contain large numbers of local granule

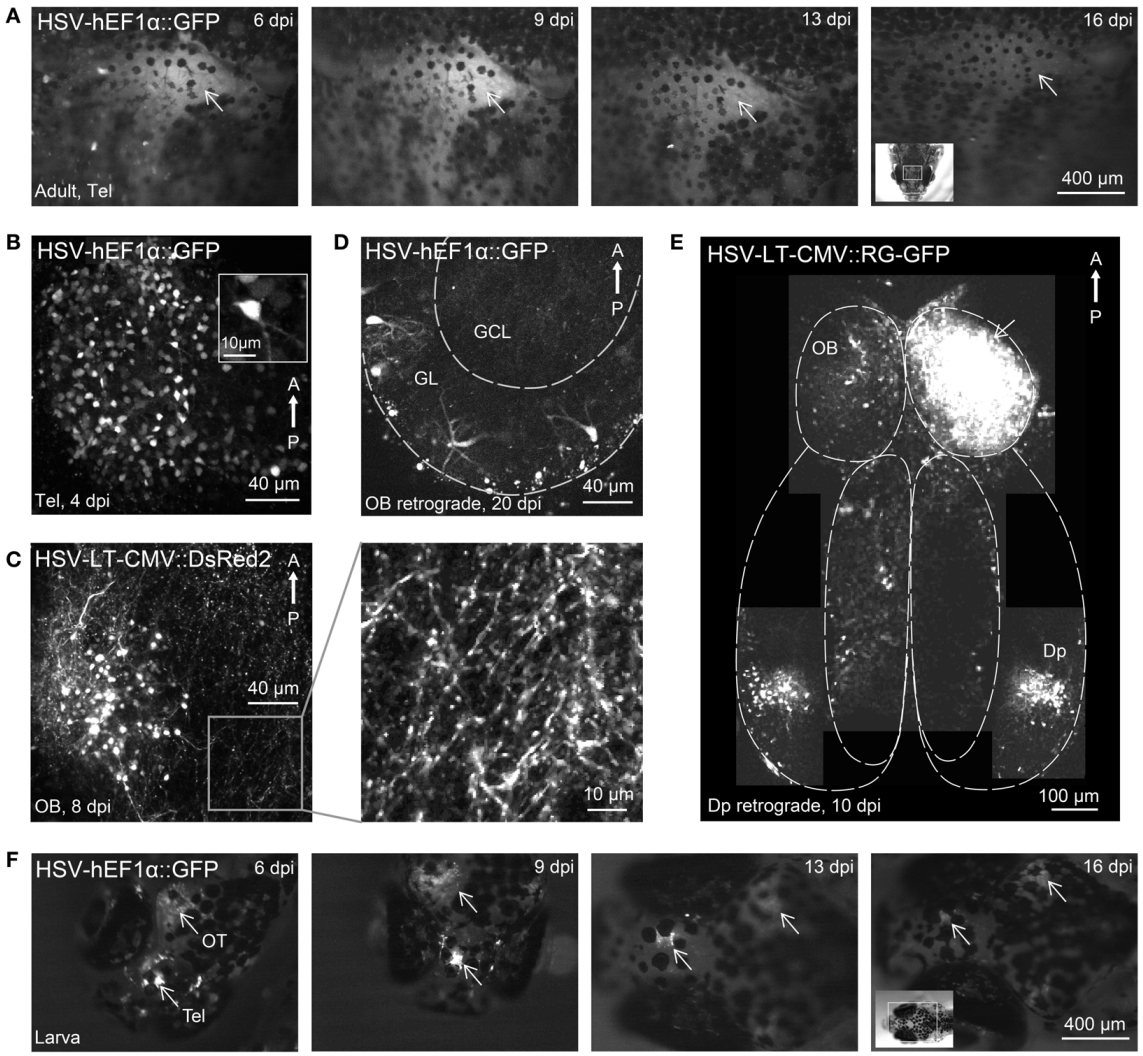


**FIGURE 2 | Gene expression in the zebrafish brain using HSV-1. (A)** Fluorescence images of the dorsal head of an adult zebrafish at different time points after injection of HSV-1 (#1). Images were taken with a fluorescence stereomicroscope; arrow indicates region of strong fluorescence. **(B)** Telencephalic neurons expressing GFP 4 days after injection of HSV-1 into the dorsal telencephalon (#1; *z*-projection of multiphoton stack). **(C)** Olfactory bulb neurons expressing DsRed2 8 days after injection of HSV-1 into the olfactory bulb (#7; *z*-projection of multiphoton stack). Boxed region is shown at higher magnification on the right. **(D)** Transgene expression in olfactory bulb neurons, presumably mitral cells, 20 days after injection of HSV-1 (#1) into Dp. GL, glomerular/mitral cell layer; GCL, granule cell layer. **(E)** Composite image (multiple z-projections of multiphoton stacks) showing transgene expression throughout the ventral forebrain after injection of HSV-1 (#11) into one olfactory bulb (arrow). Note strong bilateral expression in Dp but not in other telencephalic areas. **(F)** Fluorescence images of the dorsal head of a zebrafish larva at different time points after injection of HSV-1 (#1). Virus was injected at two sites, the telencephalon (Tel) and the optic tectum (OT). Arrows indicate strong fluorescence around the injection sites.

cells. Injections into the olfactory bulb labeled somata in Dp, which provides strong bilateral projections to the olfactory bulb (**Figure 2E**). Very few labeled cells were seen in telencephalic areas between the olfactory bulb and Dp. Hence, HSV-1 vectors can infect projection neurons retrogradely via their axons, consistent with observations in other species.

Injection of HSV-1 into the larval brain (virus #1; $n = 10$ fish) also produced robust fluorescence for $> 2$ weeks around the injection site (**Figure 2F**). These results show that modified HSV-1 viruses are efficient tools for gene transfer into the zebrafish brain.

## GENE TRANSFER BY ELECTROPORATION

Electroporation has been used in zebrafish to introduce DNA constructs into larval neurons, adult retinal neurons or adult muscle cells (Rambabu et al., 2005; Hendricks and Jesuthasan, 2007; Bianco et al., 2008; Kustermann et al., 2008). However, the procedures used in these studies cannot be used to express transgenes in the adult zebrafish brain without major modifications.

We first developed a simple procedure to electroporate plasmids into neurons of the dorsal telencephalon without high spatial precision. Plasmid DNA (hEF1α::GFP, plasmid #1, **Table 2**; 200–500 nl) was injected into the dorsal telencephalon through

a small craniotomy. After withdrawal of the injection pipette, a pair of electrodes was placed outside the skull, flanking the injection site, and train of voltage pulses was delivered (Methods; **Figure 1D**, left). Fish were then returned to their home tanks and inspected for fluorescence through the intact skull at successive time points. Fluorescence was observed after a few days even in pilot experiments before optimization of experimental parameters. Based on these initial observations we tested different electrodes, electrode positions, pulse settings, DNA concentrations and solvents to maximize the observable fluorescence signal. Strong expression was achieved with a pair of parallel, sharp stainless steel needles, separated by approximately 1 mm (**Figure 1E**, left; Methods), when one electrode was located near the craniotomy and the other was located near the edge of the ipsilateral eye (**Figure 1D**, left). The preferred pulse protocol consisted of five square pulses of 25 ms delivered at 1 Hz with an amplitude of 70 V (**Figure 1E**, left). DNA was usually dissolved in $Ca^{2+}$-free Ringer solution at a concentration of 1 μg/μl (Methods). We refer to this approach as "external-electrode-electroporation" (EEP).

Using EEP in the dorsal telencephalon and plasmid #1 (hEF1α::GFP), strong and widespread fluorescence was observed through the intact skull in 11/12 fish. Fluorescence was first detected 3 days post-electroporation (dpe), peaked around 8–12 dpe, and thereafter remained high for weeks (**Figures 3A,B**). Multiphoton imaging in the dorsal telencephalon showed strong GFP expression in hundreds of cells (estimated number: $650 \pm 250$ cells/fish, mean $\pm$ *SD*; $n = 4$ fish; **Figure 3B**). GFP-expressing neurons were distributed throughout a large volume, sometimes the entire dorsal side of the telencephalic hemisphere. Neurons had normal morphologies without obvious signs and no obvious signs of cell death or tissue damage were observed. Some neurons had long processes, consistent with previous anatomical descriptions of neurons in the dorsal telencephalon (Aoki et al., 2013), and some neurons had spiny dendrites (**Figure 3C**).

Co-electroporation of two plasmids harboring reporters of different colors frequently resulted in overlapping expression of the reporters in the same cells (plasmids #15 and #18; **Figure 3D**; $n = 3$ fish). Moreover, co-electroporation of a plasmid containing a Tet driver construct (plasmid #12) and a second plasmid containing a Tet responder construct (plasmid #13) resulted in transgene expression in a substantial number of cells (**Figure 3E**). Hence, electroporation can be used to co-express multiple transgenes from different plasmids, consistent with previous observations (Barnabé-Heider et al., 2008).

When plasmids were injected into Dp, the same electroporation protocol produced no detectable expression within Dp although some labeled neurons were found near the craniotomy in the dorsal telencephalon. EEP is therefore not equally effective throughout the brain, implying that gene transfer by EEP cannot easily be targeted and confined to small brain areas. Dp is located approximately 400–600 μm below the dorsal skull (**Figure 1B**, bottom) next to a prominent bone, suggesting that the efficiency of electroporation is non-uniform because the electrical field is distorted by inhomogeneities of the tissue, particularly around bones. In order to overcome these problems we fabricated pairs of electrodes from insulated Pt wires with a diameter of 25 μm. Wires were glued together in parallel with a spacing of approximately 400 μm and the insulation was removed only at the tips. Electrodes were then inserted into the brain together with a glass pipette containing the plasmid suspension. The wire electrodes and the pipette were targeted to Dp using a stereotactic procedure (Methods), plasmid suspension was injected between the two wire electrodes, and voltage pulses were applied across the electrodes. This injection and electroporation sequence was repeated at three different depths in Dp, spaced by approximately 100 μm (Methods; **Figure 1D**, right).

Targeted electroporation using internal electrodes resulted in expression of fluorescent markers in Dp. In most cases, the expression was completely restricted to a volume of approximately $200 \times 200 \times 200\,\mu m^3$ within Dp. The careful design of voltage pulse trains can reduce damage and substantially enhance the efficiency of electroporation (Šatkauskas et al., 2012). Generally, it is recommended to use pulse trains consisting of a pair of brief, high-amplitude poring pulses of opposite polarity to permeabilize the plasma membrane followed by a train of longer pulses with lower amplitude and changing polarity to transfer the DNA into the cell. Furthermore, it is useful to adjust the amplitude of voltage pulses to the tissue impedance in each experiment in order to generate a reproducible current (Šatkauskas et al., 2012). We found that these procedures considerably improved electroporation results as compared to simpler pulse trains. Best results were obtained when the calculated poring currents were 4–6 mA and when the pulse trains were designed as specified in **Table 3**. This optimized protocol resulted in reliable expression of transgenes that lasted for weeks (see below). We refer to this protocol as "internal-electrode-electroporation" (IEP).

Using IEP and plasmid #1 (hEF1α::GFP; $n = 7$ fish) or plasmid #2 (hEF1α::ChR2tc-GFP; $n = 40$ fish), reporter gene expression in Dp was observed in 85% of fish (**Figure 3F**, left). In a subset of fish electroporated with plasmid #2, fluorescent neurons were counted throughout Dp. On average, reporter expression was detected in $23 \pm 5$ cells per Dp (mean $\pm$ SD; $n = 26$ fish). The morphology of GFP-expressing neurons was normal without obvious signs of damage. In most cells, expression appeared strong compared to the expression of the same or similar transgenes in stable transgenic lines (not shown). Strong fluorescence was observed even for transgenes that are usually difficult to express at high levels such as fusion proteins containing ChR2 (**Figure 3F**, left). IEP is therefore a fast and reliable method to express transgenes in spatially restricted populations of neurons at high levels.

### CHARACTERIZATION OF PROMOTERS FOR EXPRESSION IN THE ADULT ZEBRAFISH BRAIN

The intensity, cell type specificity and time course of transgene expression is expected to depend critically on the promoter in an expression construct. In stable transgenic lines, many promoters drive much broader expression at early developmental stages than in the adult brain (Stamatoyannopoulos et al., 1993; Goldman et al., 2001; Li et al., 2005; Zhu et al., 2009), raising the possibility that expression of transgenes in the adult brain is difficult to achieve. However, little is known about the activity of promoters when developmental processes are bypassed by

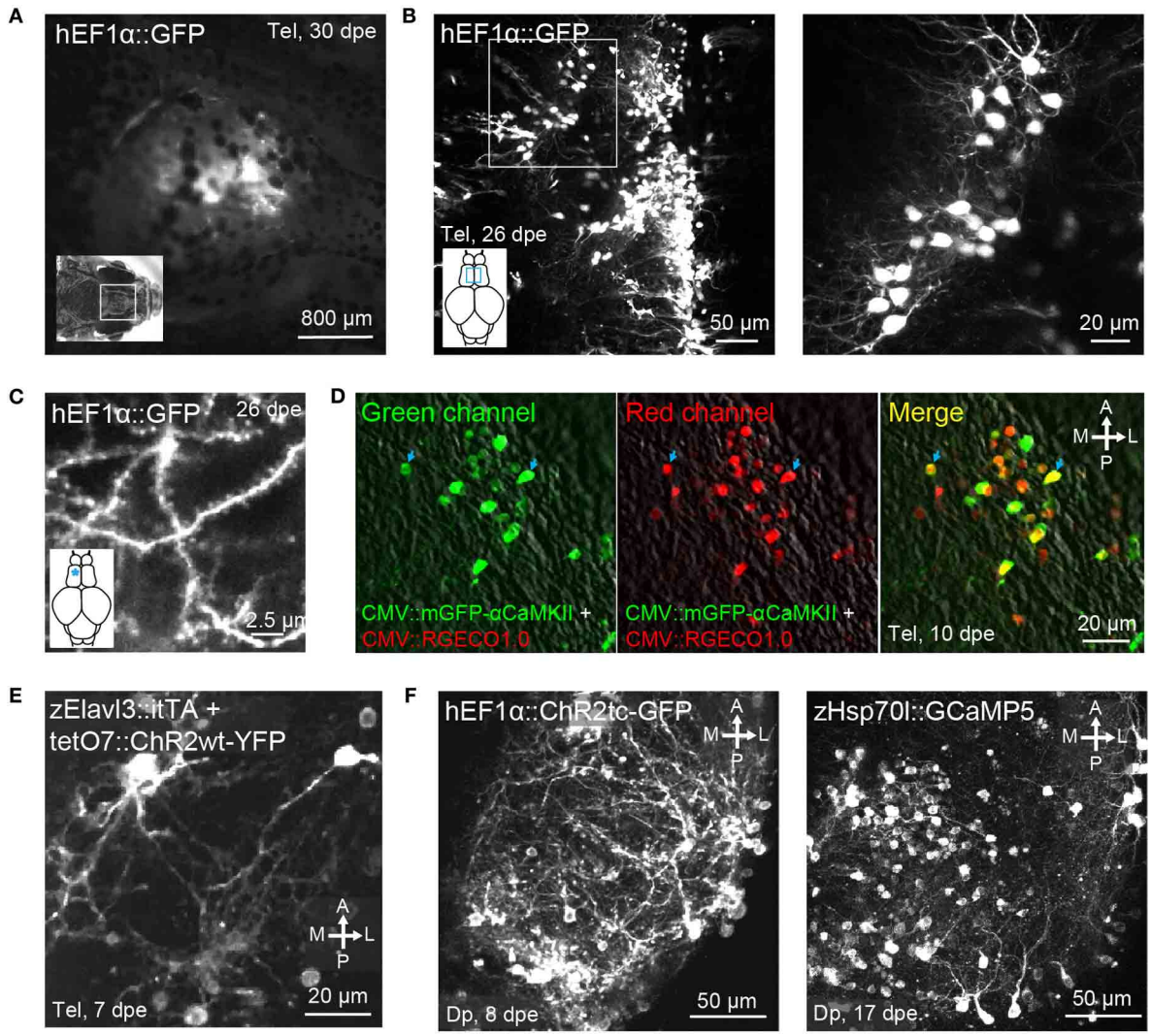


G

| # | Promoter | Transgene | Plasmid # | 5 dpe | 10 dpe | 15 dpe | 20 dpe | 30 dpe | 45 dpe |
|---|---|---|---|---|---|---|---|---|---|
| 1 | hSyn | ChR2wt-GFP-mbd | #10 | 0.5 | 1.0 | 0.7 | 0.4 | 0 | n.a. |
| 2 | zElavl3 | GCaMP5 | #11 | 0.5 | 1.2 | 0.8 | 0.5 | 0.4 | n.a. |
| 3 | αCaMKII | GFP | #9 | 0 | 0 | n.a. | n.a. | n.a. | n.a. |
| 4 | CMV | mRuby | #14 | 2.0 | 1.2 | 1.0 | 0.8 | 0.4 | 0 |
| 5 | CAG | Cre-GFP | #7 | 0.5 | 1.0 | 0.5 | 0 | n.a. | n.a. |
| 6 | hEF1α | GFP | #1 | 0.8 | 2.0 | 1.5 | 1.2 | 1.0 | 0.7 |
| 7 | xEF1α | GFP | #4 | 0.8 | 1.8 | 1.5 | 1.1 | 0.9 | 0.7 |
| 8 | zHsp70l | GFP | #5 | 1.5 | 2.0 | 2.0 | 2.0 | 2.0 | 2.0 |

**FIGURE 3 | Gene expression in the adult zebrafish brain using electroporation. (A)** Fluorescence image of the dorsal head of an adult zebrafish 30 days after electroporation (dpe) of plasmid #1 (EEP; hEF1α::GFP). Image was taken with a fluorescence stereomicroscope. **(B)** Expression of GFP in the dorsal telencephalon after electroporation of plasmid #1 (EEP; *z*-projection of multiphoton image stack). Boxed area is shown at higher magnification on the right. **(C)** GFP expression in spiny dendrites (same fish as in **B**; location is indicated by asterisk). **(D)** Expression of mGFP-αCaMKII (green channel, left) and RGECO1.0 (red channel, center) after co-electroporation of plasmids #15 and #18 (EEP in the dorsal telencephalon). Right: overlay showing co-expression. **(E)** Expression of ChR2wt-YFP after co-electroporation of a plasmid harboring the Tet activator (itTA; #12) and another plasmid containing the responder element (tetO7::ChR2wt-YFP; #13; EEP in the dorsal telencephalon). **(F)** Expression of ChR2tc-GFP (plasmid #2; left) and GCaMP5 (plasmid #6; right) in Dp after

*(Continued)*

**FIGURE 3 | Continued**
targeted electroporation using internal wire electrodes (IEP; z-projections of multiphoton image stacks). **(G)** Fluorescence intensity observed through the dorsal skull at different time points after electroporation of different constructs (EEP in dorsal telencephalon). Fluorescence intensity was scored manually through a fluorescence stereomicroscope and normalized to the intensity observed 10 days after electroporation of plasmid #10, which contains promoter #1 (hSyn::ChR2wt-GFP-mbd; Methods). n.a, not analyzed.

introducing expression constructs directly into the adult brain. We therefore analyzed transgene expression under the control of eight promoters that drive broad expression at early developmental stages (**Table 4**; **Figure 3G**). Electroporation was preferred over HSV-1 for gene delivery because available plasmids could be used without the need to generate viral vectors.

EEP was performed in the dorsal telencephalon and fluorescence was examined through the intact skull at different time points (**Table 4**; **Figure 3G**; $n = 4$–6 fish; 1 μg/μl for all plasmids). Fluorescence intensity was scored relative to the signal observed 10 days after electroporation of construct #10 (hSyn::ChR2wt-GFP-mbd), which produced intermediate expression levels. The intensity and time course of expression varied between constructs but only one promoter (αCaMKII::GFP; plasmids #8 and #9) failed to produce detectable expression. The fastest onset of expression was produced by construct #14 (CMV::mRuby), reaching peak levels at 5 dpe. Thereafter, expression gradually declined until it became undetectable at 45 dpe. Expression driven by other constructs usually peaked at 10 dpe and declined more slowly. Three constructs (#1, #4, #5) still generated substantial expression at 45 dpe. These constructs contained the human EF1α promoter (hEF1α), the EF1α promoter from Xenopus (xEF1α), and a heat-shock promoter from zebrafish (zHsp70l).

The same plasmids, along with the plasmid containing the CMV promoter (#14), also produced the highest peak fluorescence signals. Somewhat weaker but still substantial fluorescence was observed after electroporation of plasmids #7, #10, and #11, which harbored the human synapsin-1 promoter (hSyn), the zebrafish Elavl3 promoter (HuC) and the chimeric CAG promoter (Miyazaki et al., 1989), respectively. The constructs containing hSyn and zElavl3 had ChR2YFP and GCaMP5, respectively, as fluorescent reporters, which are usually less bright than the reporters of plasmids #1, #4, #5, and #14 (GFP or mRuby). The somewhat lower fluorescence generated by plasmids #10 and #11 may thus be due to the reporter, rather than the promoter. Plasmid #7 may have produced lower fluorescence because the CAG promoter is weaker than other promoters in zebrafish (Rothenaigner et al., 2011), because the reporter (Cre-GFP) is less bright, or both. Together, these results show that a broad range of promoters can drive strong and long-lasting expression of transgenes when they are introduced into the adult zebrafish brain.

The fluorescence signal produced by plasmid #5 (zHsp70l::GFP) was particularly strong and outlasted the fluorescence signals of other plasmids containing the same reporter (**Figure 3G**). To further examine gene expression using zHsp70l promoter, we electroporated plasmid #6 (zHsp70l::GCaMP5) into Dp by targeted IEP and found that the number of GCaMP5-expressing neurons was four times higher (92 ± 39 cells, mean ± *SD*.; $n = 6$ fish; **Figure 3F**, right) than the number of GFP-expressing neurons observed after electroporation of plasmid #2 (hEF1α::ChR2tc-GFP; 23 ± 5 cells, mean ± SD.; $n = 26$ fish; see above). Strong and widespread expression using the zHsp70l promoter was observed without application of a heat shock. Expression may therefore be driven by basal activity of the promoter or activated by a cellular response to the electroporation event. These results indicate that the zHsp70l promoter is particularly effective in driving expression of transgenes in a wide range of neurons when introduced into the adult zebrafish brain, consistent with previous reports (Hans et al., 2011).

## FUNCTIONALITY OF CHANNELRHODOPSIN VARIANTS AND GENETICALLY ENCODED CALCIUM INDICATORS

Gene transfer by HSV-1 or electroporation provides the opportunity to rapidly characterize the function of optogenetic probes, GECIs and other molecular tools in adult zebrafish. We used EEP to express four variants of ChR2, fused to fluorescent reporters, in the dorsal telencephalon of adult zebrafish (**Table 2**, plasmids #2, #3, #10, and #13; $n = 4$ for each plasmid). Moreover, we used targeted IEP to express plasmid #2 in Dp neurons. All constructs produced high-level expression. Labeled neurons had normal morphologies except for those electroporated with plasmid #3 (ChR2tc-mEos2), which sometimes showed unusual dendritic shapes and hot spots of fluorescence that may reflect protein aggregation. Targeted whole cell patch clamp recordings were performed from neurons expressing ChR2tc-GFP ($n = 11$ neurons in Dp) or ChR2wt-GFP-mbd ($n = 2$ neurons in the dorsal telencephalon) in an explant preparation of the whole brain (Zhu et al., 2012) at 7 dpe. All neurons had normal resting potentials between −60 and −75 mV. Whole-field light pulses (460 nm) of fixed intensity (250–300 $\mu W/mm^2$) and different durations (1, 2, 5, 10, 20, 50 ms) were delivered at 1 Hz. In all neurons, action potentials were triggered reliably (probability > 90 %) when the duration of light pulses was 10 ms or longer (**Figure 4A**). Some neurons reliably fired action potentials even when light pulses were as short as 2 ms or 1 ms (not shown).

In order to examine synaptic transmission in Dp we expressed hEF1α::ChR2tc-GFP (plasmid #2) in Dp neurons by targeted IEP and prepared brain explant preparations at 7–10 dpe. Neurons were optically stimulated with trains of wide-field light pulses (460 nm; 10 ms duration, 10 pulses at 5 or 10 Hz). Whole cell voltage clamp recordings were performed from ChR2tc negative neurons in Dp that were usually intermingled with ChR2tc positive neurons ($n = 42$ neurons in 9 fish). Excitatory post-synaptic currents (EPSCs) and inhibitory post-synaptic currents (IPSCs) were measured by holding the recorded neurons close to the reversal potentials for chloride currents (−70 mV) and cation currents (0 mV), respectively. EPSCs time-locked to the optical stimulus were observed in only one neuron, and stimulus-locked IPSCs were observed in two neurons (**Figures 4B,C**). The EPSC and one of the IPSCs had short latencies (< 6 ms;

**Table 4 | Promoters compared by electroporation.**

| No. | Promoter | Size | Transgene | Number of fish (EEP) | Description |
|---|---|---|---|---|---|
| **PAN NEURONAL EXPRESSION** | | | | | |
| 1 | hSyn | 0.6 kb | ChR2wt-GFP-mbd | $n = 5$ | Human synapsin-1 promoter (see plasmid #10) |
| 2 | zElavl3 | 8.7 kb | GCaMP5 | $n = 4$ | Zebrafish Elavl3 (or HuC) promoter (see plasmid #11) |
| **EXCITATORY GLUTAMATERGIC NEURON EXPRESSION** | | | | | |
| 3 | αCaMKII | 1.3 kb | GFP | $n = 6$ | Alpha $Ca^{2+}$ /calmodulin-dependent protein kinase II promoter (see plasmid #9) |
| **UBIQUITOUS EXPRESSION** | | | | | |
| 4 | CMV | 0.6 kb | mRuby | $n = 5$ | Cytomegalovirus immediate-early promoter (see plasmid #14) |
| 5 | CAG | 1.7 kb | Cre-GFP | $n = 4$ | Chimeric promoter with sequences from cytomegalovirus immediate-early gene, chicken beta-actin gene, and rabbit beta-globin gene (see plasmid #7) |
| 6 | hEF1α | 1.2 kb | GFP | $n = 6$ | Human elongation factor 1 alpha promoter (see plasmid #1) |
| 7 | xEF1α | 1.2 kb | GFP | $n = 5$ | Xenopus elongation factor 1 alpha promoter (see plasmid #4) |
| 8 | zHsp70l | 1.5 kb | GFP | $n = 5$ | Zebrafish heat-shock protein 70l promoter (see plasmid #5) |

*N indicates number of fish used in EEP experiments. See **Figure 3G** for expression levels.*

**Figures 4B,C**), consistent with monosynaptic connections, while the second IPSC had a longer latency. These results demonstrate that monoysnaptic connectivity among Dp neurons is sparse. In addition, we observed slow inhibitory or excitatory currents that were not time-locked to the stimulus pulses in 23 of the 42 Dp neurons (**Figure 4D**). Together, these results show that electroporation can be used to introduce optogenetic probes into adult neurons to examine functional connectivity in the intact brain.

We next used EEP in the dorsal telencephalon to express different GECIs including the green-fluorescent probes GCaMP5 (Akerboom et al., 2012), GCaMP6f (fast variant of GCaMP6) (Chen et al., 2013), GCaMP6s (slow variant of GCaMP6) (Chen et al., 2013) and the red-fluorescent indicators RGECO1.0 (Zhao et al., 2011) and RCaMP1.07 (Ohkura et al., 2012) (**Table 2**, plasmids #11, #16, #17, #18, and #19; $n = 3$ or 4 fish for each GECI). At 7–10 dpe, fluorescence was examined by multiphoton microscopy in the *ex-vivo* preparation. In order to produce large changes in intracellular calcium concentration we applied the $GABA_A$ receptor blocker Gabazine (1 μM) through the bath. This treatment is known to induce epileptiform bursting of many neurons in the forebrain at low inter-burst frequency (Tabor et al., 2008). Gabzine induced large changes in fluorescence intensity (ΔF/F) throughout the soma and dendrites of many GECI-expressing cells that occurred at frequencies of approximately 0.1–0.3 Hz (**Figures 5A–C**). The amplitude of these events was measured at the soma and at dendritic locations where the fluorescence in the time-averaged ΔF/F map was large. This procedure provides a simple assay to compare fluorescence changes of different GECIs produced by intense bursting of adult telencephalic neurons (**Figure 5C**).

Mean changes of GECI fluorescence in the presence of Gabazine were approximately 180–400% at somata and even larger in dendrites (**Figure 5C**; $n = 9$ neurons from 3 fish for each GECI). Particularly large fluorescence changes were observed with GCaMP6s (soma: approximately 300%; dendrite: approximately 1000%). Calcium transients observed with GCaMP6s (**Figure 5B** bottom) decayed more slowly than those produced by other GECIs, consistent with the slow kinetics of this probe (Chen et al., 2013). Substantial fluorescence transients were also observed with all other calcium sensors including the red-fluorescent indicators, RGECO1.0 and RCaMP1.07 (**Figure 5C**).

In Dp neurons expressing GCaMP5 (plasmid #6) by IEP we also measured fluorescence changes evoked by odor stimulation. Previous electrophysiological studies showed that many Dp neurons receive depolarizing synaptic input during odor stimulation but only a small subset fires action potentials (Yaksi et al., 2009; Blumhagen et al., 2011). In some Dp neurons, odor stimulation produced a calcium signal at the soma and a global calcium signal throughout the dendrite, indicative of action potential firing. In addition, we frequently observed smaller, highly localized calcium transients that most likely reflect subthreshold synaptic input in dendrites (**Figure 5D**). Similar calcium transients were also evoked by electrical stimulation (0.5 ms pulse duration, 10 pulses at 20 Hz) in the posterior olfactory bulb (**Figure 5E**). Together, these results show that various green- and red-fluorescent GECIs function efficiently in adult telencephalic neurons when they are introduced by electroporation.

## DISCUSSION

We report methods to directly express transgenes in neurons of the adult zebrafish brain by HSV-1 or electroporation. Both methods are simple, efficient and can produce strong and long-lasting gene expression without obvious toxicity. In other species, fast gene transfer can be achieved using AAVs or lentiviruses but comparable methods have been lacking in zebrafish. This gap in the molecular toolbox for zebrafish may therefore be filled by HSV-1 and targeted electroporation.

HSV-1 is used for gene transfer in other species because it exhibits a high potential to infect neurons and low levels of toxicity. Our observations in zebrafish are fully consistent with these properties of HSV-1. However, we observed substantial variation in reporter gene expression between different HSV-1 viruses, presumably depending on the method of virus production and other factors. HSV-1 can produce dense expression of transgenes, which is important to target large populations of neurons. The ability of HSV-1 to retrogradely infect neurons via

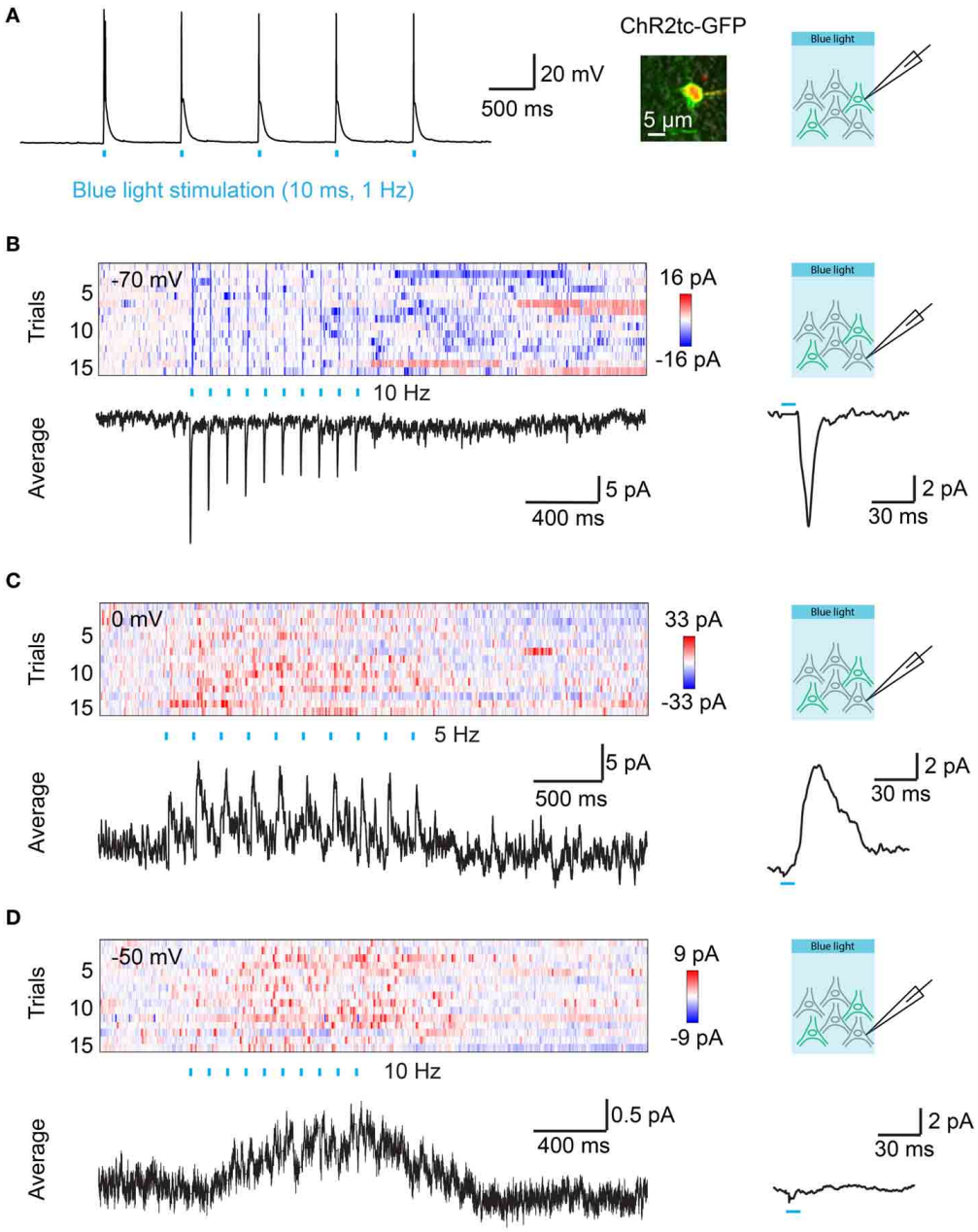


**FIGURE 4 | Optical control of synaptic transmission after targeted electroporation of channelrhodopsin-2 in Dp. (A)** Action potentials evoked by blue light pulses (10 ms; 1 Hz) in a Dp neuron expressing ChR2tc-GFP after targeted IEP of plasmid #2. Image shows overlay of GFP fluorescence (green), Alexa594 fluorescence (red; included in pipette solution), and transmitted light (gray) images. **(B)** Color plot shows currents recorded at a holding potential of −70 mV in a ChR2tc-GFP-negative Dp neuron as a function of time. ChR2tc-GFP was expressed in other Dp neurons by targeted IEP of plasmid #2. Rows represent successive trials. Blue ticks indicate pulses of blue light to stimulate ChR2tc-GFP-expressing Dp neurons (10 pulses of 10 ms at 10 Hz). Black traces show the average over all 15 trials (left) and the average over all 150 individual pulses (right). The pulse-triggered current average shows a fast onset and decay, indicating that the EPSC contains a monosynaptic component. **(C)** Currents recorded at a holding potential of 0 mV in another ChR2tc-GFP-negative Dp neuron after targeted IEP of plasmid #2 (different fish). The pulse-triggered current average shows a fast onset, consistent with a monosynaptic component in the IPSC. **(D)** Currents recorded at a holding potential of −50 mV in another ChR2tc-GFP-negative Dp neuron after targeted IEP of plasmid #2 (different fish). Note a slow current but no fast EPSCs or IPSCs.

their axons can be exploited to target defined projection neurons. Conceivably, additional cell type selectivity may be generated by the choice of the promoter, which can be exchanged using established procedures (Simonato et al., 1999). We therefore expect that HSV-1 will become an important tool for gene transfer in zebrafish.

We established reliable protocols for gene transfer by electroporation using external or internal electrodes. Compared to

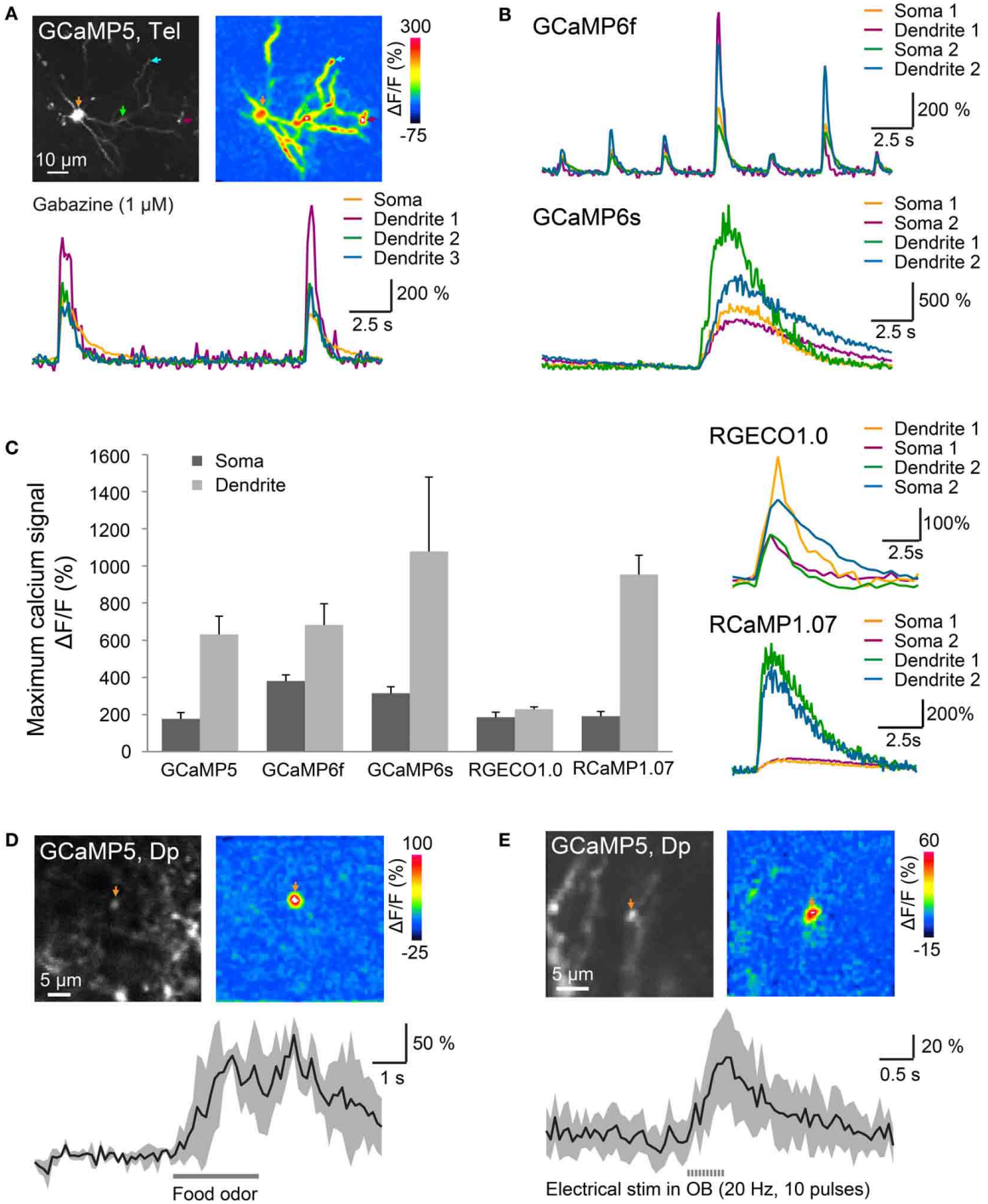


**FIGURE 5 | Optical measurements of calcium signals after targeted electroporation of GECIs. (A)** Top left: expression of GCaMP5 in a neuron of the dorsal telencephalon after EEP of plasmid #11. Bottom: change in GCaMP5 fluorescence as a function of time. Colored traces correspond to the locations indicated by colored arrows in the images above. Large, low-frequency calcium transients were induced by Gabazine (1 µM), which causes epileptiform population activity. Top right: spatial distribution of fluorescence changes (ΔF/F) during a calcium transient, relative to baseline before the transient. **(B)** Calcium transients in the presence of Gabazine (1 µM) measured with GCaMP6f and GCaMP6s. **(C)** Mean amplitude (±SD) of calcium transients at the soma and at a dendritic location measured with different GECIs ($n = 9$ neurons from 3 fish for each GECI). Right: fluorescence transients of red calcium indicators in the presence of Gabazine. **(D)** Localized calcium transient in a Dp neuron expressing GCaMP5 (IEP of plasmid #6; 11 dpe), evoked by odor stimulation (food extract; average over 3 trials). **(E)** Localized calcium transients in a Dp neuron expressing GCaMP5 (IEP of plasmid #6; 8 dpe), evoked by electrical stimulation in the olfactory bulb (20 Hz, 10 pulses; average over 10 trials).

gene transfer by HSV-1, transgene expression was sparser but strong. One advantage of electroporation is that plasmids can be introduced directly into neurons without the need to package genetic material into viruses or other vectors (Barnabé-Heider et al., 2008). The time to produce reagents for gene transfer and the risk of immune responses or other potential complications are therefore reduced. Moreover, the efficiency of electroporation should not vary substantially between cell types, brain areas and even species because electroporation relies on physical rather than molecular mechanisms. Electroporation is therefore a particularly fast and versatile method for gene transfer.

Electroporation has been used previously to introduce DNA into individual or small groups of neurons (Haas et al., 2001; Bianco et al., 2008; Kitamura et al., 2008) and to transfer transgenes into populations of cells near the ventricle (Barnabé-Heider et al., 2008). In order to target neuronal populations in specific brain regions we used internal electrodes (IEP) to create a local electrical field (Nishi et al., 1996). Physical damage was minimal because the electrodes were made of thin wires (25 μm) and the electrical pulses were adjusted to the local tissue parameters in each experiment. The procedure is not substantially more difficult to perform than viral injections and most likely applicable in different brain areas and species.

Efficient gene expression in the adult brain was achieved with a wide range of promoters that drive broad gene expression at early developmental stages. This result was not necessarily expected because gene expression in stable transgenic lines often becomes restricted in the adult brain (Stamatoyannopoulos et al., 1993; Goldman et al., 2001; Li et al., 2005; Zhu et al., 2009). A possible explanation for this result is that gene transfer into the adult brain bypasses silencing processes during development. Among the promoters tested, the heat-shock promoter zHsp70l appeared particularly promising to achieve broad, cell type-independent expression of transgenes.

We took advantage of electroporation to express a variety of ChR2 variants and GECIs in the adult telencephalon. Using a simple procedure to assess basic functional properties of GECIs in the intact brain we observed functional differences between GECIs that corresponded well to previous observations in other assays and species (Akerboom et al., 2012; Chen et al., 2013). For example, largest but also slowest fluorescence signals were observed with GCaMP6s (Chen et al., 2013). Consistent with previous results obtained in larvae (Walker et al., 2013) we observed substantial fluorescence signals using the red-fluorescent indicator RGECO1.0 (Zhao et al., 2011). Moreover, we obtained large fluorescence signals with another red-fluorescent GECI, RCaMP1.07 (Ohkura et al., 2012). These probes are therefore promising tools for multicolor calcium imaging.

Dp is a telencephalic brain area that is homologous to mammalian olfactory cortex (Mueller and Wullimann, 2009; Mueller et al., 2011) and assumed to be involved in olfactory memory (Wilson and Sullivan, 2011). Functional synaptic connectivity between principal neurons in olfactory cortex is difficult to analyze by paired electrophysiological recordings because it is very sparse (Johnson et al., 2000; Franks et al., 2011). This problem can be overcome by optogenetic stimulation of multiple neurons to increase the probability of finding a monosynaptically connected post-synaptic neuron (Franks et al., 2011). When ChR2tc was expressed in multiple Dp neurons by IEP we detected short-latency EPSCs or IPSCs in a small fraction of the recorded ChR2tc-negative neurons. Monosynaptic connectivity in Dp is therefore sparse, consistent with recurrent connectivity in mammalian olfactory cortex. Further experiments using this approach may now be performed to quantify connectivity in more detail. In Dp neurons expressing GECIs, odor stimulation evoked localized dendritic calcium transients that most likely reflect subthreshold synaptic input. Hence, sparse expression of GECIs by IEP is a promising approach to measure the tuning of synaptic inputs at different dendritic locations of Dp neurons. Conceptually similar experiments have provided insights into the processing of synaptic inputs in other brain areas such as the visual and auditory cortex (Jia et al., 2010; Chen et al., 2011). In summary, we conclude that gene transfer by HSV-1 and electroporation have a wide range of potential applications in zebrafish neuroscience. Moreover, electroporation is likely to be a useful technique for gene transfer in species in which genetic methods are not well established.

## ACKNOWLEDGMENTS

We thank J. Letzkus, K. Yonehara and B. Roska for HSV-1 reagents, C. Xu for the hEF1α promoter, K. Kawakami for the xEF1α promoter, A. Schier for the zElavl3 promoter, A. Fine for the αCaMKII promoters, T. Oertner for plasmids containing ChR2tc and ChR2wt-GFP-mbd, R. Campbell for RGECO1.0, L. Looger and D. Kim for GCaMP variants, J. Wiedenmann for mRuby, and M. Ohkura and J. Nakai for RCaMP1.07. We are grateful to E. Arn Bouldoires for expert help with molecular biology. This work was supported by the Novartis Research Foundation, the Swiss Nationalfonds, the Deutsche Forschungsgemeinschaft, the Human Frontiers Science Program (RWF) and by the Canadian Institutes of Health Research and the Natural Science and Engineering Research Council of Canada (PDK).

## REFERENCES

Akerboom, J., Chen, T.-W., Wardill, T. J., Tian, L., Marvin, J. S., Mutlu, S., et al. (2012). Optimization of a GCaMP calcium indicator for neural activity imaging. *J. Neurosci.* 32, 13819–13840. doi: 10.1523/JNEUROSCI.2601-12.2012

Aoki, T., Kinoshita, M., Aoki, R., Agetsuma, M., Aizawa, H., Yamazaki, M., et al. (2013). Imaging of neural ensemble for the retrieval of a learned behavioral program. *Neuron* 78, 881–894. doi: 10.1016/j.neuron.2013.04.009

Barnabé-Heider, F., Meletis, K., Eriksson, M., Bergmann, O., Sabelström, H., Harvey, M. A., et al. (2008). Genetic manipulation of adult mouse neurogenic niches by *in vivo* electroporation. *Nat. Methods* 5, 189–196. doi: 10.1038/nmeth.1174

Berndt, A., Schoenenberger, P., Mattis, J., Tye, K. M., Deisseroth, K., Hegemann, P., et al. (2011). High-efficiency channelrhodopsins for fast neuronal stimulation at low light levels. *Proc. Natl. Acad. Sci. U.S.A.* 108, 7595–7600. doi: 10.1073/pnas.1017210108

Bianco, I. H., Carl, M., Russell, C., Clarke, J. D., and Wilson, S. W. (2008). Brain asymmetry is encoded at the level of axon terminal morphology. *Neural Dev.* 3:9. doi: 10.1186/1749-8104-3-9

Blumhagen, F., Zhu, P., Shum, J., Schärer, Y.-P. Z., Yaksi, E., Deisseroth, K., et al. (2011). Neuronal filtering of multiplexed odour representations. *Nature* 479, 493–498. doi: 10.1038/nature10633

Burgos, J. S., Ripoll-Gomez, J., Alfaro, J. M., Sastre, I., and Valdivieso, F. (2008). Zebrafish as a new model for herpes simplex virus type 1 infection. *Zebrafish* 5, 323–333. doi: 10.1089/zeb.2008.0552

Cerda, G. A., Thomas, J. E., Allende, M. L., Karlstrom, R. O., and Palma, V. (2006). Electroporation of DNA, RNA, and morpholinos into zebrafish embryos. *Methods* 39, 207–211. doi: 10.1016/j.ymeth.2005.12.009

Chen, T.-W., Wardill, T. J., Sun, Y., Pulver, S. R., Renninger, S. L., Baohan, A., et al. (2013). Ultrasensitive fluorescent proteins for imaging neuronal activity. *Nature* 499, 295–300. doi: 10.1038/nature12354

Chen, X., Leischner, U., Rochefort, N. L., Nelken, I., and Konnerth, A. (2011). Functional mapping of single spines in cortical neurons *in vivo*. *Nature* 475, 501–505. doi: 10.1038/nature10193

De Vry, J., Martínez-Martínez, P., Losen, M., Temel, Y., Steckler, T., Steinbusch, H. W. M., et al. (2010). *In vivo* electroporation of the central nervous system: a non-viral approach for targeted gene delivery. *Prog. Neurobiol.* 92, 227–244. doi: 10.1016/j.pneurobio.2010.10.001

Franks, K. M., Russo, M. J., Sosulski, D. L., Mulligan, A. A., Siegelbaum, S. A., and Axel, R. (2011). Recurrent circuitry dynamically shapes the activation of piriform cortex. *Neuron* 72, 49–56. doi: 10.1016/j.neuron.2011.08.020

Friedrich, R. W., Genoud, C., and Wanner, A. A. (2013). Analyzing the structure and function of neuronal circuits in zebrafish. *Front. Neural Circuits* 7:71. doi: 10.3389/fncir.2013.00071

Friedrich, R. W., Jacobson, G. A., and Zhu, P. (2010). Circuit neuroscience in zebrafish. *Curr. Biol.* 20, R371–R381. doi: 10.1016/j.cub.2010.02.039

Goldman, D., Hankin, M., Li, Z., Dai, X., and Ding, J. (2001). Transgenic zebrafish for studying nervous system development and regeneration. *Transgenic Res.* 10, 21–33. doi: 10.1023/A:1008998832552

Haas, K., Sin, W. C., Javaherian, A., Li, Z., and Cline, H. T. (2001). Single-cell electroporation for gene transfer *in vivo*. *Neuron* 29, 583–591. doi: 10.1016/S0896-6273(01)00235-5

Halloran, M. C., Sato-Maeda, M., Warren, J. T., Su, F., Lele, Z., Krone, P. H., et al. (2000). Laser-induced gene expression in specific cells of transgenic zebrafish. *Development* 127, 1953–1960.

Hans, S., Freudenreich, D., Geffarth, M., Kaslin, J., Machate, A., and Brand, M. (2011). Generation of a non-leaky heat shock-inducible cre line for conditional cre/lox strategies in zebrafish. *Dev. Dyn.* 240, 108–115. doi: 10.1002/dvdy.22497

Hendricks, M., and Jesuthasan, S. (2007). Electroporation-based methods for *in vivo*, whole mount and primary culture analysis of zebrafish brain development. *Neural Dev.* 2:6. doi: 10.1186/1749-8104-2-6

Hudmon, A., LeBel, E., Roy, H., Sik, A., Schulman, H., Waxham, M. N., et al. (2005). A Mechanism for Ca2+/calmodulin-dependent protein kinase II clustering at synaptic and nonsynaptic sites based on self-association. *J. Neurosci.* 25, 6971–6983. doi: 10.1523/JNEUROSCI.4698-04.2005

Jia, H., Rochefort, N. L., Chen, X., and Konnerth, A. (2010). Dendritic organization of sensory input to cortical neurons *in vivo*. *Nature* 464, 1307–1312. doi: 10.1038/nature08947

Johnson, A. D., and Krieg, P. A. (1994). pXeX, a vector for efficient expression of cloned sequences in Xenopus embryos. *Gene* 147, 223–226. doi: 10.1016/0378-1119(94)90070-1

Johnson, D. M. G., Illig, K. R., Behan, M., and Haberly, L. B. (2000). New features of connectivity in piriform cortex visualized by intracellular injection of pyramidal cells suggest that "primary" olfactory cortex functions like "association" cortex in other sensory systems. *J. Neurosci.* 20, 6974–6982.

Kim, D. W., Uetsuki, T., Kaziro, Y., Yamaguchi, N., and Sugano, S. (1990). Use of the human elongation factor 1 alpha promoter as a versatile and efficient expression system. *Gene* 91, 217–223. doi: 10.1016/0378-1119(90)90091-5

Kitamura, K., Judkewitz, B., Kano, M., Denk, W., and Häusser, M. (2008). Targeted patch-clamp recordings and single-cell electroporation of unlabeled neurons *in vivo*. *Nat. Methods* 5, 61–67. doi: 10.1038/nmeth1150

Knöpfel, T., Lin, M. Z., Levskaya, A., Tian, L., Lin, J. Y., and Boyden, E. S. (2010). Toward the second generation of optogenetic tools. *J. Neurosci.* 30, 14998–15004. doi: 10.1523/JNEUROSCI.4190-10.2010

Kredel, S., Oswald, F., Nienhaus, K., Deuschle, K., Röcker, C., Wolff, M., et al. (2009). mRuby, a bright monomeric red fluorescent protein for labeling of subcellular structures. *PLoS ONE* 4:e4391. doi: 10.1371/journal.pone.0004391

Kügler, S., Kilic, E., and Bähr, M. (2003). Human synapsin 1 gene promoter confers highly neuron-specific long-term transgene expression from an adenoviral vector in the adult rat brain depending on the transduced area. *Gene Ther.* 10, 337–347. doi: 10.1038/sj.gt.3301905

Kustermann, S., Schmid, S., Biehlmaier, O., and Kohler, K. (2008). Survival, excitability, and transfection of retinal neurons in an organotypic culture of mature zebrafish retina. *Cell Tissue Res.* 332, 195–209. doi: 10.1007/s00441-008-0589-5

Kwan, K. M., Fujimoto, E., Grabher, C., Mangum, B. D., Hardy, M. E., Campbell, D. S., et al. (2007). The Tol2kit: a multisite gateway-based construction kit for Tol2 transposon transgenesis constructs. *Dev. Dyn.* 236, 3088–3099. doi: 10.1002/dvdy.21343

Leung, L. C., Wang, G. X., and Mourrain, P. (2013). Imaging zebrafish neural circuitry from whole brain to synapse. *Front. Neural Circuits* 7:76. doi: 10.3389/fncir.2013.00076

Lewis, T. L. Jr., Mao, T., Svoboda, K., and Arnold, D. B. (2009). Myosin-dependent targeting of transmembrane proteins to neuronal dendrites. *Nat. Neurosci.* 12, 568–576. doi: 10.1038/nn.2318

Li, J., Mack, J. A., Souren, M., Yaksi, E., Higashijima, S., Mione, M., et al. (2005). Early development of functional spatial maps in the zebrafish olfactory bulb. *J. Neurosci.* 25, 5784–5795. doi: 10.1523/JNEUROSCI.0922-05.2005

Luo, L., Callaway, E. M., and Svoboda, K. (2008). Genetic dissection of neural circuits. *Neuron* 57, 634–660. doi: 10.1016/j.neuron.2008.01.002

Mathieson, W. B., and Maler, L. (1988). Morphological and electrophysiological properties of a novel *in vitro* preparation: the electrosensory lateral line lobe brain slice. *J. Comp. Physiol.* 163, 489–506. doi: 10.1007/BF00604903

Matsuda, T., and Cepko, C. L. (2007). Controlled expression of transgenes introduced by *in vivo* electroporation. *Proc. Natl. Acad. Sci. U.S.A.* 104, 1027–1032. doi: 10.1073/pnas.0610155104

Mayford, M., Bach, M. E., Huang, Y. Y., Wang, L., Hawkins, R. D., and Kandel, E. R. (1996). Control of memory formation through regulated expression of a CaMKII transgene. *Science* 274, 1678–1683. doi: 10.1126/science.274.5293.1678

McKinney, S. A., Murphy, C. S., Hazelwood, K. L., Davidson, M. W., and Looger, L. L. (2009). A bright and photostable photoconvertible fluorescent protein. *Nat. Methods* 6, 131–133. doi: 10.1038/nmeth.1296

Miyazaki, J., Takaki, S., Araki, K., Tashiro, F., Tominaga, A., Takatsu, K., et al. (1989). Expression vector system based on the chicken beta-actin promoter directs efficient production of interleukin-5. *Gene* 79, 269–277. doi: 10.1016/0378-1119(89)90209-6

Mueller, T., Dong, Z., Berberoglu, M. A., and Guo, S. (2011). The dorsal pallium in zebrafish, Danio rerio (*Cyprinidae, Teleostei*). *Brain Res.* 1381, 95–105. doi: 10.1016/j.brainres.2010.12.089

Mueller, T., and Wullimann, M. F. (2009). An evolutionary interpretation of teleostean forebrain anatomy. *Brain. Behav. Evol.* 74, 30–42. doi: 10.1159/000229011

Nishi, T., Yoshizato, K., Yamashiro, S., Takeshima, H., Sato, K., Hamada, K., et al. (1996). High-efficiency *in vivo* gene transfer using intraarterial plasmid DNA injection following *in vivo* electroporation. *Cancer Res.* 56, 1050–1055.

Ohkura, M., Sasaki, T., Kobayashi, C., Ikegaya, Y., and Nakai, J. (2012). An improved genetically encoded red fluorescent Ca2+ indicator for detecting optically evoked action potentials. *PLoS ONE* 7:e39933. doi: 10.1371/journal.pone.0039933

Palella, T. D., Hidaka, Y., Silverman, L. J., Levine, M., Glorioso, J., and Kelley, W. N. (1989). Expression of human HPRT mRNA in brains of mice infected with a recombinant herpes simplex virus-1 vector. *Gene* 80, 137–144. doi: 10.1016/0378-1119(89)90258-8

Park, H. C., Kim, C. H., Bae, Y. K., Yeo, S. Y., Kim, S. H., Hong, S. K., et al. (2000). Analysis of upstream elements in the HuC promoter leads to the establishment of transgenic zebrafish with fluorescent neurons. *Dev. Biol.* 227, 279–293. doi: 10.1006/dbio.2000.9898

Pérez Koldenkova, V., and Nagai, T. (2013). Genetically encoded Ca2 + indicators: properties and evaluation. *Biochim. Biophys. Acta* 1833, 1787–1797. doi: 10.1016/j.bbamcr.2013.01.011

Pologruto, T. A., Sabatini, B. L., and Svoboda, K. (2003). ScanImage: flexible software for operating laser scanning microscopes. *Biomed. Eng. Online* 2:13. doi: 10.1186/1475-925X-2-13

Rambabu, K. M., Rao, S. H. N., and Rao, N. M. (2005). Efficient expression of transgenes in adult zebrafish by electroporation. *BMC Biotechnol.* 5:29. doi: 10.1186/1472-6750-5-29

Rothenaigner, I., Krecsmarik, M., Hayes, J. A., Bahn, B., Lepier, A., Fortin, G., et al. (2011). Clonal analysis by distinct viral vectors identifies bona fide neural stem cells in the adult zebrafish telencephalon and characterizes their division properties and fate. *Development* 138, 1459–1469. doi: 10.1242/dev.058156

Šatkauskas, S., Ruzgys, P., and Venslauskas, M. S. (2012). Towards the mechanisms for efficient gene transfer into cells and tissues by means of cell electroporation.

*Expert Opin. Biol. Ther.* 12, 275–286. doi: 10.1517/14712598.2012.654775

Simonato, M., Marconi, P., Glorioso, J., and Manservigi, R. (1999). Molecular analysis of behavior by gene transfer into neurons with herpes simplex vectors. *Brain Res.* 835, 37–45. doi: 10.1016/S0006-8993(99)01245-7

Stamatoyannopoulos, G., Josephson, B., Zhang, J. W., and Li, Q. (1993). Developmental regulation of human gamma-globin genes in transgenic mice. *Mol. Cell. Biol.* 13, 7636–7644.

Suter, B. A., O'Connor, T., Iyer, V., Petreanu, L. T., Hooks, B. M., Kiritani, T., et al. (2010). Ephus: multipurpose data acquisition software for neuroscience experiments. *Front. Neural Circuits* 4:100. doi: 10.3389/fncir.2010.00100

Tabata, H., and Nakajima, K. (2001). Efficient *in utero* gene transfer system to the developing mouse brain using electroporation: visualization of neuronal migration in the developing cortex. *Neuroscience* 103, 865–872. doi: 10.1016/S0306-4522(01)00016-1

Tabor, R., Yaksi, E., and Friedrich, R. W. (2008). Multiple functions of GABA A and GABA B receptors during pattern processing in the zebrafish olfactory bulb. *Eur. J. Neurosci.* 28, 117–127. doi: 10.1111/j.1460-9568.2008.06316.x

Tabor, R., Yaksi, E., Weislogel, J.-M., and Friedrich, R. W. (2004). Processing of odor mixtures in the zebrafish olfactory bulb. *J. Neurosci.* 24, 6611–6620. doi: 10.1523/JNEUROSCI.1834-04.2004

Thomsen, D. R., Stenberg, R. M., Goins, W. F., and Stinski, M. F. (1984). Promoter-regulatory region of the major immediate early gene of human cytomegalovirus. *Proc. Natl. Acad. Sci. U.S.A.* 81, 659–663. doi: 10.1073/pnas.81.3.659

Ugolini, G., Kuypers, H. G., and Simmons, A. (1987). Retrograde transneuronal transfer of herpes simplex virus type 1 (HSV 1) from motoneurones. *Brain Res.* 422, 242–256. doi: 10.1016/0006-8993(87)90931-0

Wagle, M., Grunewald, B., Subburaju, S., Barzaghi, C., Le Guyader, S., Chan, J., et al. (2004). EphrinB2a in the zebrafish retinotectal system. *J. Neurobiol.* 59, 57–65. doi: 10.1002/neu.10340

Wagle, M., and Jesuthasan, S. (2003). Baculovirus-mediated gene expression in zebrafish. *Mar. Biotechnol.* 5, 58–63. doi: 10.1007/s10126-002-0050-9

Walker, A. S., Burrone, J., and Meyer, M. P. (2013). Functional imaging in the zebrafish retinotectal system using RGECO. *Front. Neural Circuits* 7:34. doi: 10.3389/fncir.2013.00034

Wilson, D. A., and Sullivan, R. M. (2011). Cortical processing of odor objects. *Neuron* 72, 506–519. doi: 10.1016/j.neuron.2011.10.027

Wullimann, M. F., and Reichert, H. (1996). *Neuroanatomy of the Zebrafish Brain: A Topological Atlas [. . . ] [. . . .]*. Basel: Birkhäuser. doi: 10.1007/978-3-0348-8979-7

Yaksi, E., von Saint Paul, F., Niessing, J., Bundschuh, S. T., and Friedrich, R. W. (2009). Transformation of odor representations in target areas of the olfactory bulb. *Nat. Neurosci.* 12, 474–482. doi: 10.1038/nn.2288

Yizhar, O., Fenno, L. E., Davidson, T. J., Mogri, M., and Deisseroth, K. (2011). Optogenetics in neural systems. *Neuron* 71, 9–34. doi: 10.1016/j.neuron.2011.06.004

Yonehara, K., Balint, K., Noda, M., Nagel, G., Bamberg, E., and Roska, B. (2011). Spatially asymmetric reorganization of inhibition establishes a motion-sensitive circuit. *Nature* 469, 407–410. doi: 10.1038/nature09711

Zhao, Y., Araki, S., Wu, J., Teramoto, T., Chang, Y.-F., Nakano, M., et al. (2011). An expanded palette of genetically encoded Ca2+ indicators. *Science* 333, 1888–1891. doi: 10.1126/science.1208592

Zhu, P., Fajardo, O., Shum, J., Zhang Schärer, Y.-P., and Friedrich, R. W. (2012). High-resolution optical control of spatiotemporal neuronal activity patterns in zebrafish using a digital micromirror device. *Nat. Protoc.* 7, 1410–1425. doi: 10.1038/nprot.2012.072

Zhu, P., Narita, Y., Bundschuh, S. T., Fajardo, O., Schärer, Y.-P. Z., Chattopadhyaya, B., et al. (2009). Optogenetic dissection of neuronal circuits in zebrafish using viral gene transfer and the Tet system. *Front. Neural Circuits* 3:21. doi: 10.3389/neuro.04.021.2009

**Conflict of Interest Statement:** The authors declare that the research was conducted in the absence of any commercial or financial relationships that could be construed as a potential conflict of interest.

*Received: 06 February 2014; accepted: 04 April 2014; published online: 06 May 2014.*
*Citation: Zou M, De Koninck P, Neve RL and Friedrich RW (2014) Fast gene transfer into the adult zebrafish brain by herpes simplex virus 1 (HSV-1) and electroporation: methods and optogenetic applications. Front. Neural Circuits* ***8****:41. doi: 10.3389/fncir.2014.00041*
*This article was submitted to the journal Frontiers in Neural Circuits.*

# *Chapter 3: Results Part II*

## Synaptic connectivity and plasticity in the zebrafish homolog of olfactory cortex.

Ming Zou, Rainer W. Friedrich*

*Manuscript in preparation.*

*Correspondence

**Contributions:**

MZ performed all experiments and data analysis, MZ and RWF conceived the study and wrote the manuscript.

# Statistics and plasticity of synaptic connections in the zebrafish homolog of olfactory cortex

Ming Zou[1,2], Rainer W. Friedrich[1,2] *

[1] Friedrich Miescher Institute for Biomedical Research, CH-4058 Basel, Switzerland.

[2] University of Basel, CH-4003 Basel, Switzerland

*Correspondence: Rainer W. Friedrich, Friedrich Miescher Institute for Biomedical Research, Maulbeerstrasse 66, CH-4058 Basel, Switzerland. e-mail: rainer.friedrich@fmi.ch

## ABSTRACT

Piriform cortex is the main target area of the olfactory bulb (OB) and contains distributed, sparse and plastic recurrent connections that have been proposed to function as an autoassociative memory network. In teleosts including zebrafish, the posterior zone of dorsal telencephalon (Dp) is directly homologous to mammalian olfactory cortex but the cytoarchitecture is different because the teleost pallium does not undergo the inside-out development that leads to cortical layering. We examined whether functional synaptic connectivity and plasticity in Dp of adult zebrafish is similar to mammalian olfactory cortex using a combination of optogenetics, electrophysiology, and pharmacology. We found that both intrinsic excitatory and inhibitory synaptic transmissions consist large amplitude (>2 pA) and stable responses, as well as small amplitude (<2 pA) but unstable responses. The intrinsic excitatory connectivity is extremely sparse (connection probability ~0.19 % – 1.31 %). Inhibitory connectivity is also sparse although estimates of inhibitory connection probability are somewhat higher (~0.61 % – 2.15 %). No obvious interdependence between excitatory and inhibitory connectivity was observed. Cholinergic agonists reduced inhibitory, but not excitatory, synaptic transmission in Dp. Electrical stimulation protocols designed to produce spike timing-dependent synaptic plasticity (STDP) resulted in long-term potentiation in Dp. These results indicate that the functional architecture of Dp is similar to piriform cortex and suggest that Dp may function as a distributed memory network.

# INTRODUCTION

Olfactory cortex is thought to establish synthetic representations of odor objects and to function as a distributed memory system for the autoassociative storage and retrieval of odor information (Haberly, 2001; Wilson and Sullivan, 2011). Insights into the functional organization of olfactory cortex may therefore be important to understand how odor information is encoded and used to guide behavior. Moreover, the structure and function of olfactory cortical circuits may provide insights into elementary mechanisms of associative cortical computations.

Mammalian olfactory cortex encompasses paleocortical brain areas that receive direct input from the olfactory bulb (OB), the largest of which is piriform cortex. One characteristic of piriform cortex is the absence of an obvious columnar organization: unlike in neocortex, the probability of connections between pyramidal neurons appears to be independent of distance (Franks et al., 2011; Johnson et al., 2000). Moreover, excitatory connectivity is very sparse: the probability of an excitatory connection between arbitrary pairs of pyramidal neurons is <1 % (Franks et al., 2011). Physiological experiments indicate that these recurrent connections can undergo long-term potentiation (Hasselmo and Barkai, 1995), and that cholinergic agonists decrease inhibitory synaptic transmission (Patil and Hasselmo, 1999). Computational circuit models that incorporate these findings can learn attractor-like representations of odors and perform pattern completion or pattern separation during retrieval, giving rise to the hypothesis that olfactory cortex functions as an autoassociative memory network (Hasselmo et al., 1990; Haberly, 2001). Recent in vivo studies are supporting this hypothesis (Wilson, 2003; Choi et al., 2011; Barnes et al., 2008; Chapuis and Wilson, 2011). However, in rodents, detailed analyses of odor-evoked activity patterns and their dynamics are challenging because olfactory cortex is large and difficult to access.

The adult zebrafish brain contains a pallial brain area, the posterior zone of the dorsal telencephalon (Dp), that is directly homologous to olfactory cortex (Mueller et al., 2011). Though, the histological appearance differs from mammalian piriform cortex because the teleost pallium undergoes a morphogenetic process during development ("eversion") that is different from the telencephalic "evagination" in other vertebrate classes. As a consequence, pallial areas of the teleost telencephalon do not show the distinct layering of cortical brain areas in other vertebrates. It is, however, unclear whether the basic connectivity and function is preserved between homologous pallial brain areas of teleosts and other vertebrates.

Measurements of odor-evoked responses in Dp showed convergence of diverse input channels from the OB and scattered, but not extremely sparse, activity patterns, as well as pronounced mixture suppression (Yaksi et al., 2009; Blumhagen et al., 2011; Schärer et al., 2012). These findings are generally consistent with activity patterns observed in piriform cortex (Apicella et al., 2010; Stettler and Axel, 2009) and provide support to functional similarities between Dp and the piriform cortex.

However, cellular architecture, synaptic properties and synaptic modulation are still unknown in Dp.

To address these questions, here we used a combination of optogenetics, electrophysiology, and pharmacology to investigate the intrinsic connectivity and plasticity of synapses in zebrafish Dp. The results show that both intrinsic excitatory and inhibitory connections in Dp are sparse and the local inhibition is reduced during cholinergic pharmacological application. The data further prove the existence of activity-dependent synaptic plasticity and spike-timing-dependent long-term potentiation (STDP type LTP) in Dp, shedding light on pattern learning in this brain region. Dp may therefore be an interesting model system to study autoassociative network function in a small genetically modifiable vertebrate.

## MATERIALS AND METHODS

### Animals and *in vivo* electroporation

Experiments were performed in wild-type zebrafish (*Danio rerio*) of both sexes that were raised at 25-28°C with a 14/10 hour on/off light cycle. Adult fish were > 3 months old. All experimental protocols were approved by the Veterinary Department of the Canton Basel-Stadt (Switzerland).

The procedures for spatially targeted *in vivo* electroporation in the adult zebrafish brain was described previously (Zou et al., 2014). Briefly, fish were anesthetized with 0.01% tricaine methanesulfonate (MS-222, Sigma-Aldrich) and fixed in a custom-made stereotactic chamber with a sponge filled holder and a pair of lateral stabilizers. The chamber was placed under a tilted stereomicroscope (Olympus SZX16 or Wild) and the fish was continuously supplied with fresh fish water containing MS-222 through a cannula in the mouth. To access Dp, a craniotomy was made on the skull, as described previously (Zou et al., 2014), at the suture between the bones over the telencephalon and tectum where Dp is located underneath.

A pair of custom-made wire electrodes (Pt, 25 µm diameter, ~400 µm distance, modified from FHC Inc. CE2C40) together with a micropipette containing DNA plasmid (hEF1α::ChR2tc-GFP, Berndt et al., 2011; Zou et al., 2014) were vertically inserted into the tissue. Approximately 70 nl of DNA solution was ejected slowly at each of three depths below the level of the bone (approximately 400 µm, 500 µm and 600 µm). After every injection, the tissue impedance was measured and according to that a set of pre-programmed square electrical pulses was selected and applied immediately (NEPA21 electroporator, NEPAGENE, Japan). Pulse trains created with the NEPA21 electroporator consist of a biphasic, high-amplitude cell membrane poring pulse that followed by a train of lower-amplitude DNA transfer pulses and aim

to maximize the electroporation efficiency and minimize tissue damage (Zou et al., 2014). The polarity of the transfer pulses was reversed after 50% of pulses were applied. The voltage amplitude of the poring pulses was adjusted based on tissue impedance to yield currents of 4 – 6 mA and the transfer pulses was 20% of the amplitude of the poring pulse. For tissue with an impedance of 16 – 20 kΩ, for example, the pulse train consisted of one biphasic square pulse of 0.1 ms and 96 V for membrane poring followed by 50 square pulses of 1 ms, 19.2 V and 10 Hz for DNA transfer and another 50 square pulses with the same parameters but opposite polarity.

After electroporation, fish were returned to standard tanks and further experiments were performed 7 – 10 days later until ChR2tc expression. The ChR2tc expressing neurons are most likely random in Dp because ChR2tc is driven by a ubiquitous human EF1α promoter and the electroporation process is not selective for cell types. Since the majority neurons in Dp are glutamatergic (**Figure 1 A1**), most of the ChR2tc positive cells are assumed to be excitatory.

### *Ex-vivo* preparations and pharmacology

Physiological experiments were performed in an *ex-vivo* preparation of the nose and brain from adult zebrafish (Zhu et al., 2012). In short, fish with were cold-anesthetized, decapitated, and the ventral forebrain was exposed by removal of the jaw and palate. The preparation was transferred into a custom-made fixing chamber with continuous perfusion of teleost artificial cerebrospinal fluid (ACSF) (Mathieson and Maler, 1988) and warmed up to room temperature.

For pharmacology, the cholinergic agonist Carbachol (CCh, Sigma, USA) was prepared as a stock solution (10 mM) in distilled water and stored at -20°C. Immediately before application, the stock was thawed and diluted to a final concentration of 10 µM in ACSF. The drug wash-in in our experimental settings usually takes less than 2 min (Bundschuh et al., 2012). The effects of CCh were accessed after 5 min of wash-in. CCh was washed out for at least 10 min before testing the recovery of synaptic transmission. Analysis was performed only for cells with full drug wash-in and wash-out data set.

### Imaging, electrophysiology, optical and electrical stimulations

High-resolution imaging of ChR2tc-GFP expression and targeted whole-cell recordings were performed using a multiphoton microscope custom-built on an Olympus BX-51 body (Bundschuh et al., 2012). The microscope and related equipment were controlled by ScanImage and Ephus software (Pologruto et al., 2003; Suter et al., 2010).

Whole-cell patch clamp recordings were carried out using borosilicate pipettes (8 – 14 MΩ), a Multiclamp 700 B amplifier (Molecular Devices) and Ephus software (Suter et al., 2010). Neurons were targeted by a combination of multiphoton fluorescence and laser differential interference contrast (DIC) imaging. Pipettes were filled with an intracellular solution containing 130 mM potassium gluconate, 10 mM sodium gluconate, 10 mM sodium phosphocreatine, 4 mM sodium chloride, 4 mM magnesium-ATP, 0.3 mM sodium-GTP, 10 mM HEPES (pH 7.2, 300 mOsm) and 10 μM Alexa Fluor 594 (Invitrogen). Signals were digitized at 10 kHz. Synaptic transmission was studied with voltage clamp hold at either -70 mV for excitatory responses or 0 mV for inhibitory responses.

For optical stimulation of ChR2tc-expressing neurons in Dp (we call it "chrDp"), a 1-m length optic fiber (BFL22-200, Thorlabs, USA) was mounted on a strong blue LED (470 nm; Luxeon STAR, USA) and targeted at Dp using a micromanipulator (Sutter MP-285, USA). The distance between the optical fiber and Dp was ~500 μm. The light power projected on Dp was estimated to be ~16.9 mW/mm$^2$. The blue light stimulation contains a set of 10-trial 10-pulse trains at 6 ms width, 10 Hz, and 11 s inter-trial interval (ITI) and is triggered by TTL signal. In a few early experiments, the stimulation was performed with a 460 nm LED that mounted in the epifluorescence lamphouse at the back of the Olympus BX-51 body (> 10 trials, 10-pulse trains at 10 ms, 10 Hz or 5 Hz, and 12 s ITI; light power under objective ~0.2 – 0.3 mW/mm$^2$).

Electrical stimulation in the OB (we call it "eleOB") was performed by placing a glass pipette (tip diameter, 30 – 50μm) filled with 1 M NaCl or ACSF at the posterior end of the OB. For probing the excitatory and inhibitory synaptic transmissions in Dp, a train of 10 pulses at 0.5 ms width, 10 Hz, -35 V, was delivered 10 times at an ITI of 11 s. For LTP experiments, the eleOB test pulses used consist 2 pulses at 0.5 ms width, 5 Hz, -10 V and 30 s ITI. After recording the baseline synaptic responses evoked by the test pulses for 10 min, the STDP pairing protocol was applied. The pairing protocol consists 3 pair of pre- and post-synaptic stimulation pulses given at 12.5 Hz, and repeated for 10 trials (15 s ITI). The paired pulses contains a pulse for pre-synaptic eleOB stimulation (0.5 ms width, -20 V) and a pulse for post-synaptic depolarization of the Dp neuron at current clamp mode (15 ms delay, 6 ms width, amplitude adjusted from cell to cell so that just enough to induce action potentials, usually 200 pA). After STDP pairing protocol, the test pulses were applied again for at least 50 min.

**Data analysis**

Electrophysiology data were analyzed using custom routines written in Matlab. For studying the excitatory or inhibitory synaptic connections, synaptic currents evoked by chrDp or eleOB stimulations were measured by whole-cell voltage clamp recordings and averaged over 100 pulses (10 trials with 10 pulses each). The response

/ max amplitudes of the averaged pulse traces were measured as the peak currents within a 30-ms time window after the stimulation offset relative to pre-stimulus baseline. If an amplitude exceeds 3X standard deviation (SD) of the averaged pulse trace and lasts for at least 1 ms, the response is considered to be significant. The synaptic latency of the significant responses were estimated manually as the time between the offset of the stimulation and the first inflection of the averaged current trace. Furthermore, the large amplitude and stable excitatory post-synaptic currents (EPSCs) and inhibitory post-synaptic currents (IPSCs) were defined using a 2-pA cutoff threshold for the response amplitudes. For analyzing the synaptic plasticity within EPSCs or IPSCs evoked by the chrDp 10-pulse train, only large amplitude (>2 pA) cells are considered. The traces averaged over 10 trials was used and values were collected from each of the 10 pulses. The area under the curve (AUC) was calculated over an 80-ms time window after stimulation offset.

For LTP experiments, excitatory synaptic currents were recorded with voltage clamp and AUC was calculated for each pulse over a 30-ms time window after eleOB stimulation offset. AUC values over every 10-min period after STDP protocol were compared with the values before STDP protocol. Only cells with significant increase of AUC after 30 min were considered as LTP. Cells with significant decrease of AUC after 30 min were considered as long-term depression (LTD). Results are reported as mean ± SD or standard error (SE) as indicated. Statistical significance was assessed using a non-parametric Wilcoxon rank-sum test for unpaired samples and a non-parametric sign-rank test for paired samples.

## RESULTS

### Sparse excitatory and inhibitory connectivity in Dp

It is well known that in the mammalian olfactory cortex, the majority neurons are excitatory. By checking a BAC transgenic zebrafish line that specifically labels glutamatergic neurons (Vglut2a::DsRed, Miyasaka et al., 2009), we found that most cells in zebrafish Dp are also excitatory (**Figure 1 A**). Functional synaptic connectivity between principal neurons in the olfactory cortex is difficult to analyze by paired electrophysiological recordings because it is very sparse (connection probability < 1 %) (Franks et al., 2011; Hagiwara et al., 2012). Paired recordings of neurons in Dp show the same difficulty (0 connections from over 100 pairs, Y.P. Zhang Schaerer and J. Shum, unpublished data), suggesting the connectivity in Dp may also be sparse. However, this problem can be overcome by optogenetic stimulation of multiple neurons to increase the probability of finding a mono-synaptically connected post-synaptic neuron (Franks et al., 2011). In order to examine the synaptic transmissions within the Dp excitatory neurons, we used the channelrhodopsion-2 (ChR2) and electrophysiology in the experiments.

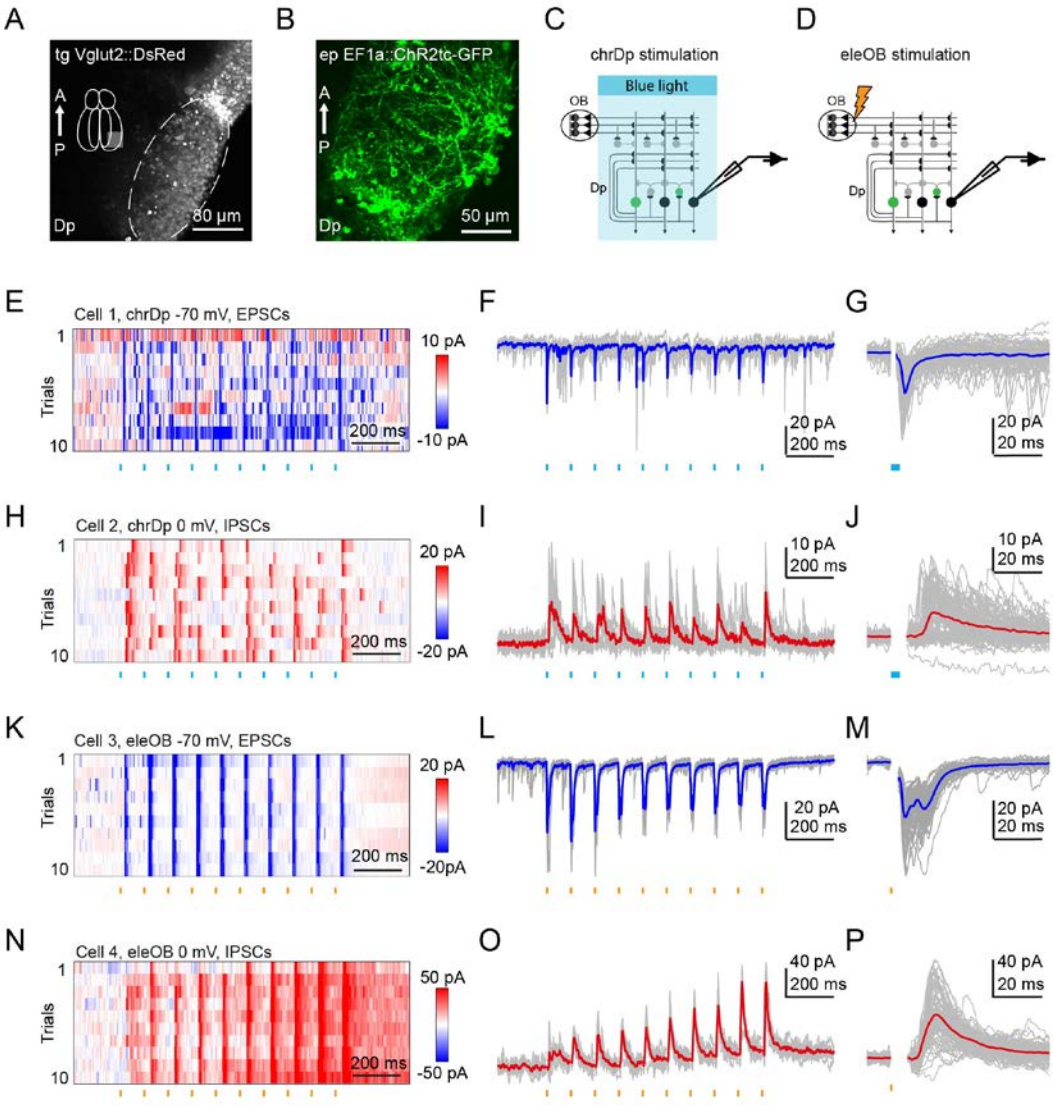


**Figure 1 | Excitatory and inhibitory synaptic transmissions in Dp. (A)** Dp excitatory neurons labeled by DsRed (z-projection of multi-photon stack) in a BAC transgenic fish. Inset shows the ventral view of adult forebrain and the position for taking the image. Dash line circles Dp area. A, anterio; P, posterior; tg, transgenic. **(B)** Sparse set of neurons in Dp labeled by ChR2tc-GFP through in vivo electroporation (ep) (z-projection of multi-photon stack). **(C, D)** Schemes for chrDp and eleOB stimulations to study neuronal connectivity in Dp. ChR2tc was expressed in sparse set of cells in Dp (green circles). ChR2tc negative neurons were recorded with whole cell voltage clamp. **(E)** Color plot shows 10 trails of currents recorded at a holding potential of -70 mV in a ChR2tc negative Dp neuron. Light blue ticks, chrDp blue light pulses. **(F)** The raw traces from (E) are shown in gray and the average of all trials is shown in dark blue. **(G)** Overlay of averaged pulse trace (blue) and raw traces from all pulses over all trials (gray). Stimulation artifact is blanked and the blue bar indicates blue light stimulation. **(H – J)** Like (E – G), the plots show inhibitory currents (in red) recorded at chrDp 0 mV condition. **(K – M)** Similar to (E – G), the plots show excitatory currents (in blue) recorded at eleOB -70 mV condition. The orange ticks indicate extracellular electrical stimulation pulses for OB. Note the multiple peaks in (M). **(N – P)** Like (K – M), the plots show inhibitory currents (in red) recorded at eleOB 0 mV condition.

Briefly, a plasmid DNA containing ChR2tc, a ChR2 mutant with higher cation current and higher probability to induce action potential in neurons (Berndt et al., 2011), was introduced into a sparse set of Dp neurons (n = 35 fish, **Figure 1 B**) by spatially targeted *in vivo* electroporation (Zou et al., 2014). ChR2tc was expressed in 23 ± 5 cells (mean ± SD, counted from 26 fish) that are assumed to be random because ChR2tc is driven by a ubiquitous human EF1α promoter and the electroporation process is not selective for cell types. In addition, most of the ChR2tc positive cells would be excitatory because the majority neurons in Dp are glutamatergic (**Figure 1 A**). ChR2tc was stimulated by trains of blue light pulses (10 trials of 6-ms, 10-pulse train at 10 Hz) delivered through an optic fiber illuminating the whole Dp. The successful rate of ChR2tc to trigger action potentials is > 90 % (Berndt et al., 2011; Zou et al., 2014). Responses were recorded from ChR2tc negative neurons by whole-cell voltage clamp recordings (**Figure 1 C**). As a comparison, we also recorded responses activated by extracellular electrical stimulation of the ipsilateral olfactory bulb output axon bundle (10 trials of 0.5-ms, 10-pulse train at 10 Hz), which is an afferent input path to Dp (**Figure 1 D**). Hereafter we refer to Dp ChR2tc stimulation as "chrDp" and OB output axon electrical stimulation as "eleOB".

By holding the recorded neuron at -70 mV and 0 mV, we could measure both excitatory and inhibitory synaptic transmissions in Dp. Therefore, together we collected data from four types of conditions: chrDp -70 mV and eleOB -70 mV conditions for excitatory responses, and chrDp 0 mV and eleOB 0 mV conditions for inhibitory responses. We observed both excitatory post-synaptic currents (EPSCs) and inhibitory post-synaptic currents (IPSCs) evoked by chrDp stimulation (**Figure 1 E – J**). The chrDp EPSCs show an early onset (< 4 ms after stimulation offset), indicating that the EPSCs contain a mono-synaptic component (**Figure 1 G**). In contrast, the chrDp IPSCs often show a late onset (> 4 ms after stimulation offset), indicating the IPSCs may be polysynaptic responses (**Figure 1 J**). The typical EPSCs and IPSCs triggered by eleOB stimulation have larger amplitudes and last longer time (**Figure 1 K – P**). The onset of eleOB EPSCs are also fast (< 4 ms after stimulation offset) but usually contain multiple peaks (**Figure 1 M**), suggesting a monosynaptic component in the EPSCs and recurrent excitations across multiple synapses/cells in Dp. The late onset of eleOB IPSCs (> 4 ms after stimulation offset) also suggest that most of them may be polysynaptic responses (**Figure 1 P**).

To analyze the cell to cell connection probabilities and properties, we obtained large numbers of stimulation-recording cell pairs under each condition. Altogether we collected data from 189 neurons in the 35 fish (5.4 ± 2.9 cells per fish, mean ± SD) and there are 169 cells under chrDp -70 mV condition, 163 cells under chrDp 0 mV condition, 142 cells under eleOB -70 mV condition, and 138 cells under eleOB 0 mV condition. 116 cells possess data under all 4 conditions. The averaged pulse traces from each cell under each condition are displayed as color plots (**Figure 2 A – D**). We defined a neuron's response to be significant if the current amplitudes exceed 3X SD of the averaged pulse trace and last for at least 1 ms (**Figure 2 E – H**). We found that

there are only a few chrDp induced significant excitatory responses (40 out of 169, **Figure 2 A, E**) and inhibitory responses (63 out of 163, **Figure 2 B, F**). In contrast, eleOB triggered more significant responses with much larger amplitudes (excitatory, 116 out of 142, **Figure 2 C, G**; inhibitory, 108 out of 138, **Figure 2 D, H**). The inhibitory responses often decay slower than excitatory responses and last longer time (**Figure 2 A – D**). We also measured the onset latencies of all the significant

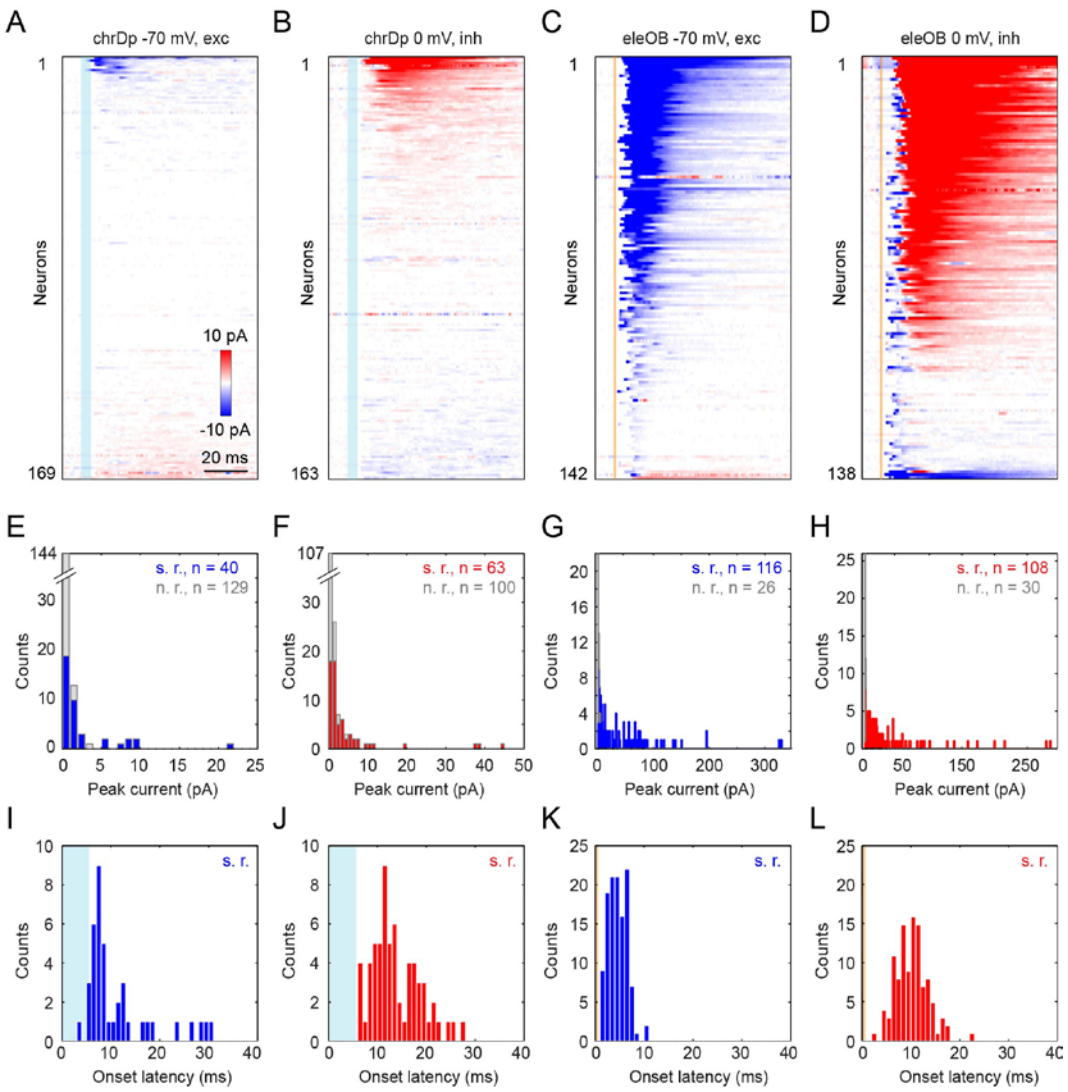


**Figure 2 | Sparse intrinsic excitatory and inhibitory connectivity in Dp. (A – D)** Color plots show averaged excitatory (exc, hold at -70 mV, in blue) or inhibitory (inh, hold at 0 mV, in red) pulse currents of individual neurons under chrDp or eleOB stimulation. Cells in each condition are sorted by their area under curve (AUC) over 80 ms time window after stimulation offset. Blue bars and orange bars indicate blue light or electrical pulse stimulation. **(E – H)** Histograms of peak currents/ response amplitudes collected from averaged pulse traces in each condition above (A – D). The counts of significant responses (s. r.) in each condition are shown in blue for excitatory or red for inhibitory. The counts of non-significant responses (n. r.) are shown in gray. Note the long tail distributions of significant responses. **(I – L)** Histograms of the onset latencies manually collected for all significant excitatory (in blue) and inhibitory (in red) responses from the averaged pulse traces under each condition in (A – D).

excitatory and inhibitory responses (**Figure 2 I – L**). The latency histogram for chrDp stimulation triggered significant excitatory responses shows an early peak at 8 ms and a second peak at 13 ms (**Figure 2 I**). For the chrDp inhibitory responses, the latency histogram also shows two pronounced peaks at 12 ms and 18 ms (**Figure 2 J**). As we don't know the exact wiring diagrams between the stimulated neurons and recorded neurons, we are not able to confirm whether the responses are monosynaptic or polysynaptic.

Because of the low frequency to observe chrDp significant responses (**Figure 2 A, B**) and the small amplitudes of most chrDp significant responses (compared to that of eleOB significant responses, **Figure 2 E, F** vs. **G, H**), it is unlikely that many of the chrDp significant excitatory and inhibitory responses will contain multiple synaptic events from simultaneous activation of multiple ChR2 expressing neurons. In contrast, the large amplitudes of eleOB significant responses suggest that they contain multiple events. The reason may be that electrical stimulation activates much more pre-synaptic neurons. Interestingly, the long tail distribution of the peak synaptic currents suggest that there are some rare large-amplitude synaptic connections in the Dp excitatory and inhibitory circuits (**Figure 2 E – H**). This was frequently reported in studies of other cortical circuits but so far not in the piriform cortex (Lefort et al., 2009; Holmgren et al., 2003; Feldmeyer et al., 2002; Markram et al., 1997).

We found that within the chrDp significant responses, it would be obvious to distinguish the large amplitude responses with a 2-pA cutoff (**Figure 3 A**). Together we sorted out 9 large amplitude EPSCs out of the 40 chrDp significant excitatory responses and 28 large amplitude IPSCs out of the 63 chrDp significant inhibitory responses. The large amplitude responses are usually stable across the individual raw traces (**Figure 1 G, J**), which is not the case for low amplitude responses. The inconsistency of low amplitude significant responses across the individual raw traces suggests either that the synaptic connections are weak and unstable or that it is a false positive response. The later is less likely because we are using relatively stringent filtering rules.

Nevertheless, to estimate the connection probabilities, we could use the large amplitude stable events to define the lower bound and the overall significant responses to define the upper bound. Taken together, the 9 large amplitude chrDp EPSCs out of 23(± 5) x 169 stimulation-recording cell pairs mean that the lower bound of intrinsic functional excitatory connection porbability in Dp could be as sparse as 0.19 % – 0.30 %. The upper bound based on the 40 significant excitatory responses would be ~0.85 % – 1.31 %. It is interesting to find out that this excitatory connection probability in Dp is similar to that reported in the piriform (< 1 %, Franks et al., 2011; Hagiwara et al., 2012). Moreover, the 28 large amplitude chrDp IPSCs out of 23(± 5) x 163 stimulation-recording cell pairs mean that the lower bound of intrinsic feedback inhibition connection probability may be slightly higher, around 0.61 % – 0.95 %. And the upper bound for inhibitory connection probability based on the 63 significant inhibitory responses would be ~1.38 % – 2.15 %.

In addition, we wanted to know whether there are any correlations between the excitatory and inhibitory responses induced by either chrDp or eleOB stimulation in the same neurons. We picked out the 116 cells that have data in all the 4 conditions and calculated the correlation coefficients between response amplitudes of any pair of the 4 conditions. The results indicate weak correlation among responses from each condition (p values: chrDp excitation vs. chrDp inhibition, 0.49; chrDp excitation vs. eleOB excitation, 0.48; chrDp inhibition vs. eleOB inhibition, 0.80; and eleOB excitation vs. eleOB inhibition, 0.31). Scatter plots of response amplitudes for chrDp excitation vs. inhibitory and eleOB excitation vs. inhibition show weak or no correlation between each of the two (**Figure 3 B, C**). With the 2-pA cutoff, the 116 cells could be simply sorted into four groups: cells with only large EPSCs (ChRepsc, n = 6, **Figure 3 B,** blue dots), cells with only large IPSCs (ChRipsc, n = 22, **Figure 3 B,** red dots), cells with both large EPSCs and large IPSCs (ChRepip, n = 2, **Figure 3 B,** green dots), and cells weak or null responses (ChRwenu, n = 86, **Figure 3 B,** black dots). However, these four groups of cells do not show obvious clustering in the eleOB excitation and inhibition correlation plot (**Figure 3 C**).

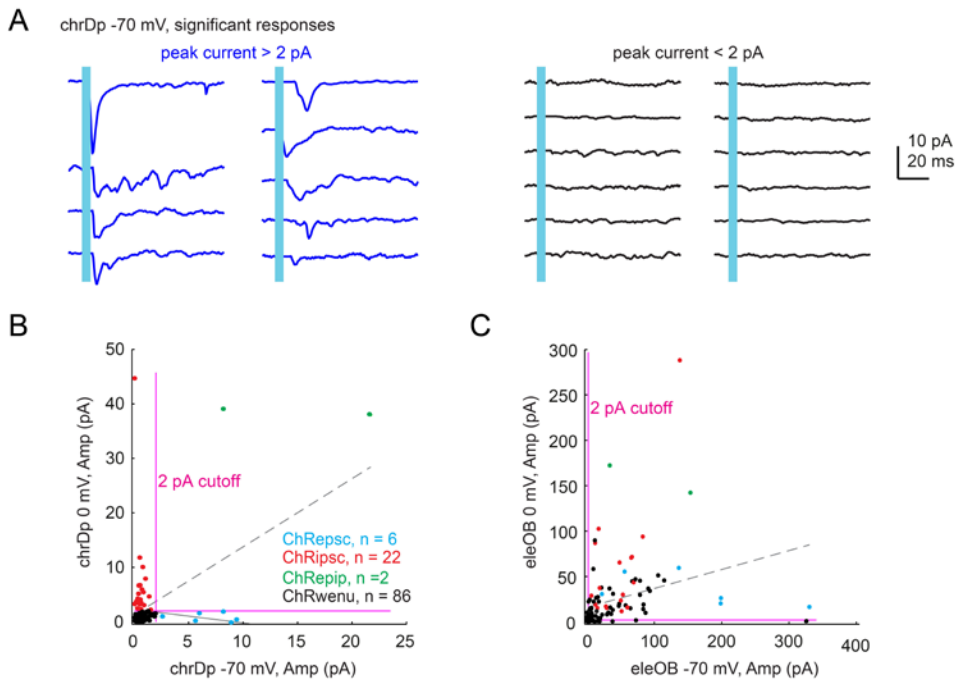


**Figure 3 | Large amplitude excitatory and inhibitory responses induced by chrDp.** **(A)** With a 2-pA peak current cutoff, the significant chrDp excitatory responses could be separated to large amplitude EPSCs (in blue) and low amplitude ones (in black). **(B)** Response amplitudes (Amp) of the 116 cells at chrDp -70 mV condition as a function of that at chrDp 0 mV. With 2-pA cutoff (magenta line), 4 groups of cells are shown: with only large EPSCs (ChRepsc, n = 6, blue dots); with only large IPSCs (ChRipsc, n = 22, red dots); with both large EPSCs and large IPSCs (ChRepip, n = 2, green dots); and with only weak or null responses (ChRwenu, n = 86, black dots). Gray dash line is a linear fit of the data; gray solid line is a linear fit of the data that removing the two green dots. **(C)** Correlation scatter plot of response amplitudes for the 116 cells under eleOB -70 mV and eleOB 0 mV conditions. Gray dash line is a linear fit of the data.

From the results above, we conclude that both intrinsic excitatory and inhibitory connectivity within Dp are sparse (excitatory connection probability, ~0.19 % – 1.31 %; inhibitory connection probability, ~0.61 % – 2.15 %). There are slightly more intrinsic inhibitory connections than excitatory connections but there is no obvious interdependence between excitatory and inhibitory connectivity.

**Inhibition is reduced by cholinergic modulation**

Cholinergic system is known to have intensive axonal projections in the mammalian cortex and modulate the cortical processing of both bottom-up sensory inputs and inter-regional feedback signals (Giocomo and Hasselmo, 2007; Fumitaka, 2000; J. Josh, 2008; Muñoz and Rudy, 2014). In the olfactory cortex, cholinergic modulation is involved in various plasticity, learning, and memory (Hasselmo and Bower, 1992; Hunter and Murray, 1989; Ravel et al., 1992; Lévy et al., 1997; De Rosa and Hasselmo, 2000; Wilson et al., 2004; Giocomo and Hasselmo, 2007; Fletcher and Chen, 2010). The cholinergic system also spread intensive axon fibers in the zebrafish Dp area (Edwards et al., 2007; Clemente et al., 2004), but their functions are still poorly known. Therefore, in some connectivity probing experiments, we also washed in the cholinergic agonist carbachol (CCh, 10 µM in ACSF) to examine whether it could modulate the excitatory and inhibitory synaptic transmissions in Dp.

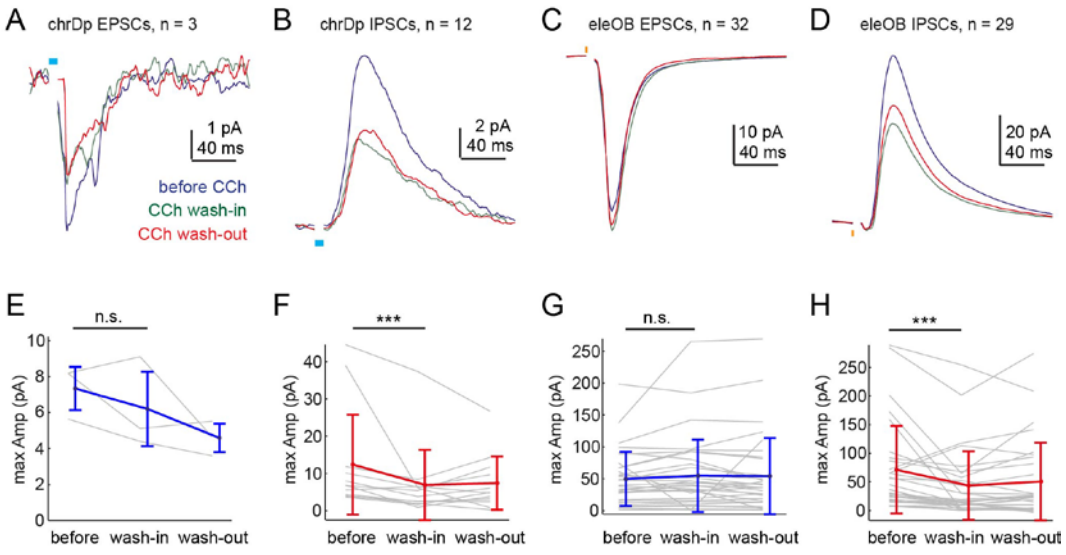


**Figure 4 | Intrinsic inhibition in Dp are reduced by cholinergic modulation. (A – D)** Mean EPSC or IPSC traces of multiple cells before (blue), during (green), and after (red) CCh wash-in are shown for each condition. Blue bar, chrDp blue light pulses; orange tick, eleOB electrical pulses. Stimulation artifact is blanked. **(E – H)** EPSC or IPSC response amplitudes are collected from mean traces of each cell in (A – D). Raw values are shown in gray and mean ± SD are shown in blue (for EPSC) and in red (for IPSC). ***, Wilcoxon sign-rank test p<0.001; n.s., not significant.

**Figure 4 A – D** show the mean traces of the large amplitude EPSCs and IPSCs (with 2-pA cutoff) from multiple cells obtained before, during, and after CCh application under the 4 conditions. We observed significant decrease of response amplitudes from IPSCs triggered by both chrDp (n = 12) and eleOB (n = 29) stimulations (**Figure 4 F, H**). In contrast, the EPSCs triggered by chrDp and eleOB stimulations were not significantly affected by cholinergic modulation (**Figure 4 E, G**). Together, the data show that intrinsic inhibitory connections within Dp are reduced by cholinergic activation.

## Activity-dependent synaptic plasticity

We also analyzed the short-term changes of responses within the 10 pulses for all the large amplitude EPSCs and IPSCs under chrDp stimulation (**Figure 5 A, E**). By measuring the response amplitudes and AUC of each of the 10 pulses, we observed significant synaptic depression at the late pulses in both chrDp EPSCs and chrDp IPSCs ($p < 0.05$, **Figure 5 B, C, F, and G**). The overlay of the averaged traces of the 10 pulses from all cells in either condition suggests that the responses to the first pulse has slower decay (**Figure 5 D, H**). These short-term synaptic depressions are activity-dependent and could result from interaction of different types of pre-synaptic interneurons, similar to that in the piriform (Suzuki and Bekkers, 2010; Stokes and Isaacson, 2010).

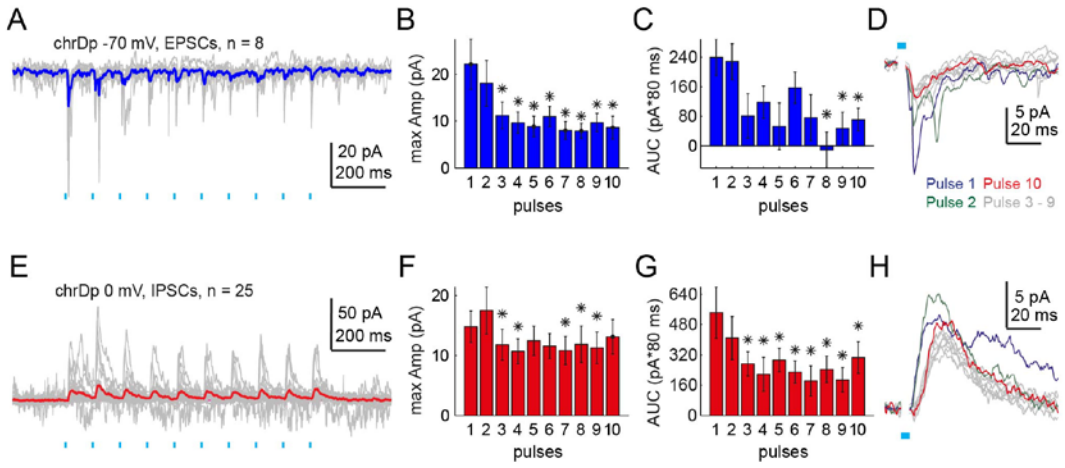


**Figure 5 | Activity-dependent synaptic depression in Dp. (A)** Mean trial traces from individual cells that with chrDp large amplitude EPSCs are shown in gray. The averaged trace of all cells is shown in dark blue. Light blue ticks, chrDp blue light pulses. **(B, C)** Averages of response amplitudes and AUC for each of the 10 consecutive pulses from all cells in (A) are calculated. There're significant depression in the train of chrDp evoked EPSCs (*, $p < 0.05$). **(D)** Mean pulse traces of the 10 pulses from all cells are overlaid. Stimulation artifact is blanked. Dark blue, pulse 1; green, pulse 2; red, pulse 10; gray, pulse 3 – 9; light blue bar, chrDp blue light pulse. Note the decay of pulse 1 (dark blue). **(E – H)** The same plots as in (A – D) for cells with chrDp large amplitude IPSCs.

Furthermore, we examined the possibility to induce LTP (Bliss and Collingridge, 1993; Morris and Frey, 1997) in the intrinsic excitatory synapses of Dp since LTP could be a very important mechanism for learning and memory of different odor-induced activity patterns. For convenience, we used the eleOB stimulation as the pre-synaptic stimulation and optimized the LTP induction protocol based on common STDP induction methods (Bi and Poo, 1998; Song et al., 2000; Feldman, 2012).

Our preferred LTP induction protocol contains the eleOB test pulses and the STDP pairing protocol. The eleOB test pulses used consist 2 pulses at 0.5 ms width, 5 Hz, -10 V and 30 s ITI. After recording the baseline synaptic responses evoked by the test pulses for 10 min, the STDP pairing protocol was applied. The pairing protocol consists 3 pairs of pre- and post-synaptic stimulation pulses given at 12.5 Hz, and repeated for 10 trials (15 s ITI). The paired pulses contains a pulse for pre-synaptic eleOB stimulation (0.5 ms width, -20 V) and a pulse for post-synaptic depolarization of the Dp neuron at current clamp mode (15 ms delay, 6 ms width, amplitude adjusted from cell to cell so that just enough to evoke spikes, usually 200 pA). After STDP

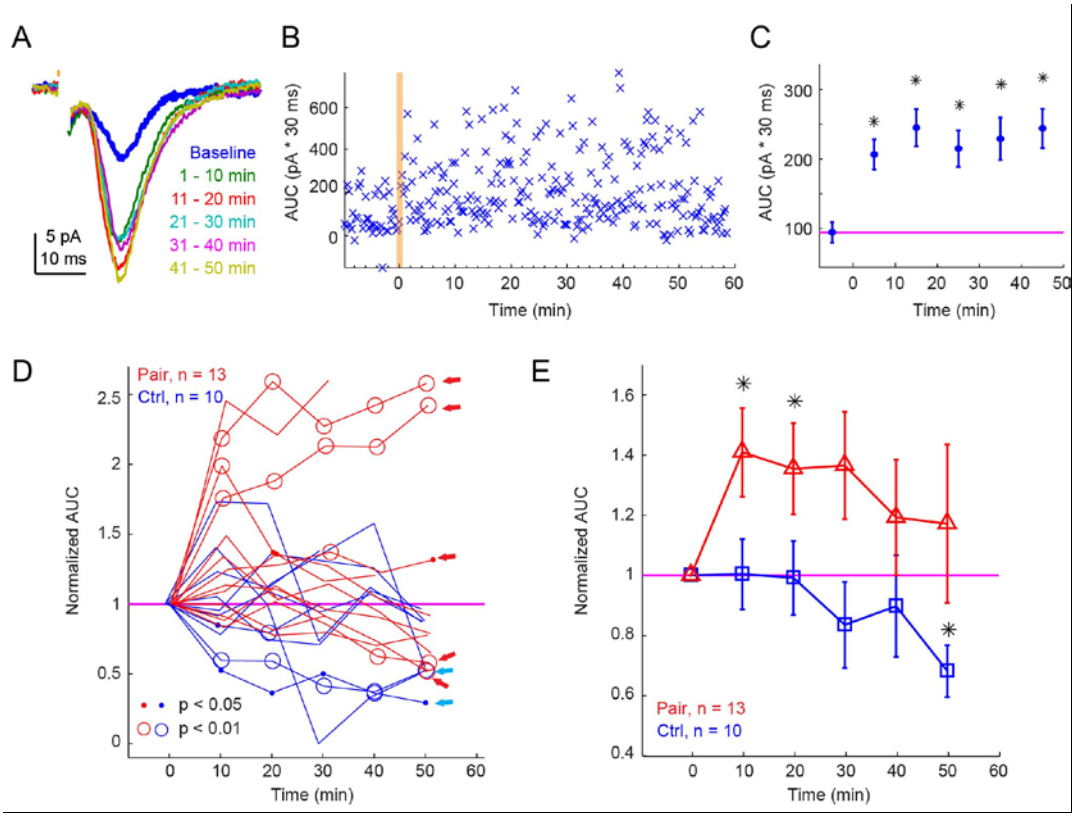


**Figure 6 | Long-term potentiation in Dp. (A – C)** Sample cell with LTP triggered by STDP pairing protocol. **(A)** Mean traces of test pulses over every 10-min period before and after STDP pairing. Orange tick indicates the eleOB stimulation time. **(B)** AUC of test pulses as a function of time. Orange bar indicates STDP protocol was given at 0 min. **(C)** The 10-min-bin AUC values (mean ± SE) from data in (B) are ranked to pre-pairing baseline. *, $p < 0.05$. **(D)** Normalized10-min-bin AUC data from individual cells for a control group (blue, n = 10) and STDP pairing group (red, n = 13). Arrows indicate LTP or LTD cells. **(E)** Average of all cells from each group in (D). Mean ± SE; *, $p < 0.05$.

pairing protocol, the test pulses were applied again for at least 50 min to see whether any LTP happens. The AUC over a 30-ms time window after stimulation offset was measured from each pulse for comparison to the pre-pairing baseline. A sample cell with successful LTP was shown (**Figure 6 A – C**). The mean traces over different 10-min time bins show the potentiation mainly happens at a late phase (> 8 ms after stimulation offset, **Figure 6 A**), indicating the LTP is most likely happening in the Dp intrinsic synapse(s).

With this LTP induction protocol, 3 out of 13 neurons (23%) showed significant LTP (**Figure 6 D**). While in the controls (only test pulses, no STDP pairing, n = 10), no LTP was observed. Some cells in the control group (n = 2) and also the pair group (n = 2) showed depression (**Figure 6 D**, arrows). The other cells in both groups showed no change. Overall, AUC increased significantly in the STDP group but decreased significantly in the control group (**Figure 6 E**).

Taken together, the data above show clearly that there is activity-dependent synaptic plasticity in Dp intrinsic excitatory and inhibitory synapses and that STDP type LTP could be induced in Dp.

## DISCUSSION

In this study, we used a combination of optogenetics, electrophysiology, and pharmacology to probe the connectivity and plasticity of intrinsic neural circuits in the zebrafish Dp, an area homologous to mammalian olfactory cortex. We found that both the intrinsic excitatory and local feedback inhibitory connections in Dp are sparse. We also demonstrate that there is activity-dependent synaptic plasticity as well as STDP type LTP in the Dp neural circuits. Furthermore, we found that inhibitory synaptic transmissions are reduced via cholinergic innervation. Our work obtains new insights on the synaptic organization of neural circuits in Dp and may shed light on odor pattern learning in this region.

Dp is a telencephalic brain area that is homolog of mammalian olfactory cortex (Mueller et al., 2011; Wullimann and Mueller, 2004) and assumed to be involved in olfactory memory (Haberly, 2001; Wilson and Sullivan, 2011; Friedrich, 2013). We found that functional synaptic connectivity between excitatory neurons in Dp is very sparse (< 1.5 %), which is in the similar range of that in olfactory cortex (Franks et al., 2011; Hagiwara et al., 2012). Surprisingly, we observed that the feedback inhibition connection probability in Dp is also sparse (< 2.5 %). This is different from what was suggested for the olfactory cortex that inhibition is widespread (Stokes and Isaacson, 2010). Our observation infers that the tuning of inhibition in Dp may be narrow and as a consequence inhibitory neurons could shape response profiles of Dp output neurons. Furthermore, we report, for the first time in vertebrate olfactory

forebrain, that the distribution of synaptic transmissions is skewed, which indicates that the activity in Dp may be processed by some strongly connected units. This is similar to that found in other cortical regions (Lefort et al., 2009; Holmgren et al., 2003; Feldmeyer et al., 2002; Markram et al., 1997) but so far not reported for the olfactory cortex.

In our experiments, the inhibitory synaptic neurotransmissions in Dp neural circuits are reduced by cholinergic system. The same phenomena has been observed in the piriform cortex (Patil and Hasselmo, 1999). The mechanisms for the reduced feedback inhibition are still unclear. In rodents, it is shown that cholinergic activation of feed-forward inhibitory neurons in layer 1 results in inhibition of layer 2/3 local feedback interneurons (Letzkus et al., 2011). Similar circuits may also exist in Dp. Taken together, cholinergic system may function similarly to affect odor information processing in both Dp and olfactory cortex.

STDP is a type of long-term synaptic plasticity that depends on the relative timing of pre- and post-synaptic action potentials (Bi and Poo, 1998; Song et al., 2000; Feldman, 2012). STDP mechanism has only been reported in the rodent olfactory bulb (Ma et al., 2012) and insect higher olfactory brain area mushroom body (Cassenaer and Laurent, 2007, 2012), but not yet in the vertebrate olfactory forebrain. Here, for the first time that we show STDP phenomena in the vertebrate higher olfactory forebrain, Dp. This type of plasticity reveals that the odor activity pattern from olfactory bulb could most likely be learned and stored by Dp.

In conclusion, we found that synaptic organization of Dp is consistent with mammalian piriform cortex. To our best knowledge, this is the first study that functionally demonstrates common circuit organization between a teleost pallial brain area and its mammalian homologue. Based on this study, it will be important to further characterize how STDP functions in Dp and how cholinergic system affect plasticity as well as odor learning and memory in zebrafish Dp. Interesting experiments could be designed to confirm that cholinergic modulation facilitates LTP in Dp excitatory synapses and allows pattern learning in the circuit level by population calcium imaging.

## Conflict of Interest Statement

The authors declare that the research was conducted in the absence of any commercial or financial relationships that could be construed as a potential conflict of interest.

**Acknowledgments**

We thank C. Xu for hEF1α promoter, T. Oertner for ChR2tc mutant, and G. Jacobson for help with data analysis. This work was supported by the Novartis Research Foundation, the Swiss Nationalfonds, the Deutsche Forschungsgemeinschaft, and the Human Frontiers Science Program.

## REFERENCES

Barnes, D. C., Hofacer, R. D., Zaman, A. R., Rennaker, R. L., and Wilson, D. A. (2008). Olfactory perceptual stability and discrimination. *Nat. Neurosci.* 11, 1378–1380. doi:10.1038/nn.2217.

Berndt, A., Schoenenberger, P., Mattis, J., Tye, K. M., Deisseroth, K., Hegemann, P., and Oertner, T. G. (2011). High-efficiency channelrhodopsins for fast neuronal stimulation at low light levels. *Proc. Natl. Acad. Sci.* 108, 7595 –7600. doi:10.1073/pnas.1017210108.

Bi, G. Q., and Poo, M. M. (1998). Synaptic modifications in cultured hippocampal neurons: dependence on spike timing, synaptic strength, and postsynaptic cell type. *J. Neurosci. Off. J. Soc. Neurosci.* 18, 10464–10472.

Bliss, T. V. P., and Collingridge, G. L. (1993). A synaptic model of memory: long-term potentiation in the hippocampus. *Nature* 361, 31–39. doi:10.1038/361031a0.

Blumhagen, F., Zhu, P., Shum, J., Schärer, Y.-P. Z., Yaksi, E., Deisseroth, K., and Friedrich, R. W. (2011). Neuronal filtering of multiplexed odour representations. *Nature* 479, 493–498. doi:10.1038/nature10633.

Bundschuh, S. T., Zhu, P., Schärer, Y.-P. Z., and Friedrich, R. W. (2012). Dopaminergic Modulation of Mitral Cells and Odor Responses in the Zebrafish Olfactory Bulb. *J. Neurosci.* 32, 6830–6840. doi:10.1523/JNEUROSCI.6026-11.2012.

Cassenaer, S., and Laurent, G. (2012). Conditional modulation of spike-timing-dependent plasticity for olfactory learning. *Nature* 482, 47–52. doi:10.1038/nature10776.

Cassenaer, S., and Laurent, G. (2007). Hebbian STDP in mushroom bodies facilitates the synchronous flow of olfactory information in locusts. *Nature* 448, 709–713. doi:10.1038/nature05973.

Chapuis, J., and Wilson, D. A. (2011). Bidirectional plasticity of cortical pattern recognition and behavioral sensory acuity. *Nat. Neurosci.* 15, 155–161. doi:10.1038/nn.2966.

Choi, G. B., Stettler, D. D., Kallman, B. R., Bhaskar, S. T., Fleischmann, A., and Axel, R. (2011). Driving Opposing Behaviors with Ensembles of Piriform Neurons. *Cell* 146, 1004–1015. doi:10.1016/j.cell.2011.07.041.

Clemente, D., Porteros, Á., Weruaga, E., Alonso, J. R., Arenzana, F. J., Aijón, J., and Arévalo, R. (2004). Cholinergic elements in the zebrafish central nervous system: Histochemical and immunohistochemical analysis. *J. Comp. Neurol.* 474, 75–107. doi:10.1002/cne.20111.

Edwards, J. G., Greig, A., Sakata, Y., Elkin, D., and Michel, W. C. (2007). Cholinergic innervation of the zebrafish olfactory bulb. *J. Comp. Neurol.* 504, 631–645. doi:10.1002/cne.21480.

Feldman, D. E. (2012). The Spike-Timing Dependence of Plasticity. *Neuron* 75, 556–571. doi:10.1016/j.neuron.2012.08.001.

Feldmeyer, D., Lübke, J., Silver, R. A., and Sakmann, B. (2002). Synaptic connections between layer 4 spiny neurone-layer 2/3 pyramidal cell pairs in juvenile rat barrel cortex: physiology and anatomy of interlaminar signalling within a cortical column. *J. Physiol.* 538, 803–822.

Fletcher, M. L., and Chen, W. R. (2010). Neural correlates of olfactory learning: Critical role of centrifugal neuromodulation. *Learn. Mem.* 17, 561–570. doi:10.1101/lm.941510.

Franks, K. M., Russo, M. J., Sosulski, D. L., Mulligan, A. A., Siegelbaum, S. A., and Axel, R. (2011). Recurrent Circuitry Dynamically Shapes the Activation of Piriform Cortex. *Neuron* 72, 49–56. doi:10.1016/j.neuron.2011.08.020.

Friedrich, R. W. (2013). Neuronal Computations in the Olfactory System of Zebrafish. *Annu. Rev. Neurosci.* 36, 383–402. doi:10.1146/annurev-neuro-062111-150504.

Fumitaka, K. (2000). Cholinergic modulation of cortical function: A hypothetical role in shifting the dynamics in cortical network. *Neurosci. Res.* 38, 19–26. doi:10.1016/S0168-0102(00)00151-6.

Giocomo, L. M., and Hasselmo, M. E. (2007). Neuromodulation by Glutamate and Acetylcholine can Change Circuit Dynamics by Regulating the Relative Influence of Afferent Input and Excitatory Feedback. *Mol. Neurobiol.* 36, 184–200. doi:10.1007/s12035-007-0032-z.

Haberly, L. B. (2001). Parallel-distributed Processing in Olfactory Cortex: New Insights from Morphological and Physiological Analysis of Neuronal Circuitry. *Chem. Senses* 26, 551–576. doi:10.1093/chemse/26.5.551.

Hagiwara, A., Pal, S. K., Sato, T. F., Wienisch, M., and Murthy, V. N. (2012). Optophysiological analysis of associational circuits in the olfactory cortex. *Front. Neural Circuits* 6, 18. doi:10.3389/fncir.2012.00018.

Hasselmo, M. E., and Barkai, E. (1995). Cholinergic modulation of activity-dependent synaptic plasticity in the piriform cortex and associative memory function in a network biophysical simulation. *J. Neurosci. Off. J. Soc. Neurosci.* 15, 6592–6604.

Hasselmo, M. E., and Bower, J. M. (1992). Cholinergic suppression specific to intrinsic not afferent fiber synapses in rat piriform (olfactory) cortex. *J. Neurophysiol.* 67, 1222–1229.

Hasselmo, M. E., Wilson, M. A., Anderson, B. P., and Bower, J. M. (1990). Associative memory function in piriform (olfactory) cortex: computational modeling and neuropharmacology. *Cold Spring Harb. Symp. Quant. Biol.* 55, 599–610.

Holmgren, C., Harkany, T., Svennenfors, B., and Zilberter, Y. (2003). Pyramidal cell communication within local networks in layer 2/3 of rat neocortex. *J. Physiol.* 551, 139–153. doi:10.1113/jphysiol.2003.044784.

Hunter, A. J., and Murray, T. K. (1989). Cholinergic mechanisms in a simple test of olfactory learning in the rat. *Psychopharmacology (Berl.)* 99, 270–275.

J. Josh, L. (2008). Cholinergic control of GABA release: emerging parallels between neocortex and hippocampus. *Trends Neurosci.* 31, 317–327. doi:10.1016/j.tins.2008.03.008.

Johnson, D. M. G., Illig, K. R., Behan, M., and Haberly, L. B. (2000). New Features of Connectivity in Piriform Cortex Visualized by Intracellular Injection of Pyramidal Cells Suggest that "Primary" Olfactory Cortex Functions Like "Association" Cortex in Other Sensory Systems. *J. Neurosci.* 20, 6974–6982.

Lefort, S., Tomm, C., Floyd Sarria, J.-C., and Petersen, C. C. H. (2009). The Excitatory Neuronal Network of the C2 Barrel Column in Mouse Primary Somatosensory Cortex. *Neuron* 61, 301–316. doi:10.1016/j.neuron.2008.12.020.

Letzkus, J. J., Wolff, S. B. E., Meyer, E. M. M., Tovote, P., Courtin, J., Herry, C., and Lüthi, A. (2011). A disinhibitory microcircuit for associative fear learning in the auditory cortex. *Nature* 480, 331–335. doi:10.1038/nature10674.

Lévy, F., Richard, P., Meurisse, M., and Ravel, N. (1997). Scopolamine impairs the ability of parturient ewes to learn to recognise their lambs. *Psychopharmacology (Berl.)* 129, 85–90.

Ma, T.-F., Zhao, X.-L., Cai, L., Zhang, N., Ren, S.-Q., Ji, F., Tian, T., and Lu, W. (2012). Regulation of spike timing-dependent plasticity of olfactory inputs in mitral cells in the rat olfactory bulb. *PloS One* 7, e35001. doi:10.1371/journal.pone.0035001.

Markram, H., Lübke, J., Frotscher, M., Roth, A., and Sakmann, B. (1997). Physiology and anatomy of synaptic connections between thick tufted pyramidal neurones in the developing rat neocortex. *J. Physiol.* 500, 409–440.

Mathieson, W. B., and Maler, L. (1988). Morphological and electrophysiological properties of a novel in vitro preparation: the electrosensory lateral line lobe brain slice. *J. Comp. Physiol. [A]* 163, 489–506.

Miyasaka, N., Morimoto, K., Tsubokawa, T., Higashijima, S., Okamoto, H., and Yoshihara, Y. (2009). From the Olfactory Bulb to Higher Brain Centers: Genetic Visualization of Secondary Olfactory Pathways in Zebrafish. *J. Neurosci.* 29, 4756 –4767. doi:10.1523/JNEUROSCI.0118-09.2009.

Morris, R. G., and Frey, U. (1997). Hippocampal synaptic plasticity: role in spatial learning or the automatic recording of attended experience? *Philos. Trans. R. Soc. Lond. B. Biol. Sci.* 352, 1489–1503. doi:10.1098/rstb.1997.0136.

Mueller, T., Dong, Z., Berberoglu, M. A., and Guo, S. (2011). The dorsal pallium in zebrafish, Danio rerio (Cyprinidae, Teleostei). *Brain Res.* 1381, 95–105. doi:10.1016/j.brainres.2010.12.089.

Muñoz, W., and Rudy, B. (2014). Spatiotemporal specificity in cholinergic control of neocortical function. *Curr. Opin. Neurobiol.* 26, 149–160. doi:10.1016/j.conb.2014.02.015.

Patil, M. M., and Hasselmo, M. E. (1999). Modulation of inhibitory synaptic potentials in the piriform cortex. *J. Neurophysiol.* 81, 2103–2118.

Pologruto, T. A., Sabatini, B. L., and Svoboda, K. (2003). ScanImage: flexible software for operating laser scanning microscopes. *Biomed. Eng. Online* 2, 13. doi:10.1186/1475-925X-2-13.

Ravel, N., Vigouroux, M., Elaagouby, A., and Gervais, R. (1992). Scopolamine impairs delayed matching in an olfactory task in rats. *Psychopharmacology (Berl.)* 109, 439–443.

De Rosa, E., and Hasselmo, M. E. (2000). Muscarinic cholinergic neuromodulation reduces proactive interference between stored odor memories during associative learning in rats. *Behav. Neurosci.* 114, 32–41.

Schärer, Y.-P. Z., Shum, J., Moressis, A., and Friedrich, R. W. (2012). Dopaminergic modulation of synaptic transmission and neuronal activity patterns in the zebrafish homolog of olfactory cortex. *Front. Neural Circuits* 6, 76. doi:10.3389/fncir.2012.00076.

Song, S., Miller, K. D., and Abbott, L. F. (2000). Competitive Hebbian learning through spike-timing-dependent synaptic plasticity. *Nat. Neurosci.* 3, 919–926. doi:10.1038/78829.

Stokes, C. C. A., and Isaacson, J. S. (2010). From Dendrite to Soma: Dynamic Routing of Inhibition by Complementary Interneuron Microcircuits in Olfactory Cortex. *Neuron* 67, 452–465. doi:10.1016/j.neuron.2010.06.029.

Suter, B. A., O'Connor, T., Iyer, V., Petreanu, L. T., Hooks, B. M., Kiritani, T., Svoboda, K., and Shepherd, G. M. G. (2010). Ephus: multipurpose data acquisition software for neuroscience experiments. *Front. Neural Circuits* 4, 100. doi:10.3389/fncir.2010.00100.

Suzuki, N., and Bekkers, J. M. (2010). Distinctive Classes of GABAergic Interneurons Provide Layer-Specific Phasic Inhibition in the Anterior Piriform Cortex. *Cereb. Cortex N. Y. NY* 20, 2971–2984. doi:10.1093/cercor/bhq046.

Wilson, D. A. (2003). Rapid, Experience-Induced Enhancement in Odorant Discrimination by Anterior Piriform Cortex Neurons. *J. Neurophysiol.* 90, 65–72. doi:10.1152/jn.00133.2003.

Wilson, D. A., Fletcher, M. L., and Sullivan, R. M. (2004). Acetylcholine and Olfactory Perceptual Learning. *Learn. Mem.* 11, 28–34. doi:10.1101/lm.66404.

Wilson, D. A., and Sullivan, R. M. (2011). Cortical Processing of Odor Objects. *Neuron* 72, 506–519. doi:10.1016/j.neuron.2011.10.027.

Wullimann, M. F., and Mueller, T. (2004). Teleostean and mammalian forebrains contrasted: Evidence from genes to behavior. *J. Comp. Neurol.* 475, 143–162. doi:10.1002/cne.20183.

Yaksi, E., von Saint Paul, F., Niessing, J., Bundschuh, S. T., and Friedrich, R. W. (2009). Transformation of odor representations in target areas of the olfactory bulb. *Nat. Neurosci.* 12, 474–482. doi:10.1038/nn.2288.

Zhu, P., Fajardo, O., Shum, J., Zhang Schärer, Y.-P., and Friedrich, R. W. (2012). High-resolution optical control of spatiotemporal neuronal activity patterns in zebrafish using a digital micromirror device. *Nat. Protoc.* 7, 1410–1425. doi:10.1038/nprot.2012.072.

Zou, M., De Koninck, P., Neve, R. L., and Friedrich, R. W. (2014). Fast gene transfer into the adult zebrafish brain by herpes simplex virus 1 (HSV-1) and electroporation: methods and optogenetic applications. *Front. Neural Circuits* 8, 41. doi:10.3389/fncir.2014.00041.

# *Chapter 4: Discussion*

In this thesis project I developed a new approach, *in vivo* targeted electroporation, for fast gene transfer into neurons of the adult zebrafish brain. Moreover, I found that gene transfer into the adult zebrafish brain can be accomplished efficiently using HSV-1 viral vectors. I also identified promoters that produced strong long-term expression and used electroporation to screen for genetically encoded protein markers, sensors, and transducers that are suitable for zebrafish neural circuit research. These methods and results fill an important gap in the spectrum of genetic tools for zebrafish and are likely to have a wide range of applications.

I then used a combination of electroporation, optogenetics, electrophysiology, and pharmacology to investigate the intrinsic connectivity and plasticity in neural circuits of Dp, the homolog of mammalian olfactory cortex. I found that intrinsic excitatory and inhibitory connectivity in Dp is sparse and that inhibitory synaptic transmission is reduced by cholinergic agonists. Moreover, I demonstrate activity-dependent synaptic plasticity and STDP type LTP in Dp neural circuits. These findings provide new insights on the synaptic organization of neuronal circuits in Dp. The discovery of sparse recurrent connectivity and disinhibitory actions of cholinergic agonists is consistent with models of autoassociative networks for olfactory cortex. These results suggest that Dp and its mammalian homolog may indeed function as an autoassociative memory network and indicate that Dp is an excellent model system to further dissect the structure and function of such a network.

Some parts of the results have already been discussed in *Chapter 2* (*Section 2.5*) and *Chapter 3* (*Section 3.5*). The following discussion mainly concerns the general implications and future directions that emerge from this thesis project.

## 4.1 Fast gene transfer for dissecting zebrafish neural circuits

As described in *Chapter 2*, both HSV-1 viral vector and *in vivo* electroporation were established as fast and efficient approaches to express transgenes in neurons of the adult zebrafish brain. Both approaches achieve high-level expression of transgenes and are stable and non-toxic over a long period of time. For many applications, these methods can therefore alleviate the need for the time-consuming methods to generate stable transgenic fish lines. Moreover, both methods could be used to target transgenes selectively to brain regions for which selective promoters do not exist.

HSV-1 mediates broad transgene expression in both larval and adult zebrafish and could retrogradely label remote brain areas (*Chapter 2*, *Figure 2*). The widespread and remote expression may be due to retrograde viral infection via axonal projections. This raises the opportunities to study inter-regional interaction with ChR2 or GECIs by retrograde labeling of neurons that have specific long-distance projections, for instance, MCs in OB that intensively project to Dp and principal cells in Dp that send centrifugal fibers back to OB.

Electroporation, in contrast, generates local expression, presumably because the electric field is spatially restricted and the intracellular diffusion of DNA is limited (*Chapter 2*, *Figure 3*). This is particularly useful for experiments that aim to exclude expression in cells outside of the region of interest, e.g. ChR2 expression for probing intrinsic connectivity in Dp. This would be unavoidable when using HSV-1 vectors because they could infect axons from those neurons that passing through the injection site. Nevertheless, the flexibilities to easily change the injection sites, promoters and amount of DNA, as well as to further optimize the electric field generated by the electrodes and pulse settings (Šatkauskas et al., 2012) make this method convenient to be adapted according to needs. Electroporation is also cost-effective and time-effective. These advantages were exploited to screen the efficiency of different DNA constructs for gene expression in the adult zebrafish brain. This approach could, in the future, be extended to screen other molecules including RNAs, proteins or chemicals in normal brain circuits or various disease models.

Last but not least, these methods are available for multi-gene co-expression by mixing different viruses or plasmids, or putting multiple expression cassettes in one DNA backbone. For example, simultaneous expression of halorhodopsin and GCaMP6f by HSV-1 vectors in the Dp neurons that send centrifugal fibers back to OB would enable measurement and manipulation of the cells at the same time during an odor stimulation. Through careful combination of different genetic approaches, e.g. cell-type-specific promoters, binary and intersectional expression systems, loss-of-

function or gain-of-function transducers, and other genetically encoded protein markers and sensors, neural circuit research in zebrafish would be greatly advanced.

## 4.2 New genetic tools for dissecting zebrafish neural circuits

A series of powerful genetically encoded tools have emerged and been broadly applied in neural circuit research of different species (Chudakov et al., 2010; Knöpfel et al., 2010; Müller and Weber, 2013; Pérez Koldenkova and Nagai, 2013; Yizhar et al., 2011). I tested a GECI, GCaMP5, in sparse set of Dp neurons (*Chapter 2, Figure 5*) and observed that odor stimulation evokes localized dendritic calcium transients that most likely reflect subthreshold synaptic input. Similar experiments have been performed in the visual and auditory cortex of rodents (Chen et al., 2011; Jia et al., 2010) and gained important insights into the processing mechanisms of synaptic inputs in individual cortical neurons. Thus, by expression of sensitive GECIs in sparse set of Dp neurons, we could measure the tuning of synaptic inputs at different dendritic locations of Dp cells for different odors and analyze computation principles at dendrites of Dp neurons.

Moreover, these genetic markers, sensors, or transducers allow long-term repeated, non-invasive measurements and manipulations of neural circuit activities *in vitro* and *in vivo* (Ahrens et al., 2012; Chen et al., 2013; Liu et al., 2012). Therefore, they will be extremely useful for zebrafish in time-lapse experiments monitoring and manipulating neuronal activities during development, during learning and memory, and during the progression of diseases.

## 4.3 Intrinsic excitatory and inhibitory connectivity in Dp

My results show that the intrinsic excitatory and inhibitory connectivity in Dp is sparse (*Chapter 3, Figure 1 – 2*). Theoretical work has shown that sparse connectivity in an autoassociative network (e.g. CA3 of hippocampus) can enhance the memory storage capacity and enhance the pattern completion ability (Rolls, 2013; Rolls and Treves, 1998). Dp and the mammalian piriform cortex are proposed to behave like an autoassociative network (Friedrich, 2013; Haberly, 2001; Wilson and Sullivan, 2011) and therefore, analyzing the pattern storage and pattern completion function of such network would be the next important step.

The sparse connectivity results are based on statistics and cannot resolve the spatial organization of synaptic connectivity. In the experiments, ChR2 was expressed most likely in different, possibly random, types of Dp neurons, and patch clamp recordings were not targeted to specific cell types. It may thus be expected that the analysis of connectivity included a variety of different cell types in Dp. Consistent with this hypothesis, correlation plots (*Chapter 3*, *Figure 3*) of excitatory and inhibitory

response indicate that some neurons may get more inputs than others. It would now be interesting to identify different subtypes of neurons, either by activity or genetic background, and characterize their connectivity profiles in more detail. This is an important step towards understanding how excitatory and inhibitory inputs determine action potential output of Dp neurons during odor stimulation.

In addition, a dense reconstruction of wiring diagrams for all neurons in Dp will be very useful and may be feasible in the near future because Dp is relatively small (Friedrich et al., 2013). With such data set, it would be possible to identify different connection features that emerged from functional analysis of the circuit activity patterns. For example, it may be possible to analyze numbers and positions of afferent synapses from OB, afferent synapses from other brain region, intrinsic synapses from principal cells, intrinsic synapses from feed-forward interneurons, and intrinsic synapses from feedback interneurons.

## 4.4 Synaptic plasticity and cholinergic modulation in Dp

Synaptic plasticity, especially long-term potentiation, is the basis for learning and memory. I demonstrate that activity-dependent synaptic plasticity and STDP type LTP exist in the neural circuits of zebrafish Dp (*Chapter 3, 3.4.3*). STDP is a type of long-term synaptic plasticity that depends on the relative timing of pre- and postsynaptic action potentials (Bi and Poo, 1998; Feldman, 2012). This mechanism induces competition between different synapses for different activity patterns (Song et al., 2000), thus it is critical for a network with associative pattern learning, separation, and completion functions. The discovery of STDP type LTP in Dp by electrical stimulation of OB (*Chapter 3, Figure 6*) further suggests Dp to be an autoassociative network. The neural circuits in Dp are most likely to be able to store information from the OB input. In other words, Dp may be able to learn and store activity patterns from OB and thus plays a critical role for olfactory learning and memory.

I further observed that the cholinergic agonist CCh decreases intrinsic inhibition (disinhibition) in Dp (*Chapter 3, Figure 4*), which is consistent with that found in piriform cortex (Patil and Hasselmo, 1999). In zebrafish, dopaminergic neuromodulation is also shown to induce disinhibition in Dp (Schärer et al., 2012). The functional role of disinhibition by cholinergic or dopaminergic innervation is unclear. In rodents, cholinergic system induced disinhibition in layer 2/3 pyramidal cells of auditory cortex is found to be necessary for associative fear learning (Letzkus et al., 2011). Moreover, cholinergic system is found to facilitate LTP in the piriform cortex (Hasselmo and Barkai, 1995) and to be indispensable for olfactory learning and memory (Fletcher and Chen, 2010; Wilson and Sullivan, 2011; Wilson et al., 2004). Therefore, it is likely that cholinergic system may be gating circuit plasticity, learning, and memory by releasing principal neurons from inhibition in Dp. Indeed, in some preliminary experiments I found LTP could be induced in Dp through bath

application of CCh (data not shown). Future experiments could be focused on verifying the cholinergic effects on synaptic plasticity and even circuit level pattern learning by electrical or odor stimulation.

## 4.5 Olfactory learning and memory in zebrafish

The small brain size makes zebrafish an interesting model for exhaustive quantitative measurement of neuronal activity patterns. Therefore, it would be extremely useful if this advantage could be applied in a setting of learning and memory, e.g. by behavioral training of the fish to remember a specific odor (Braubach et al., 2009) and then compare the neuronal activity patterns evoked by the familiar odor to that by a naive odor in Dp. This naive odor could be a similar odor or dissimilar odor or morphing series (Niessing and Friedrich, 2010), so that experiments could be designed to test the pattern separation and pattern completion hypothesis for the Dp autoassociative network (Friedrich, 2013; Haberly, 2001).

Furthermore, by training of a fish to remember two different odors for two different choices, an olfaction based attention and decision making paradigm (Uchida and Mainen, 2003; Uchida et al., 2006) is most likely achievable and therefore quantitative analysis of higher cognitive functions in zebrafish would be possible. Zebrafish behavioral paradigms on attention and decision making have already been setup for the visual system (Arganda et al., 2012; Bilotta et al., 2005; Echevarria et al., 2011). However, the circuit level mapping of decision-making brain areas and functional analysis of the network mechanisms are still lacking. With the small zebrafish brain, it should be not that difficult to map the decision-making areas for olfactory sensory inputs. Further combination of the dense sampling of neuronal activity patterns in such higher cognitive areas would make it promising to gain new insights in information processing principles at these regions and then sheds light on top-down control mechanisms to trigger different behaviors.

## 4.6 References

Ahrens, M.B., Li, J.M., Orger, M.B., Robson, D.N., Schier, A.F., Engert, F., and Portugues, R. (2012). Brain-wide neuronal dynamics during motor adaptation in zebrafish. Nature *485*, 471–477.

Arganda, S., Pérez-Escudero, A., and Polavieja, G.G. de (2012). A common rule for decision making in animal collectives across species. Proc. Natl. Acad. Sci. *109*, 20508–20513.

Bi, G.Q., and Poo, M.M. (1998). Synaptic modifications in cultured hippocampal neurons: dependence on spike timing, synaptic strength, and postsynaptic cell type. J. Neurosci. Off. J. Soc. Neurosci. *18*, 10464–10472.

Bilotta, J., Risner, M.L., Davis, E.C., and Haggbloom, S.J. (2005). Assessing Appetitive Choice Discrimination Learning in Zebrafish. Zebrafish *2*, 259–268.

Braubach, O.R., Wood, H.-D., Gadbois, S., Fine, A., and Croll, R.P. (2009). Olfactory conditioning in the zebrafish (Danio rerio). Behav. Brain Res. *198*, 190–198.

Chen, T.-W., Wardill, T.J., Sun, Y., Pulver, S.R., Renninger, S.L., Baohan, A., Schreiter, E.R., Kerr, R.A., Orger, M.B., Jayaraman, V., et al. (2013). Ultrasensitive fluorescent proteins for imaging neuronal activity. Nature *499*, 295–300.

Chen, X., Leischner, U., Rochefort, N.L., Nelken, I., and Konnerth, A. (2011). Functional mapping of single spines in cortical neurons in vivo. Nature *475*, 501–505.

Chudakov, D.M., Matz, M.V., Lukyanov, S., and Lukyanov, K.A. (2010). Fluorescent Proteins and Their Applications in Imaging Living Cells and Tissues. Physiol. Rev. *90*, 1103–1163.

Echevarria, D.J., Jouandot, D.J., and Toms, C.N. (2011). Assessing attention in the zebrafish: Are we there yet? Prog. Neuropsychopharmacol. Biol. Psychiatry *35*, 1416–1420.

Feldman, D.E. (2012). The Spike-Timing Dependence of Plasticity. Neuron *75*, 556–571.

Fletcher, M.L., and Chen, W.R. (2010). Neural correlates of olfactory learning: Critical role of centrifugal neuromodulation. Learn. Mem. *17*, 561–570.

Friedrich, R.W. (2013). Neuronal Computations in the Olfactory System of Zebrafish. Annu. Rev. Neurosci. *36*, 383–402.

Friedrich, R.W., Genoud, C., and Wanner, A.A. (2013). Analyzing the structure and function of neuronal circuits in zebrafish. Front. Neural Circuits *7*, 71.

Haberly, L.B. (2001). Parallel-distributed Processing in Olfactory Cortex: New Insights from Morphological and Physiological Analysis of Neuronal Circuitry. Chem. Senses *26*, 551–576.

Hasselmo, M.E., and Barkai, E. (1995). Cholinergic modulation of activity-dependent synaptic plasticity in the piriform cortex and associative memory function in a network biophysical simulation. J. Neurosci. Off. J. Soc. Neurosci. *15*, 6592–6604.

Jia, H., Rochefort, N.L., Chen, X., and Konnerth, A. (2010). Dendritic organization of sensory input to cortical neurons in vivo. Nature *464*, 1307–1312.

Knöpfel, T., Lin, M.Z., Levskaya, A., Tian, L., Lin, J.Y., and Boyden, E.S. (2010). Toward the Second Generation of Optogenetic Tools. J. Neurosci. *30*, 14998 –15004.

Letzkus, J.J., Wolff, S.B.E., Meyer, E.M.M., Tovote, P., Courtin, J., Herry, C., and Lüthi, A. (2011). A disinhibitory microcircuit for associative fear learning in the auditory cortex. Nature *480*, 331–335.

Liu, X., Ramirez, S., Pang, P.T., Puryear, C.B., Govindarajan, A., Deisseroth, K., and Tonegawa, S. (2012). Optogenetic stimulation of a hippocampal engram activates fear memory recall. Nature.

Müller, K., and Weber, W. (2013). Optogenetic tools for mammalian systems. Mol. Biosyst.

Niessing, J., and Friedrich, R.W. (2010). Olfactory pattern classification by discrete neuronal network states. Nature *465*, 47–52.

Patil, M.M., and Hasselmo, M.E. (1999). Modulation of inhibitory synaptic potentials in the piriform cortex. J. Neurophysiol. *81*, 2103–2118.

Pérez Koldenkova, V., and Nagai, T. (2013). Genetically encoded Ca2 + indicators: Properties and evaluation. Biochim. Biophys. Acta BBA - Mol. Cell Res. *1833*, 1787–1797.

Rolls, E. (2013). The mechanisms for pattern completion and pattern separation in the hippocampus. Front. Syst. Neurosci. *7*, 74.

Rolls, E.T., and Treves, A. (1998). Neural Networks and Brain Function (Oxford ; New York: Oxford University Press).

Šatkauskas, S., Ruzgys, P., and Venslauskas, M.S. (2012). Towards the mechanisms for efficient gene transfer into cells and tissues by means of cell electroporation. Expert Opin. Biol. Ther. *12*, 275–286.

Schärer, Y.-P.Z., Shum, J., Moressis, A., and Friedrich, R.W. (2012). Dopaminergic modulation of synaptic transmission and neuronal activity patterns in the zebrafish homolog of olfactory cortex. Front. Neural Circuits *6*, 76.

Song, S., Miller, K.D., and Abbott, L.F. (2000). Competitive Hebbian learning through spike-timing-dependent synaptic plasticity. Nat. Neurosci. *3*, 919–926.

Uchida, N., and Mainen, Z.F. (2003). Speed and accuracy of olfactory discrimination in the rat. Nat. Neurosci. *6*, 1224–1229.

Uchida, N., Kepecs, A., and Mainen, Z.F. (2006). Seeing at a glance, smelling in a whiff: rapid forms of perceptual decision making. Nat. Rev. Neurosci. *7*, 485–491.

Wilson, D.A. (1998). Habituation of Odor Responses in the Rat Anterior Piriform Cortex. J. Neurophysiol. *79*, 1425–1440.

Wilson, D.A., and Sullivan, R.M. (2011). Cortical Processing of Odor Objects. Neuron *72*, 506–519.

Wilson, D.A., Fletcher, M.L., and Sullivan, R.M. (2004). Acetylcholine and Olfactory Perceptual Learning. Learn. Mem. *11*, 28–34.

Yizhar, O., Fenno, L.E., Davidson, T.J., Mogri, M., and Deisseroth, K. (2011). Optogenetics in Neural Systems. Neuron *71*, 9–34.

# Zou, Ming C.V.

## Education

02/09 – 07/14 PhD of Neurobiology, field Neural Circuits and Computations
Friedrich Miescher Institute for Biomedical Research
CH-4058 Basel, Switzerland

07/12 – 07/12 Summer School in Computational and Cognitive Neuroscience
Cold Spring Harbor Laboratory Asia / Tsinghua University
100083 Beijing, China

10/07 – 12/08 Master of Molecular Biosciences, major Neuroscience
University of Heidelberg
D-69120 Heidelberg, Germany

09/00 – 06/05 Bachelor of Medicine (Equivalent to MD)
Peking University, School of Medicine
100083 Beijing, China

## Research Experience

02/09 – 08/14 **PhD thesis**
Supervisor: Prof. Dr. Rainer W. Friedrich
The Laboratory of Neural Circuits and Computations
Friedrich Miescher Institute for Biomedical Research, Basel, Switzerland

05/07 – 01/09 **Visiting Scientist, Master thesis**
Supervisor: Prof. Dr. Hilmar Bading & Dr. Sheng-Jia Zhang
The Laboratory of Nuclear Calcium Signaling
Department of Neurobiology, IZN, University of Heidelberg, Germany

05/08 – 06/08 **Master Lab Intern**
Supervisor: Prof. Dr. Andreas Draguhn
The Laboratory of General Neurophysiology
Institute of Physiology and Pathophysiology, Uni. of Heidelberg, Germany

01/07 – 05/07 **Research Associate**
Supervisor: Prof. Dr. Yi Rao (Northwestern University, USA)
The Joint Laboratory of Neuroscience
National Institute of Biological Sciences (NIBS), Beijing, China

10/05 – 12/06 **Research Assistant, Lab Manager**
Supervisor: Prof. Dr. Guosong Liu (MIT, USA)
The Joint Laboratory of Learning and Memory
School of Medicine, Tsinghua University, Beijing

10/01 – 01/03 **Research Assistant**
Supervisor: Prof. Dr. Shigong Zhu
The Laboratory of Neuromodulation & Gastrointestinal Endocrine
Department of Physiology & Pathophysiology, Peking University, Beijing

## Publications

**Zou M**, Friedrich RW. Statistics and plasticity of synaptic connections in the zebrafish homolog of olfactory cortex.
*Manuscript in preparation.*

**Zou M***, De Koninck P, Neve RL, Friedrich RW. Fast gene transfer into the adult zebrafish brain by herpes simplex virus 1 (HSV-1) and electroporation: methods and optogenetic applications.
*Front. Neural Circuits* 2014 May 8:41. *** Correspondence.**

Zhang SJ, Buchthal B, Lau D, Hayer S, Dick O, Schwaninger M, Veltkamp R, **Zou M**, Weiss U, Bading H. A signaling cascade of nuclear calcium-CREB-ATF3 activated by synaptic NMDA receptors defines a gene repression module that protects against extrasynaptic NMDA receptor-induced neuronal cell death and ischemic brain damage.
*J Neurosci*. 2011 Mar 30;31(13):4978-90.

Zhang SJ, **Zou M**, Lu L, Lau D, Ditzel DA, Delucinge-Vivier C, Aso Y, Descombes P, Bading H. Nuclear calcium signaling controls expression of a large gene pool: identification of a gene program for acquired neuroprotection induced by synaptic activity.
*PLoS Genet*. 2009 Aug;5(8):e1000604. Epub 2009 Aug 14.

Zhu S, Jiang P, Kang J, Gao L, Han Z, Lu H, **Zou M**, Roles of inflammatory cytokine in the mechanism of neurodegeneration.
*Chinese Journal of Pathophysiology*, 2003, 19(11):1555.